FINAL REPORT

# Evaluating the Perched Aquifer and Ogallala Fine-Grained Zone Using Airborne Geophysics

*by Jeffrey G. Paine*

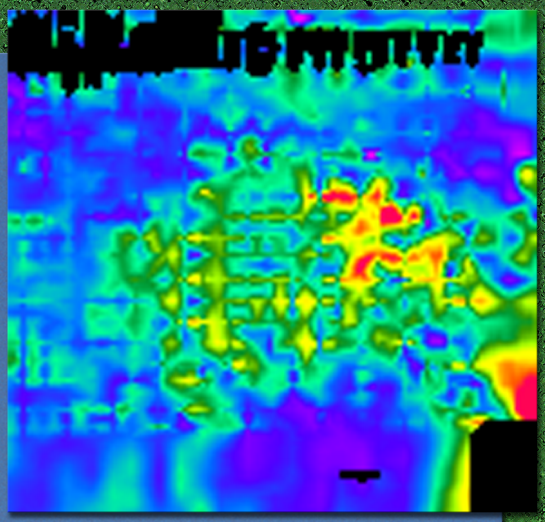

*Prepared for*

**BWXT Pantex**
**P.O. Box 30020**
**Pantex Plant**
**Amarillo, Texas 79120-0020**

**Contract no. 00026424**

**Bureau of Economic Geology**
**Scott W. Tinker, Director**
**John A. and Katherine G. Jackson School of Geosciences**
**The University of Texas at Austin**
**Austin, Texas 78713-8924**

**July 2004**

FINAL REPORT

# EVALUATING THE PERCHED AQUIFER AND OGALLALA FINE-GRAINED ZONE USING AIRBORNE GEOPHYSICS

by

Jeffrey G. Paine
Bureau of Economic Geology
John A. and Katherine G. Jackson School of Geosciences
The University of Texas at Austin

Mail address:
University Station, Box X
Austin, Texas 78713-8924

Street address:
J. J. Pickle Research Campus, Building 130
10100 Burnet Road
Austin, Texas 78758-4445
jeff.paine@beg.utexas.edu

Prepared for

BWXT Pantex
P.O. Box 30020
Pantex Plant
Amarillo, Texas 79120-0020

Contract No. 00026424

July 2004

*Page intentionally blank*

CONTENTS

FIGURES

TABLES

*Page intentionally blank*

## SUMMARY

This report summarizes results of the March 2003 airborne geophysical survey of the Pantex Plant. The survey was completed to investigate the potential for lateral and vertical migration of groundwater in the perched aquifer and to assess the integrity of the Ogallala fine-grained zone (FGZ) that perches groundwater above the Ogallala aquifer at the Pantex Plant. Airborne geophysical instruments acquired time-domain electromagnetic induction (TDEM) data along flight lines totaling 1,243 km in length within four survey blocks located north, east, south, and west of the main Pantex Plant. TDEM data were processed to produce profiles of apparent conductivity variations with depth at more than 100,000 locations within the survey blocks. Measurements with excessive noise were filtered from the final data set. We used the remaining apparent conductivity profiles to produce surveywide and local-area depth slices depicting apparent conductivity changes at 10-m depth intervals between 10- and 200-m depth. These depths are sufficient to examine apparent conductivity patterns and associated hydrologic and geologic characteristics of the upper Ogallala unsaturated zone above the perched aquifer, the perched aquifer and FGZ, the zone below the FGZ and above the Ogallala water table, the lower Ogallala Formation, and, in places, pre-Ogallala strata. In addition to surveywide conductivity data, we have extracted site-specific data for focused investigations at the Pantex Southeast plume, Playa 3, Playa 1, Playa 2, and Playa 4.

Airborne TDEM data correlated reasonably well with borehole data on the extent of the perched aquifer and its saturated thickness, but we were unable to demonstrate a separate meaningful relationship between FGZ thickness and apparent conductivity derived from airborne measurements. In part, we were unable to do so because of sparse, inconsistent data on FGZ thickness. Airborne data identified strata above the perched aquifer with elevated apparent conductivity that indicate relatively high water or clay content, including lacustrine deposits within playas that are likely to be tens of meters thick. Conductive halos surrounding major

playas suggest relatively high water content in these areas, which is associated with lateral and vertical migration of groundwater infiltrating at playas.

Elevated apparent conductivities at perched aquifer depths depicted on depth slices and cross sections are associated with increases in saturated thickness, making airborne TDEM data a useful complement to borehole data in interpolating perched aquifer configuration between boreholes and extrapolating beyond them. Because the TDEM method measures only the conductivity of the ground, these data require careful integration with existing subsurface data for us to choose among competing and conflicting possible causes of patterns depicted on horizontal or vertical conductivity images.

Notable interpretations arising from analysis of the airborne TDEM data include (1) little evidence of substantial offsite, perched aquifer saturated thicknesses, particularly east of the plant; (2) good correlations between airborne TDEM data and perched aquifer saturated thickness where cultural noise is minor, enabling identification of likely areas of local thickening and thinning of the saturated zone; (3) a recurrent apparent conductivity relationship associated with playas that is consistent with a formation mechanism that includes dissolution-induced subsidence and subsequent lacustrine deposition; and (4) relative agreement between (a) borehole data and apparent conductivity images on the bedrock configuration at the base of the Ogallala in both shallow- and deep-bedrock areas and (b) identifying likely local deepening of depth to bedrock beneath playas in shallow-bedrock areas. Possible uses of these data include guiding geologic and hydrologic interpolations and extrapolations from sparse borehole data during future characterization, remediation, monitoring, and groundwater production activities.

# INTRODUCTION

This report presents results of the airborne geophysical survey flown on and near the Pantex Plant in March 2003 (figure 1). The purpose of this survey was to measure the magnitude and variation of apparent electrical conductivity of the subsurface in order to help assess the extent of the perched aquifer and integrity of the middle Ogallala fine-grained zone (FGZ) that perches groundwater above the main Ogallala aquifer. This study follows the feasibility study conducted at the Pantex Plant in 2000 (Paine, 2000) that was part of the Innovative Treatment Remediation Demonstration (ITRD) program at Sandia National Laboratories. The feasibility studies were conducted in response to a recommendation in the "Protecting the Ogallala Aquifer II" report (U.S. Department of Energy, 2000) that "geophysical methods such as time domain electromagnetic soundings (TDEM) and seismic methods should be considered" to provide information on areal extent, thickness, and lithologic variability of the perched water aquitard in the southeast plume area. This report includes geophysical survey results that are relevant to the perched aquifer and to our understanding of underlying Ogallala hydrogeologic features.

## Geologic and Hydrologic Units

BWXT Pantex provided data from 408 wells and borings within the survey area that include depths, elevations, and thicknesses for key stratigraphic and hydrologic units. Of these wells, 287 (appendix A) are within the airborne survey blocks and can be used for direct comparison with airborne survey data. Units relevant to this study that are reported for many or most wells include the top of the Ogallala Formation (caprock caliche), the Ogallala perched aquifer, the Ogallala FGZ, the Ogallala main aquifer, and the base of the Ogallala Formation.

Airborne geophysical data were acquired at a constant height above the ground (drape survey) such that conductivity profiles have a land-surface datum. Surface elevations for 389 wells within the survey area (table 1) average 1,080 m above mean sea level. The relatively flat land surface generally rises from elevations as low as 1,057 m in the southeast part of the area to 1,096 m toward the northwest. There are local low areas where circular or elliptical basins enclose internally drained playas.

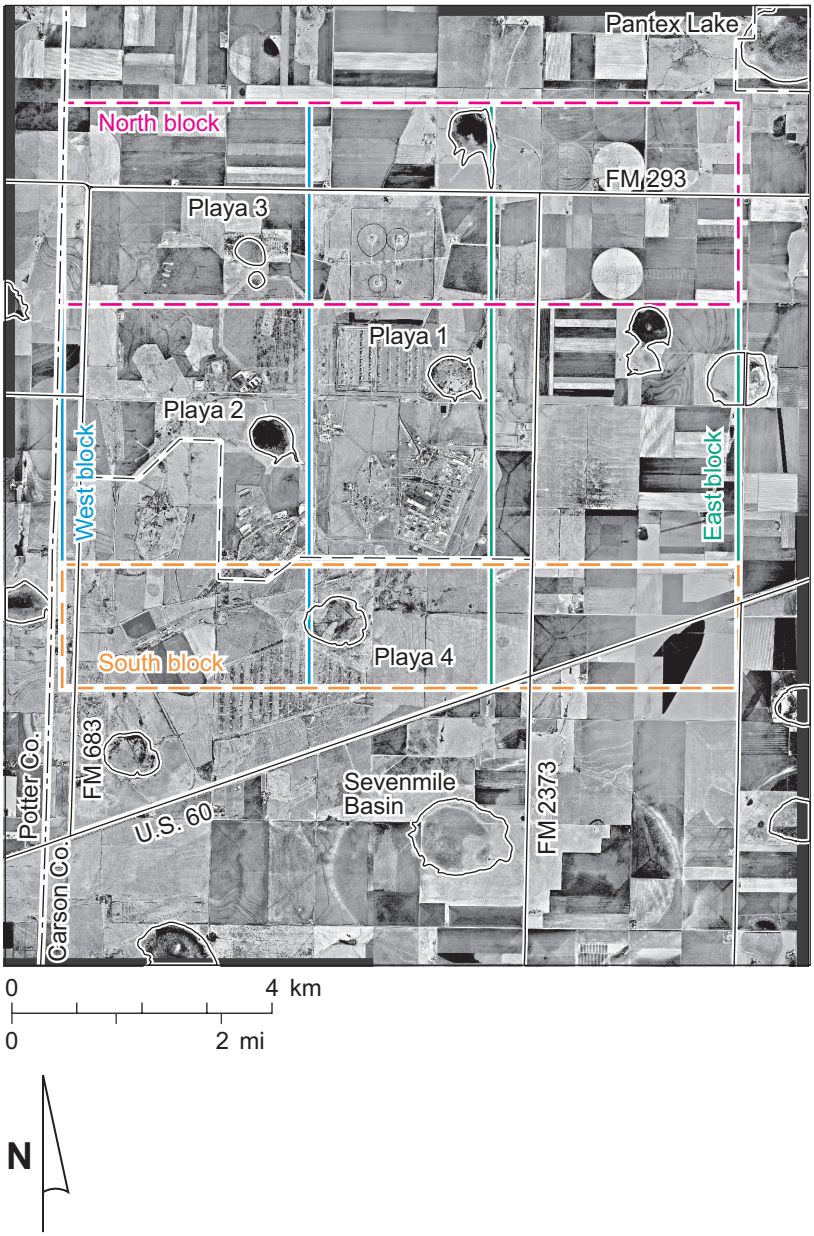


Figure 1. Aerial photomosaic of the Pantex Plant area showing the east, north, south, and west airborne geophysical survey blocks. Aerial photographs taken in 1995 and acquired from the Texas Natural Resource Information System.

Table 1. Depths and thicknesses (in meters) of selected hydrogeologic units reported from 408 wells and borings from the Pantex survey area. Data from BWXT Pantex, October 2003.

| Feature | Number | Average | Minimum | Maximum |
|---|---|---|---|---|
| Ground surface elevation | 389 | 1080 | 1057 | 1096 |
| Caprock | | | | |
| Depth to top | 363 | 22.6 | 12.2 | 31.4 |
| Thickness | 351 | 2.3 | 0.6 | 7.3 |
| Perched aquifer | | | | |
| Depth to water table | 184 | 79.8 | 52.0 | 92.2 |
| Saturated thickness (including dry wells) | 223 | 4.2 | 0.0 | 21.5 |
| Saturated thickness (excluding dry wells) | 178 | 5.3 | 0.1 | 21.5 |
| Fine-grained zone | | | | |
| Depth to top | 307 | 83.5 | 54.9 | 98.5 |
| Thickness | 72 | 14.0 | 0.6 | 47.5 |
| Combined perched aquifer and FGZ | | | | |
| Including dry wells | 11 | 13.3 | 4.5 | 29.7 |
| Excluding dry wells | 4 | 17.3 | 7.8 | 29.7 |
| Ogallala aquifer | | | | |
| Depth to water table | 33 | 136 | 99.4 | 153 |
| Base of Ogallala Formation | 44 | 216 | 106 | 271 |

Quaternary eolian, lacustrine, and alluvial silt, sand, and clay mapped as the Blackwater Draw Formation extend from the surface to reported depths of 12 to 31 m (figure 2, table 1), where the formation overlies the caprock caliche, a pedogenic carbonate-cemented zone forming the upper surface of the Miocene to Pliocene Ogallala Formation. This caliche layer, found at an average depth of 23 m, has an average thickness of 2.3 m. The surface of the caprock caliche generally mimics the land surface, but reported depths and thicknesses vary locally by as much as several meters.

The Ogallala Formation consists of fluvial, lacustrine, and eolian gravel, sand, silt, and clay that host the main Ogallala aquifer in the lower part of the formation, as well as perched aquifers in places above the middle Ogallala FGZ. The known extent of the perched aquifer has been delineated on the basis of borehole data (figure 3). Reported depths to the top of the perched aquifer range from 52 to 92 m, averaging 80 m (figure 3, table 1). Depths are shallower near significant recharge areas, such as Playa 1, where groundwater mounds have formed.

The Ogallala FGZ is considered to be the base of the perched aquifer. Depths to the FGZ average 84 m, but range widely from 55 to 99 m (figure 4, table 1) in 307 wells. Perched aquifer saturated thickness (figure 5, table 1), calculated as the difference in depth between the perched water table and the top of the FGZ, averages 5.3 m but is as great as 21.5 m. Contour maps of saturated thickness of the perched aquifer, based on borehole data, depict local increases in thickness north and west of Playa 1, south of Playa 2, and in the Pantex Southeast area.

FGZ thickness estimates are based on reports from fewer wells and borings (72) that penetrate through the FGZ. FGZ thickness averages 14 m in these wells but ranges from 0.6 to 47.5 m (figure 6, table 1). Relatively thin FGZ is reported in wells southeast, south, and southwest of the Pantex Plant, but thin examples can be found elsewhere. Thickest FGZ deposits are reported near Playa 1 and the Pratt playa. It is likely that the wide range of depths and thicknesses for this unit reflects the presence of multiple fine-grained units in the subsurface that are not necessarily correlative stratigraphically. Average thickness of the combined saturated zone and FGZ is 13 m for the few wells for which both are reported.


Figure 2. Representative depths (in meters) to the Ogallala Formation caprock caliche reported for 363 wells and borings within the Pantex survey area. Data from BWXT Pantex.


Figure 3. Representative depths (in meters) to the perched water table reported for 184 wells and borings within the Pantex survey area. Also shown is the modeled extent of perched groundwater. Data from BWXT Pantex.


Figure 4. Representative depths (in meters) to the Ogallala fine-grained zone (FGZ) reported for 307 wells and borings within the Pantex survey area. Data from BWXT Pantex.

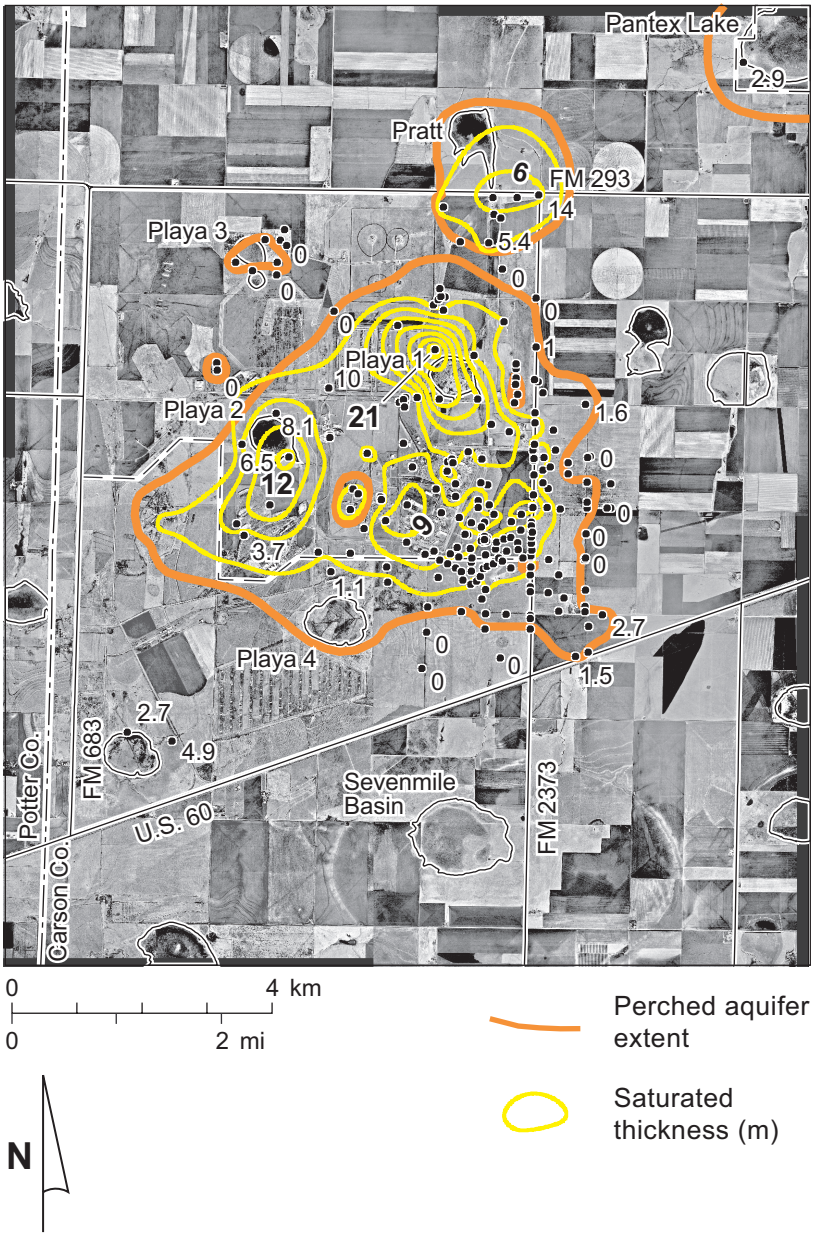


Figure 5. Representative saturated thicknesses of the perched aquifer reported for 223 wells and borings within the Pantex survey area. Well data and thickness contours from BWXT Pantex.


Figure 6. Thickness of the Ogallala FGZ (in meters) reported for 72 wells and borings within the Pantex survey area. Well data from BWXT Pantex.

Depths to the main Ogallala saturated zone generally increase northward toward the City of Amarillo water-well field. Depths of 99 to 120 m south of the plant increase to depths of 147 to 153 m north of the plant (figure 7, table 1). Average depth to the Ogallala water table is 136 m.

The designated base of the Ogallala aquifer is the base of the Ogallala Formation, which rests on a major erosional unconformity separating it from underlying Permian or Triassic sedimentary rocks. Reported depths to the base of the Ogallala also increase northward; bedrock depths increase from 106 to 120 m south of the plant to more than 260 m in places north of the plant (figure 8, table 1). Average depth to the base of the Ogallala in this area is 216 m. Saturated thickness of the main Ogallala aquifer also increases northward, from as little as a few meters south of the plant to 100 m or more north of the plant.

## FGZ Physical Properties

Numerous boreholes have reached the FGZ during Pantex Plant operation, characterization, and remediation activities. Subsurface data indicate that the FGZ is composed of several distinct clay-rich layers within a coarser matrix (Gustavson and others, 1995). Electrical logs from Pantex and surrounding wells verify the common observation that high clay content translates to increased electrical conductivity of the sediment (figure 9). Borehole seismic measurements in an Ogallala monitoring well south of Playa 2 (BEG-PTX2) document an increase in seismic velocity within the FGZ. Furthermore, water-saturated sediment within the perched aquifer most likely has density, seismic velocity, and electrical conductivity that are higher than those of similar unsaturated stratigraphic intervals. These observations from existing data suggest that seismic and electrical methods are appropriate tools for investigating the FGZ and associated perched aquifer. Variations in density, sediment type, and water saturation within the perched aquifer and FGZ might be large enough to image using seismic reflection methods, including the top and perhaps the base of the FGZ where it is sufficiently thick. Increases in electrical conductivity caused by increased saturated thickness of the perched aquifer or by increased FGZ thickness might be detected using electromagnetic induction methods, especially TDEM.


Figure 7. Representative depths (in meters) to the Ogallala water table reported for 33 wells within the Pantex survey area. Data from BWXT Pantex.


Figure 8. Depths (in meters) to the base of the Ogallala Formation reported for 44 wells within the Pantex survey area. Data from BWXT Pantex.

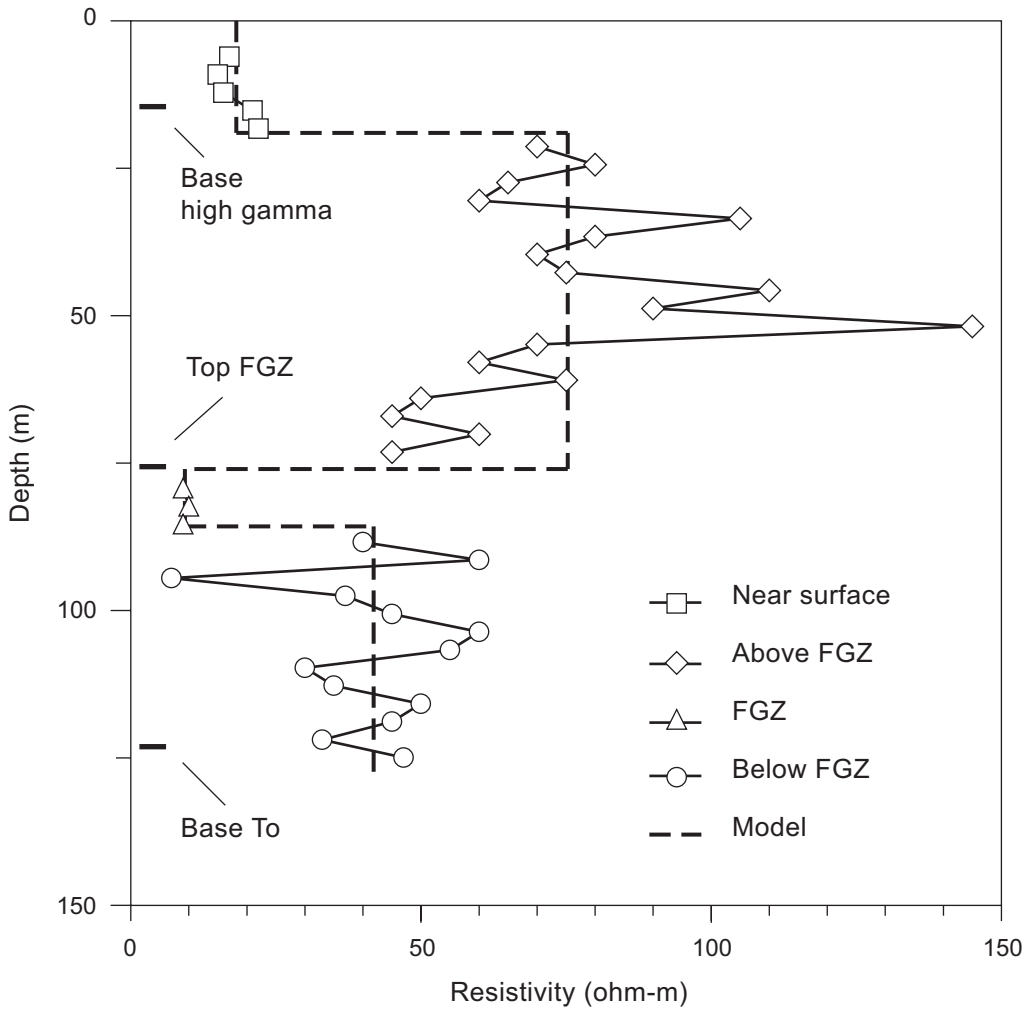


Figure 9. Resistivity log (solid line and symbols) and generalized resistivity model (dashed line) for well BEG-PTX2 in the southwest part of the Pantex Plant. Also shown are the depths to the base of the high-gamma-count zone, the top of the middle Ogallala FGZ, and the base of the Ogallala Formation (To).

The design and feasibility of seismic reflection and EM surveys depend upon the depth and thickness of the FGZ and perched aquifer. Average depth to perched water reported in recent data summaries (Pantex Plant Environmental Restoration Department, 2000; Stoller, 2004) is near 73 m, a little shallower than our calculated average of about 80 m (table 1). Saturated thickness averages about 4 m, ranging from 0 to about 22 m. The underlying FGZ is reached at an average depth of 84 m. Its thickness is poorly constrained, but borehole data suggest an average thickness of about 14 m (table 1). Consequently, the depth range of highest interest ranges from about 60 to 120 m; the combined thickness (FGZ and saturated zone) averages about 17 m.

## Preliminary Modeling and Ground-Based TDEM

We tested the feasibility of the TDEM method in addressing issues related to the perched aquifer at the Pantex Plant by performing preliminary modeling and reconnaissance field investigations in the Pantex Southeast and Playa 3 areas (Paine, 2000). Because electrical properties change with changes in clay content and water saturation, methods that measure subsurface electrical conductivity show promise in detecting subsurface changes caused by the presence or absence of the FGZ and variations in the thickness of the FGZ and the saturated thickness of the perched aquifer.

The purpose of TDEM modeling was to determine (1) appropriate acquisition parameters for the field survey and (2) whether anticipated changes in thickness of the FGZ would produce detectable differences in the TDEM data. To date, little information has been collected on the electrical properties of strata beneath the Pantex Plant; available data consist of complete induction logs for wells BEG-PTX2 and BEG-PTX3, a few partial induction logs in the Pantex Southeast and Playa 3 areas covering only the well depths below the FGZ, and resistivity logs from public water-supply wells north of the Pantex Plant.

We produced a generalized series of subsurface resistivity models on the basis of resistivity data from well BEG-PTX2, located south of Playa 2. Logs of this and other wells show that resistivity changes within the Blackwater Draw and Ogallala Formations can be generalized into four layers

(figure 9). These layers are, from shallowest to deepest: (1) a low-resistivity (about 20 ohm-m) layer a few tens of meters thick having high gamma counts and relatively high clay content that roughly corresponds to the Blackwater Draw Formation; (2) an upper Ogallala resistive layer averaging about 75 ohm-m that extends to a depth of about 75 m at BEG-PTX2; (3) a low-resistivity layer of about 9 ohm-m that is about 10-m thick, representing the middle Ogallala FGZ; and a lower Ogallala resistive layer averaging about 45 ohm-m that extends to the base of the Ogallala Formation. Geophysical logs that penetrate pre-Ogallala rocks suggest that the basal Ogallala layer is underlain by a low-resistivity unit, but that unit was not logged in well BEG-PTX2.

To simulate the effect of varying FGZ thicknesses on the TDEM data, we computed and compared the TDEM measurements that would be expected using the resistivities and layer thicknesses of the generalized model, varying the thickness of the FGZ from 0 to 10 m in 1-m increments. Predicted strength of the transient signal differs significantly, at times later than about 0.5 milliseconds (ms) after shutoff of the transmitter current, for the two end-member models of no FGZ and a 10-m thick FGZ (figure 10). When the signal strength data are converted to apparent resistivity (figure 11), the greatest divergence in the curves occurs between about 0.2 and 5 ms after current termination. If the only stratigraphic variable is the FGZ thickness, modeling data suggest that small changes in FGZ thickness are detectable and that field data be recorded between about 0.1 and 10 ms after current termination for FGZ thickness changes to be best detected.

We acquired ground-based TDEM soundings in the Playa 3 and Pantex Southeast areas (figure 12) to evaluate the method for detecting changes in Ogallala stratigraphic and hydrological properties and to determine electrical properties of the ground for airborne survey design (Paine, 2000). These soundings were acquired using a 100- × 100-m transmitter loop and a receiver at the center of the loop.

Transient signals recorded for each sounding show similar trends. According to modeling results, these signals are sufficiently long to contain information about subsurface electrical properties to depths beyond those of the FGZ. Changes in slope of each decay curve result from changes in electrical properties encountered as the primary signal travels deeper into the subsurface. Variability in decay shapes among transients indicates that the subsurface resistivity profile differs from site to site.

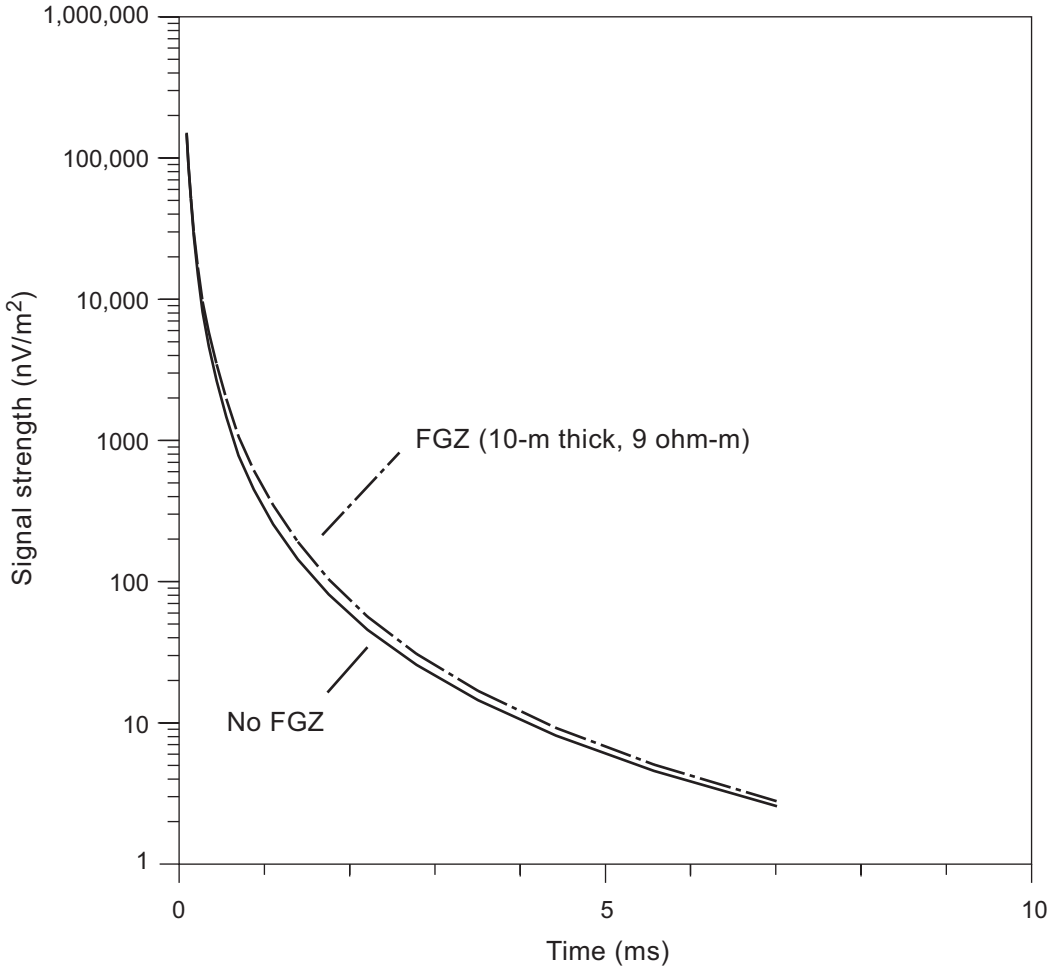


Figure 10. Predicted transient signal for the generalized resistivity model from well BEG-PTX2 with (solid line) and without (dashed line) a 10-m-thick FGZ having 9 ohm-m resistivity.

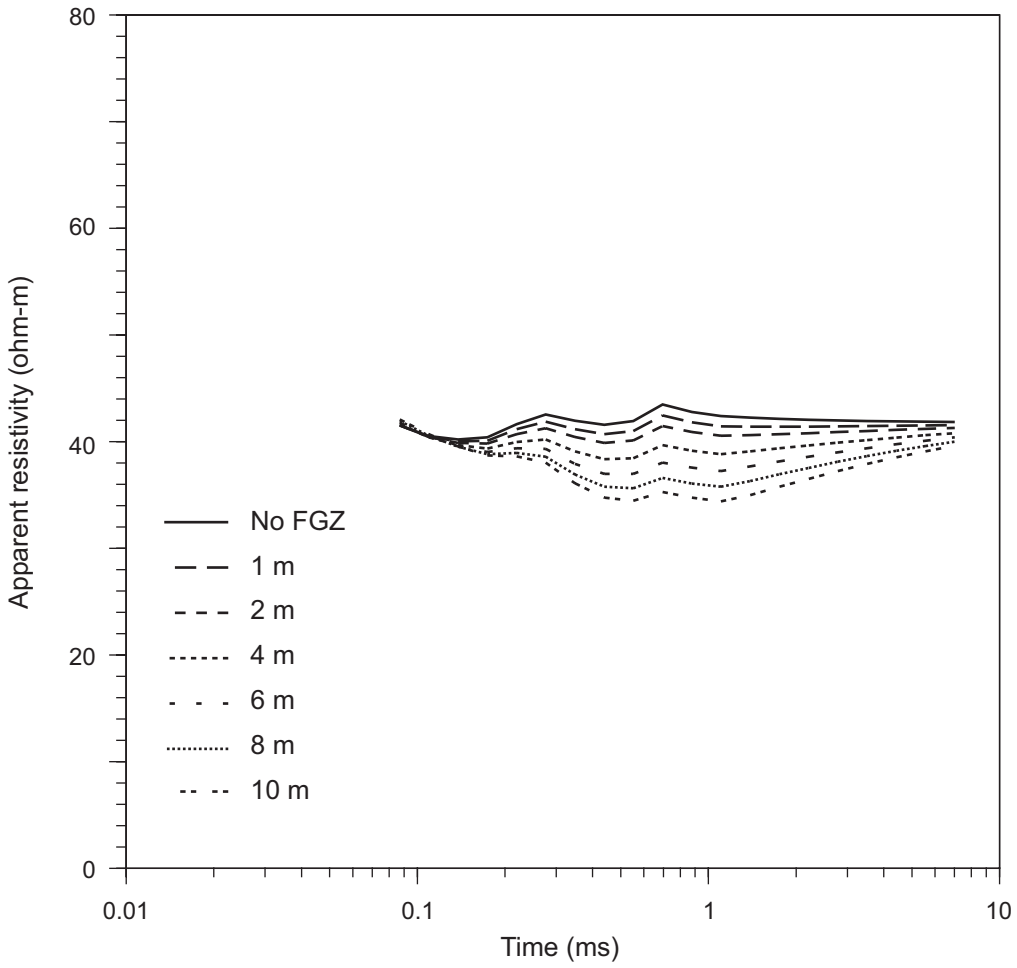


Figure 11. Predicted apparent resistivity curves for the generalized resistivity model from well BEG-PTX2 assuming FGZ thicknesses ranging from 0 (FGZ absent) to 10 m.


Figure 12. Reconnaissance ground-based TDEM sounding sites (appendix B) acquired using a 100- × 100-m transmitter loop.

At each sounding location, we constructed resistivity models of the subsurface, calculated the transient for those models, compared the calculated transients with the actual transient, and adjusted the model iteratively until it provided an adequate fit to the observed data. Two- to four-layer models constructed for soundings along the south–north series in the Pantex Southeast area differ relatively little in the near-surface low-resistivity layer (figure 13) but differ more at deeper levels. Within what would correspond to the upper Ogallala resistive zone and the middle Ogallala FGZ, resistivities decrease progressively to the north. Highest resistivities at the FGZ depth are calculated for sounding TDEM 1 at the south end of the series; lowest resistivities are calculated for TDEM 10 near the Pantex east gate. Maps of FGZ thickness derived from Ebasco seismic data (U.S. Army Corps of Engineers, 1992) show the FGZ thickness progressively increasing northward along this series, matching the TDEM trend. Perched aquifer saturated thickness also increases in this direction, possibly contributing to the increase in apparent conductivity. Upper and lower boundaries of the FGZ and overlying saturated zone are not resolved in the model, but their thicknesses appear to strongly influence the resistivity value calculated for the resistive intermediate layer that spans the depth ranges of these units. Decreases in resistivity to near 10 ohm-m in the model layers corresponding to the lower part of the Ogallala occur near the depth reported for the Ogallala water level. Further resistivity changes at deeper depths in the models are at or deeper than the reported base of the Ogallala.

## Rationale for an Airborne TDEM Survey

Modeling studies and 10 ground-based TDEM soundings showed that thickness of the FGZ can influence strength and shape of the TDEM signal, suggesting that TDEM could be used to help in evaluating the extent and integrity of the FGZ. Airborne TDEM instruments offer the ability to obtain spatially dense data required to identify expected subtle stratigraphic and hydrologic changes associated with the FGZ. These instruments are flown at low altitude along closely spaced flight lines, enabling thousands of soundings to be acquired in the same time as that required to collect a few ground-based soundings. On the basis of results of modeling and ground-based TDEM soundings and in consultation

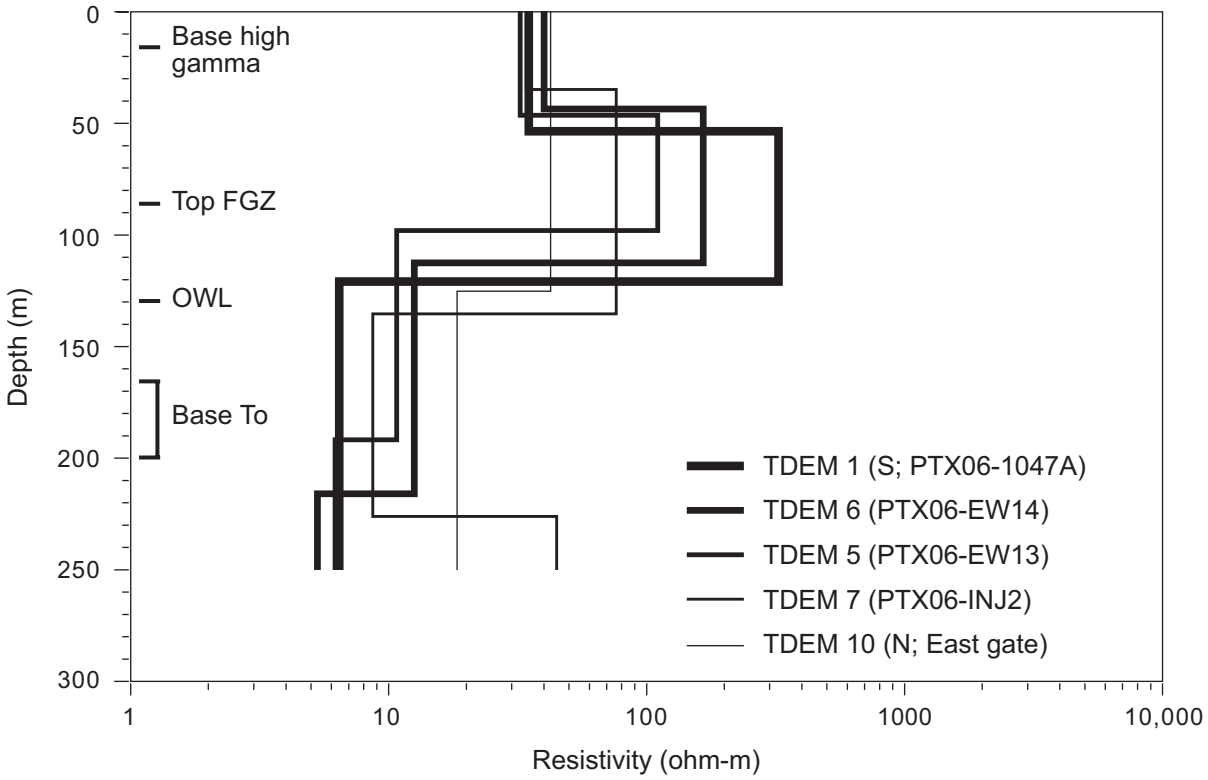


Figure 13. Two- to four-layer resistivity models that fit transients recorded at sites TDEM 1, 5, 6, 7, and 10 in the Pantex Southeast area. Also shown are the approximate depths to the base of the high-gamma-count zone, the top of the middle Ogallala FGZ, the Ogallala water level (OWL), and the base of the Ogallala Formation (To).

with Pantex Plant staff, we designed and conducted an airborne geophysical survey of four areas north, east, south, and west of the Pantex Plant (figure 1).

## METHODS

We employed airborne geophysical methods to rapidly and noninvasively measure changes in electrical conductivity with depth in the four survey blocks surrounding the Pantex Plant (figure 1). The principal geophysical method is electromagnetic induction, or EM (Parasnis, 1973; Frischknecht and others, 1991; West and Macnae, 1991). This family of geophysical methods employs a changing primary magnetic field that is created around a current-carrying transmitter wire to induce a current to flow within the ground, which in turn creates a secondary magnetic field that is sensed by a receiver coil. In general, the strength of the secondary field is proportional to the conductivity of the ground.

TDEM methods (Kaufman and Keller, 1983; Spies and Frischknecht, 1991) measure the decay of a transient, secondary magnetic field produced by the termination of an alternating primary electric current in the transmitter loop (figure 14). The secondary field, generated by current induced to flow in the ground, is measured by the receiving coil following transmitter current shutoff. Secondary-field (transient) strength at an early time gives information on conductivity in the shallow subsurface; transient strength at later times is influenced by conductivity at depth.

Airborne geophysical data, including TDEM and magnetic-field data, were acquired over the Pantex survey blocks in March 2003 by Fugro Airborne Surveys (table 2). The combined 120-km$^2$ area was covered by flying north–south lines spaced at 100 m in the east and west blocks and east–west lines spaced at 100 m in the north and south blocks (figure 15). A total of 104,880 measurement locations were acquired over the survey flight distance of 1,243 km. Fugro collected EM and magnetic-field data using its GEOTEM 1000 TDEM system and a cesium magnetometer towed behind a Casa 212 twin-engine aircraft (figure 16). Flight height was 120 m; the three-axis EM receiver was towed 130 m behind the transmitter at a height of 70 m above the ground (table 3). The primary EM field was generated by a six-turn wire loop fixed to the aircraft carrying a 30-Hz, discontinuous sinusoidal current

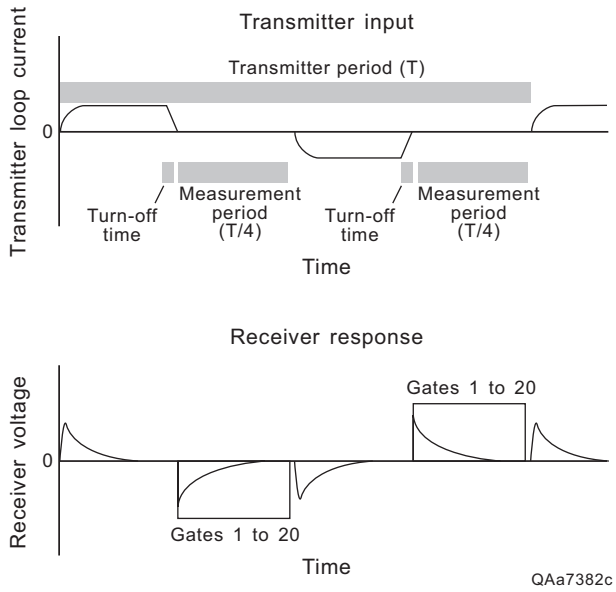


Figure 14. TDEM transmitter input (upper graphic) and receiver response (lower graphic). Adapted from Geonics Limited (1992).

Table 2. Flight specifications for the Pantex airborne geophysical survey conducted in March 2003.

| | |
|---|---|
| Company | Fugro Airborne Surveys, Ottawa, Ontario, Canada |
| Acquisition date | March 8–13, 2003 |
| Aircraft | Casa 212 (twin engine) |
| Flight line spacing | 100 m |
| Flight line direction | North–south (east and west blocks); east–west (north and south blocks) |
| Flight height | 120 m |
| Altimeter | Radar; 0.3 m sensitivity; sample frequency 1 Hz |
| Navigation | Differential GPS (~5 m accuracy); sample frequency 1 Hz |
| Flight speed | 125 knots; 145 mi/hr; 232 km/hr; 65 m/s |
| Distance surveyed | 1,243 km |
| Area surveyed | 120 $km^2$ |
| Measurement locations | 104,880 |

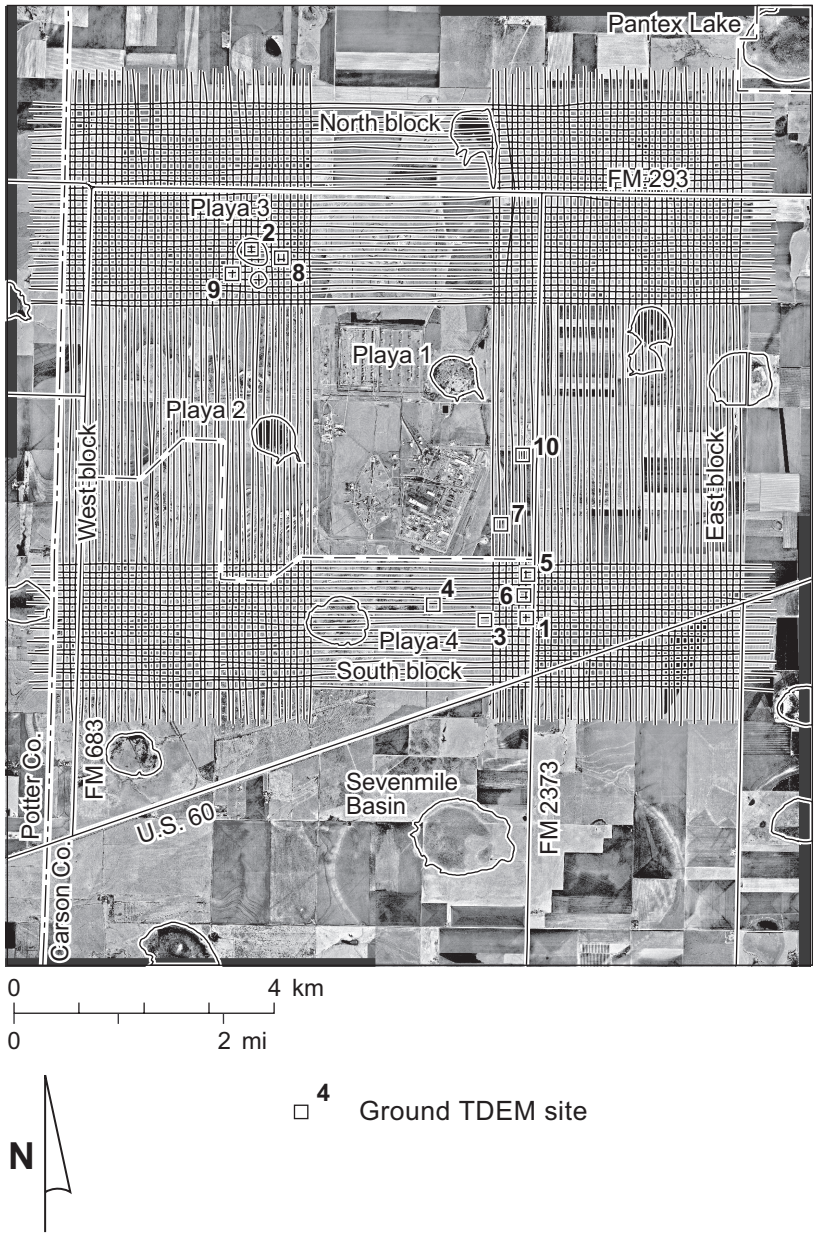


Figure 15. Map of the Pantex Plant area showing geophysical survey flight lines in the north, east, south, and west blocks. Also shown are ground TDEM locations.

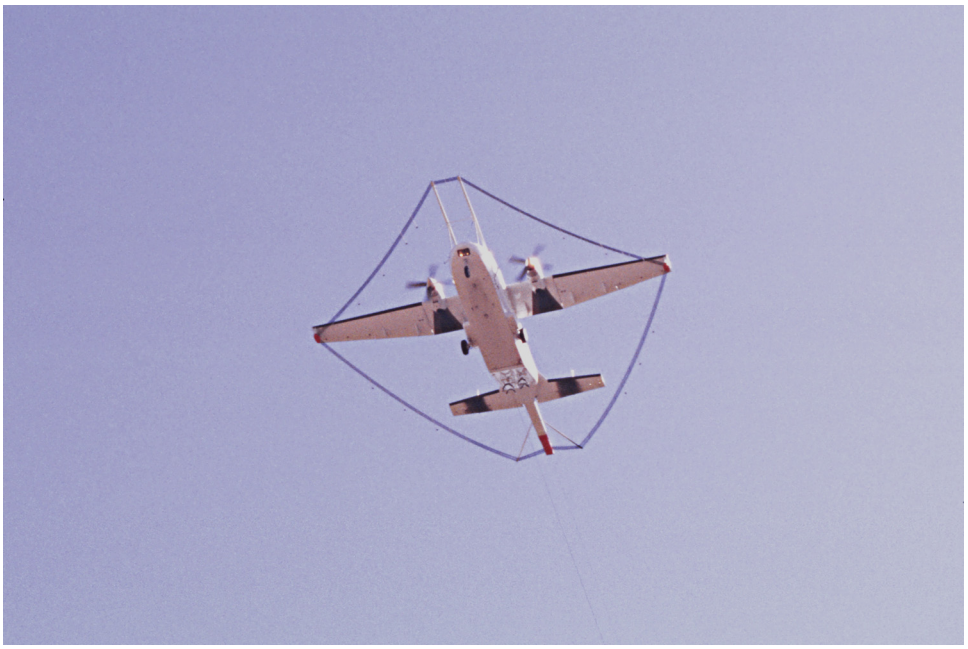

Figure 16. Casa 212 aircraft acquiring TDEM and magnetic field data in the Pantex area. The TDEM transmitter is looped around the aircraft, which is towing the TDEM receiver and magnetometer (not shown).

Table 3. GEOTEM system acquisition parameters used for the Pantex airborne electromagnetic induction survey conducted by Fugro Airborne Surveys, March 2003.

| | |
|---|---|
| EM system | GEOTEM 1000 |
| Transmitter loop area | 231 $m^2$ |
| Number of transmitter loops | 6 |
| Transmitter loop current | 560 A |
| Transmitter dipole moment | ~776,000 A-$m^2$ |
| Transmitter frequency | 30 Hz |
| Transmitter on time | 4.1 milliseconds |
| Transmitter height | 120 m |
| Receiver type | Towed 3 axis |
| Receiver height | 70 m |
| Receiver trailing distance | 130 m |
| Number of recording windows | 20 |
| Time span of recording window (from end of pulse) | -3.9 to 11.3 ms |
| Sample rate | 4 Hz |
| Sample interval | ~16 m |

of 560 amperes (A). The dipole moment, a measure of transmitter strength, was $776 \times 10^3$ A-m$^2$, more than an order of magnitude larger than the moment calculated for the ground-based instrument used in the feasibility study. Transients were recorded during the 11.3-ms window following termination of the 4-ms transmitter pulse. EM diffusion depth, the depth below which currents will not have diffused during the measurement period, is commonly used as a proxy for exploration depth. It is calculated using the equation

$$d = k ( t \ r )^{0.5}$$

where d = diffusion depth (in m), k = 503.3 (m/ohm-s)$^{0.5}$, t = latest time measured, and r = resistivity (in ohm-m) (Parasnis, 1986).

Assuming a ground conductivity of 20 to 50 mS/m (50 to 20 ohm-m resistivity) estimated from ground-based TDEM data and a latest measurement time of 11.3 ms, expected exploration depth is about 240 m for the most conductive ground and about 380 m for the least conductive ground. Measurement locations were determined from global-positioning-system (GPS) data by using a base station at the Amarillo airport and a roving receiver on the aircraft. Locational accuracy is 5 m or better. At the 30-Hz transmitter frequency (60-Hz sample frequency) and a nominal airspeed of 232 km/hr, transients were acquired every 1.1 m along the flight line. Recording stacked transients at 4 Hz resulted in a sample spacing of about 16 m. Fugro processed and delivered the data in March 2003 (Fugro Airborne Surveys, 2003).

Along with the transients measured in the *x* (parallel to the flight path), *y* (horizontal and perpendicular to the flight path), and *z* (vertical) axes by towed receiver coils, Fugro performed conductivity-depth transforms to produce relatively smooth conductivity models depicting a conductivity value at 10-m depth intervals. These transforms were performed for all 104,880 stacked transients.

We produced horizontal images of subsurface conductivity for each survey area by (1) extracting modeled conductivity values at 10-m-depth intervals, (2) gridding values within the image-processing software ERMapper using a cell size of 20 m, (3) manually rescaling the color bar for each depth slice to match the apparent conductivity range, and (4) exporting the georeferenced images using the Universal Transverse Mercator (UTM) zone 14 north projection and the 1983 North American Datum.

Digital images were imported into a GIS database. Coverages being used to analyze the relationship between the geophysical data and geological and hydrological characteristics of the area include borings, water wells, water-quality analyses, aerial photographs, and roads (and associated power lines).

The aircraft also towed a cesium magnetometer at a height of 73 m above the ground (table 4) to measure changes in the magnetic field strength caused by natural effects and local features, such as pipelines, that contain significant amounts of iron. Magnetometer data were acquired at 10 Hz, yielding a 7-m sample spacing for magnetic field data.

Table 4. Acquisition parameters used for the Pantex airborne magnetometer survey conducted by Fugro Airborne Surveys, March 2003.

| | |
|---|---|
| Magnetometer | Towed cesium vapor (Scintrex Cs-2) |
| Magnetometer height | 73 m |
| Sample rate | 10 Hz |
| Sample interval | ~7 m |
| Sensitivity | 0.01 nT; 0.2 ppm |

## AIRBORNE GEOPHYSICAL SURVEY RESULTS

Fugro Airborne Surveys processed the airborne geophysical data and delivered digital survey products that included surface topography, magnetic field strength, and several types of TDEM data. Among the types of data relevant to the TDEM measurements were power-line noise, two types of secondary signal strength, apparent ground conductivity, and transforms of the TDEM signal to pseudo-conductivity profiles (conductivity-depth transforms, or CDTs) at each measurement point.

### Terrain, Magnetic Field Strength, and Power-Line Noise

Aircraft height above the ground is one of the important parameters used in determining the electrical properties of the ground in response to an airborne instrument. GPS instruments on the aircraft and at the base station allow accurate positioning of the aircraft during the survey, but the surface topography is typically not well known. Data from an onboard altimeter can be combined with GPS data on aircraft position to produce a terrain map of the ground surface (figure 17). This map shows obvious and subtle topographic features that include a general decrease in surface elevation from northwest to southeast and prominent topographic lows associated with each of the playas and surrounding basins. Surface elevation ranges from 1,057 to 1,098 m above sea level. Minor errors in aircraft position appear as linear lows or highs along the flight-line direction (figures 15 and 17).

Magnetic field data were not a principal objective but can be helpful in identifying pipelines, wells, and other significant structures that might affect the TDEM signal. Only the total magnetic field strength is measured by the towed magnetometer, but local magnetic anomalies can be enhanced by creating a residual magnetic anomaly map (figure 18) by calculating the difference between the measured field strength and the field strength predicted from a global database of magnetic field strength values (the International Geomagnetic Reference Field, or IGRF). In addition to the dominant, northwest-trending, U-shaped feature that reflects deeper geologic structure, many local anomalies are evident that coincide with known wells and structures. Two prominent linear features that trend north-northeast and east-

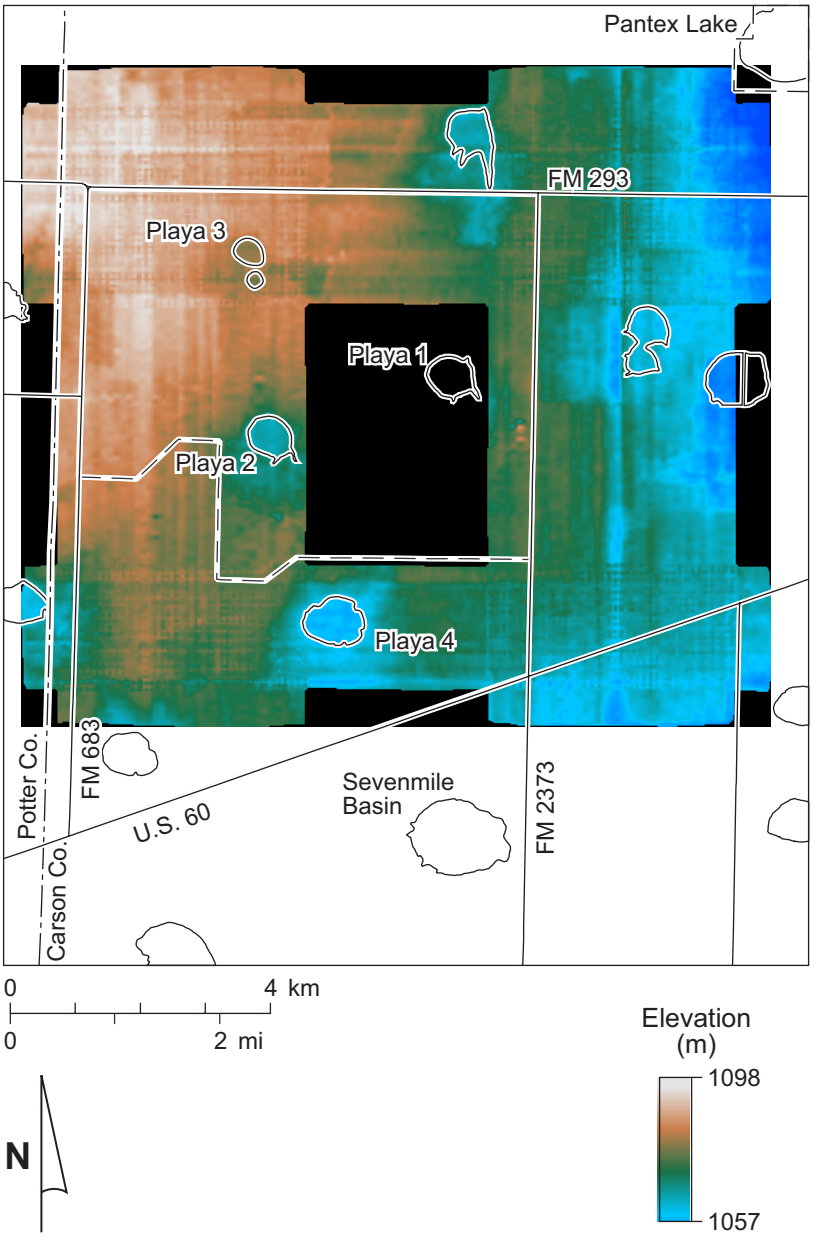


Figure 17. Terrain map of the Pantex Plant area derived from aircraft position and altimeter data.

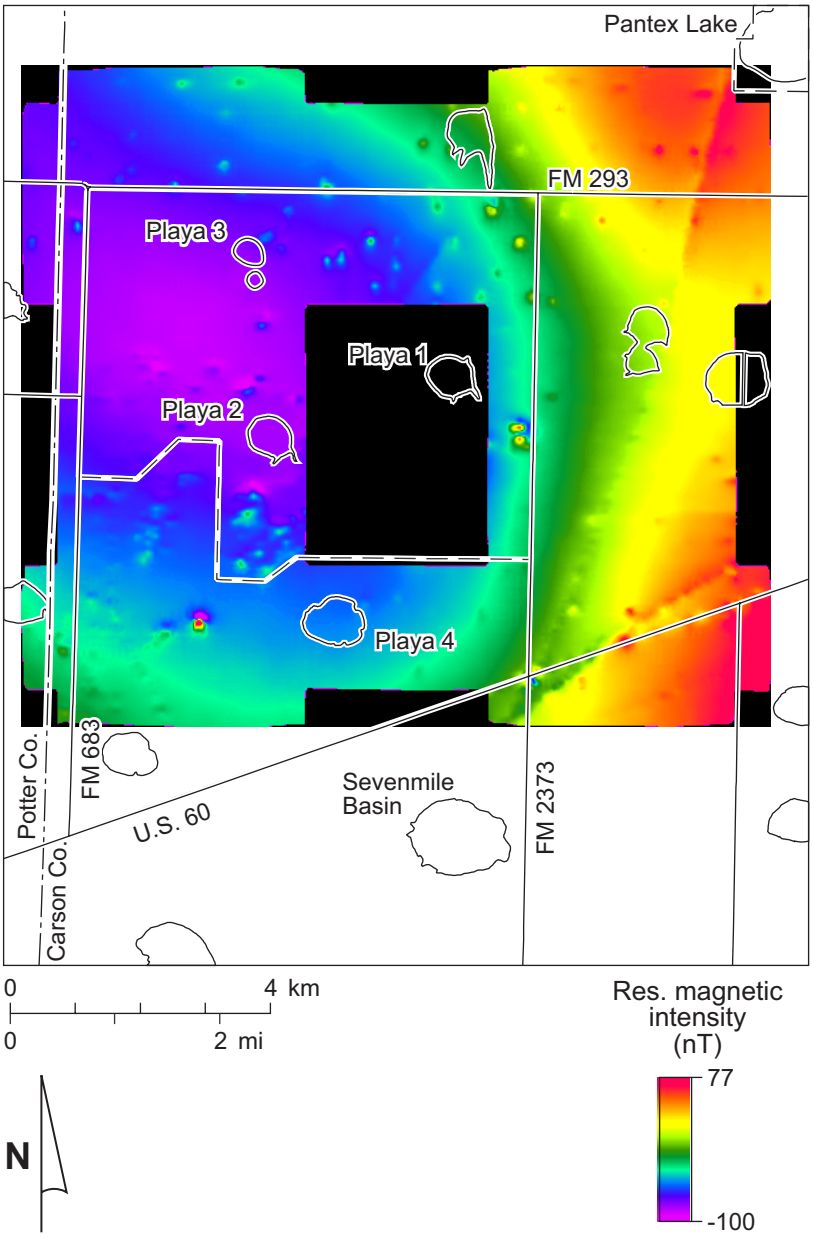


Figure 18. Residual magnetic field strength map of the Pantex Plant area. Positive values are areas where measured field strength is higher than reference field (IGRF) values; negative values are areas where measured field strength is lower than IGRF values.

northeast on the east side of the survey area are typical pipeline signatures. Total magnetic field strength ranged from 51,544 to 51,693 nanoteslas (nT) over the combined survey area.

Electric power lines carry alternating current that produces magnetic fields. These fields are strong enough to interfere with the relatively weak secondary electrical signals generated in the ground by the airborne TDEM transmitter. We used data from an onboard power-line noise monitor to create a map depicting noise levels across the survey area (figure 19) then used those values to identify excessively noise contaminated areas in the TDEM data set. Power-line noise varied greatly in strength across the area, ranging from values at or below 1 millivolt (mV) to as high as 500 mV. Highest values are observed on flight lines where the aircraft crosses major power lines. On these lines, the low-flying receiver passes closer to the power lines than it does when the flight lines are parallel to the same power lines. We used a threshold power-line noise value of 15 mV to remove excessively noisy data from the TDEM data set. Airborne TDEM soundings with power-line noise of less than 15 mV were used to generate images of apparent conductivity and conductivity-depth slices.

## TDEM Signal Strength and Noise Correlation

Calculations of apparent ground conductivity and changes in apparent conductivity with depth are based on the strength and decay of the TDEM signal recorded by the three-component receiver. The signals and mathematical manipulations of them are critical to the success of the TDEM method in assessing the extent and integrity of the FGZ. Fugro delivered processed TDEM data that included both the measured dB/dt signal (changes in the generated magnetic field strength over time) and its calculated integral, the B-field (magnetic field strength generated by the TDEM transmitter and ground response) (Smith and Annan, 2000). We examined these signals to evaluate the effects of power-line noise on the airborne TDEM data.

B-field data (figure 20) are presented in the magnetic field unit picotesla (pT, or 0.001 nT) for a single transmitter cycle. While the TDEM transmitter is on (on time, figure 20a), there are large changes in the signal magnitude and polarity, peaking at about 1000 pT (1 nT) just before the transmitter is

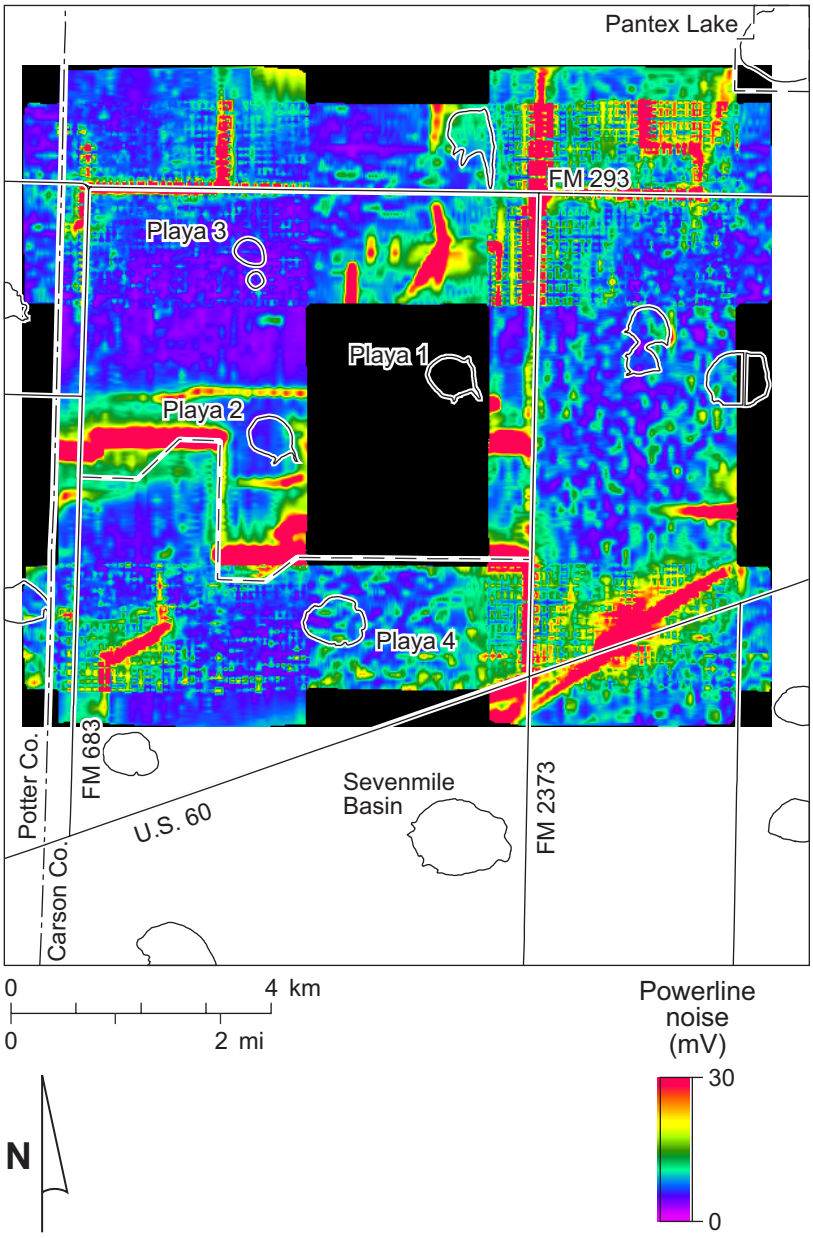


Figure 19. Power-line noise intensity map of the Pantex Plant area measured during the airborne geophysical survey.

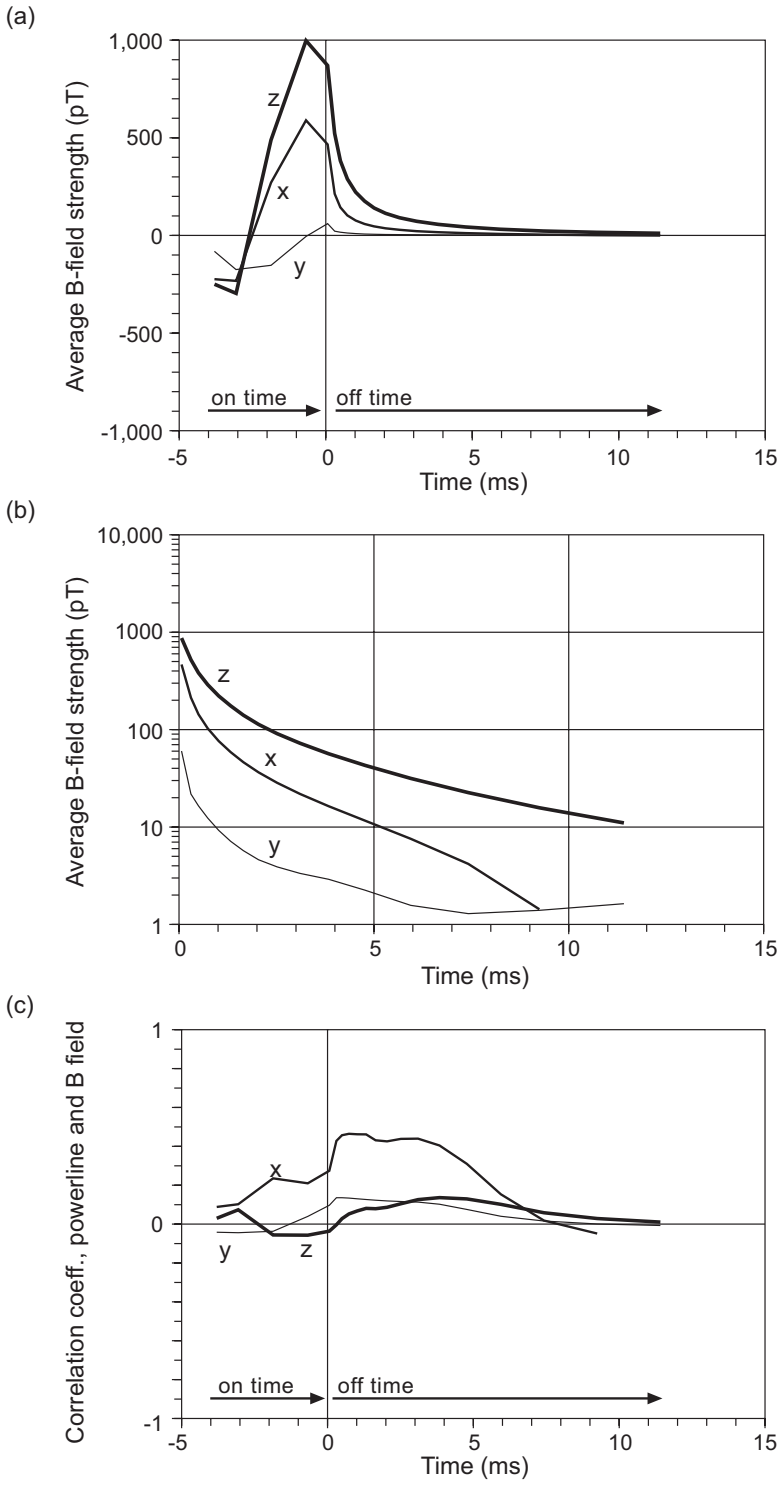


Figure 20. B-field signal strength and correlation with power-line noise. (a) B-field signal strength over one TDEM transmit and receive cycle in the *z* (vertical), *x* (inline), and *y* (transverse) directions, including both on time (TDEM transmitter on) and off time (transmitter off); (b) decay of secondary TDEM B-field signal during off time in the *z*, *x*, and *y* directions; and (c) correlation of B-field signal components with power-line noise during both on and off times.

turned off. Once the transmitter is turned off (off time, figure 20a), there is a rapid decay in the secondary signal generated by currents flowing in the ground (figure 20a, b). The strongest component is in the *z* direction (vertical), followed in strength by the *x* component (in the flight-line direction). The weakest signal is recorded in the *y* direction, transverse to the flight-line direction. Above horizontally stratified layers, the *y* component should be small because the transmitter generates the strongest signal in the *z* direction (the transmitter is a vertical dipole). A large *y* signal would suggest significant lateral changes in conductivity, which might invalidate processing assumptions that are made in determining apparent conductivity of the ground and its variation with depth. The *x* component should also be stronger than the *y* component because the receiver is recording an *x* signal by moving through a magnetic field as the aircraft acquires data.

We examined the influence of power-line noise on all components of the B-field signal by calculating a correlation coefficient between power-line noise and signal strength during both on and off times (figure 20c). The strongest correlation with noise is evident for the *x* component at relatively early off times, reaching nearly 0.5 at times of 0.5 to 1.5 ms after turnoff. Both *z* and *y* components correlate poorly with power-line noise. These data suggest that including *x*-axis data in conductivity calculations might increase the influence of unwanted noise.

The actual measured signal, dB/dt, is equivalent to the time derivative of the B-field signal and is given in units of nT/s (figure 21). While the transmitter is on, the dB/dt signal also shows polarity and large magnitude changes (figure 21a). Once the transmitter is off, the secondary signal arising from ground currents decays rapidly in all three components (figure 21a, b). The *z* component is again the strongest, decaying rapidly from initial values of more than 1,000 nT/s to final values above 1 nT/s. The *x*-component signal is significantly weaker than the *z* component but is an order of magnitude stronger than the transverse, or *y*, component. Both the *z* and *y* components are poorly correlated with power-line noise (figure 21c), but the *x* component shows a relatively high and positive correlation of about 0.5 with power-line noise, particularly at early off times.

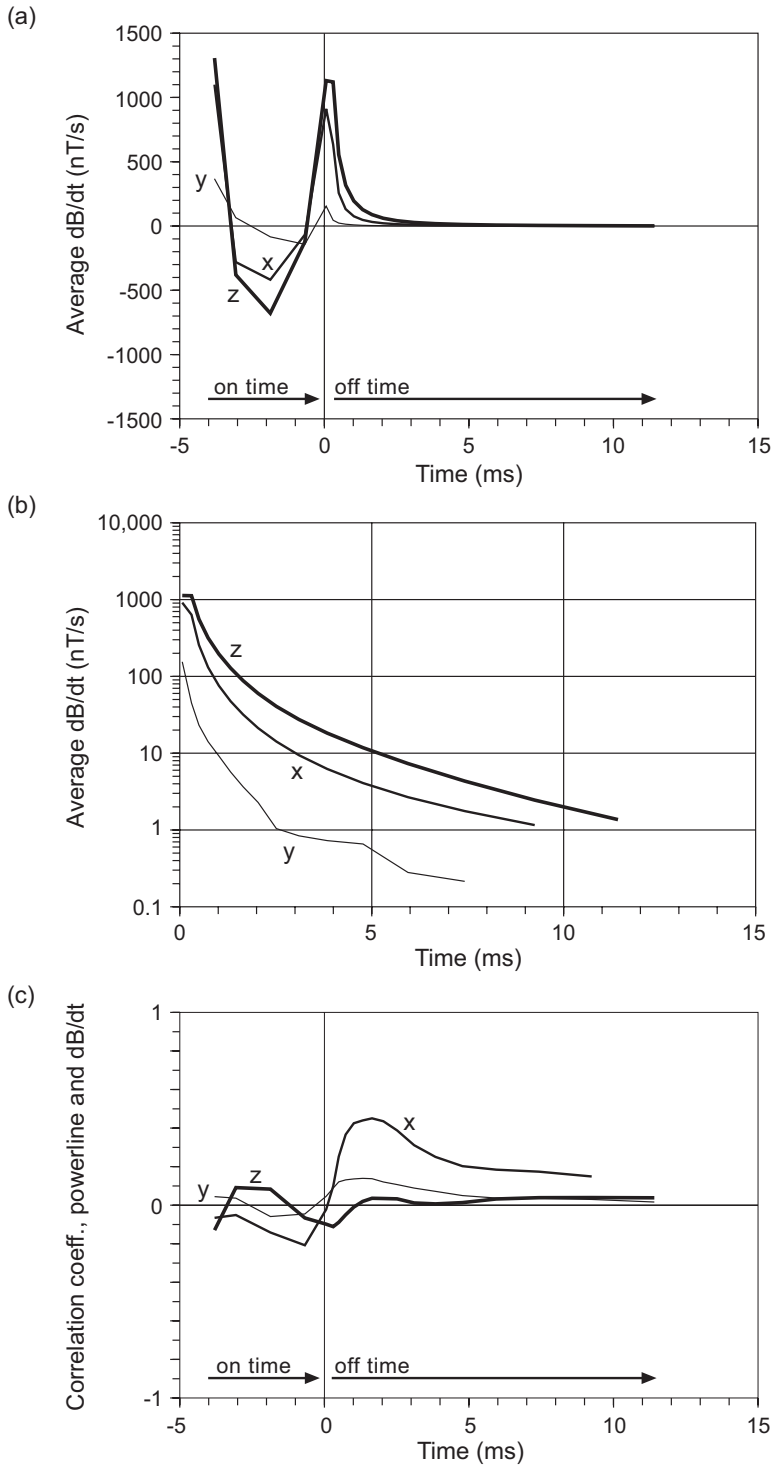


Figure 21. Time derivative (dB/dt) signal strength and correlation with power-line noise. (a) dB/dt signal strength over one TDEM transmit and receive cycle in the *z* (vertical), *x* (inline), and *y* (transverse) directions, including both on time (TDEM transmitter on) and off time (transmitter off); (b) decay of secondary TDEM dB/dt signal during off time in the *z*, *x*, and *y* directions; and (c) correlation of dB/dt field signal components with power-line noise during both on and off times.

## Apparent Ground Conductivity

Rather than produce maps depicting TDEM signal strength at various times during signal decay, the TDEM signals can be processed to generate apparent conductivity models of the ground that would produce the observed signal decay. The simplest of these is a single value of apparent conductivity that best fits the observed decay at a sounding location, assuming that the ground beneath the instrument is electrically homogeneous. This image (figure 22), with noisy soundings removed, can be used to observe general trends. Calculated apparent conductivities for the combined survey blocks range from 38 to 102 mS/m. Relatively high values are present at each of the on- and off-plant playas, over a large area north of FM 293 (both west and east of the Pratt playa) and within areas extending east and southeast of the Pantex Plant. Relatively conductive areas such as these suggest higher clay and water content within the exploration depth of the instrument.

## Conductivity-Depth Transforms (CDTs)

Single apparent conductivity values for each sounding location are useful for establishing basic electrical properties of an area and identifying major trends but are an oversimplification of the ground's electrical properties at Pantex, which are known to vary significantly as sediment type and water saturation change with depth (figure 9). During TDEM processing, Fugro also produced "transforms" depicting changes in apparent conductivity with depth (CDTs) at each sounding location. These are not full, robust inversions of the TDEM data (Wolfgram and Karlik, 1995) but do produce pseudo-depth profiles from z- and x-axis data that reflect changes in signal strength with time.

### CDT Correlation with Noise

We have shown that power-line noise has a small positive correlation with the *x*-axis signal that is also used in the depth transforms (figure 21c). Power-line noise might also influence depth transforms. We examined this possible influence by calculating the average correlation coefficient between calcu-

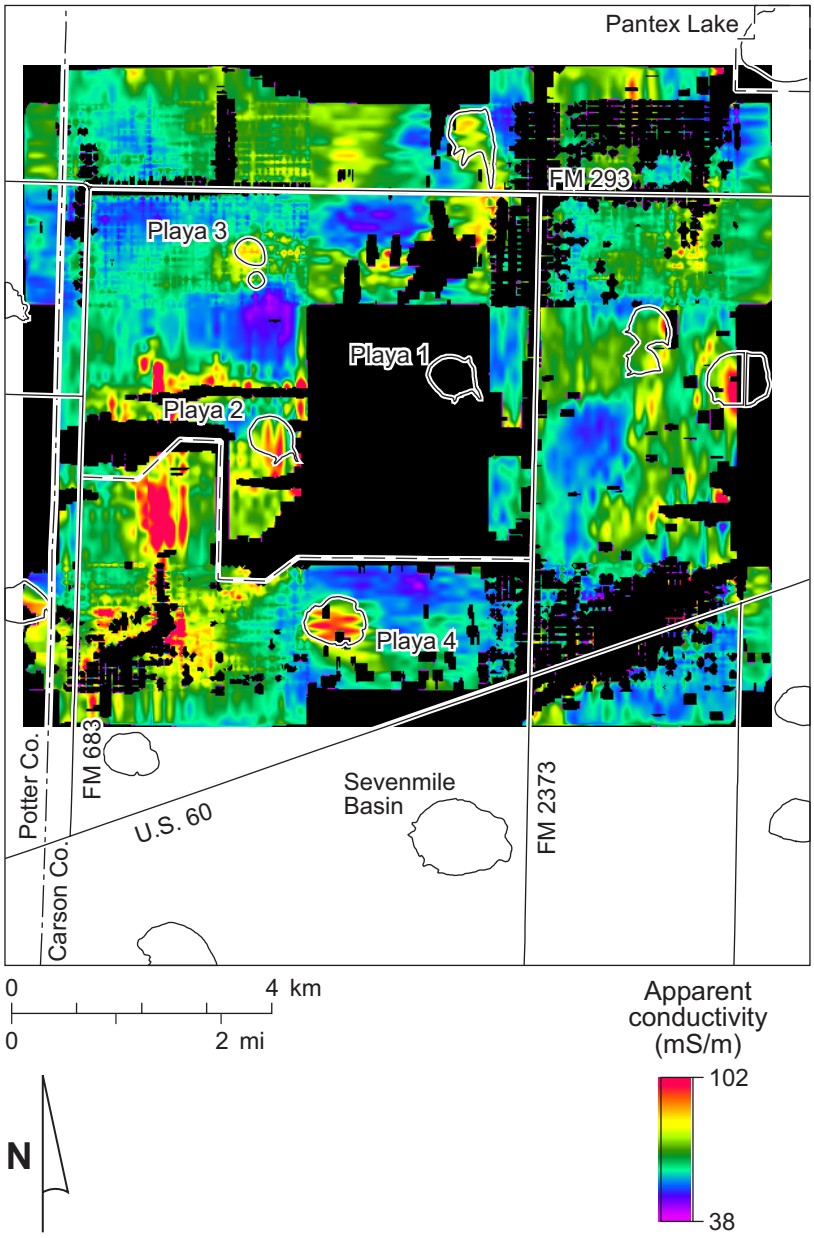


Figure 22. Apparent conductivity map of the Pantex Plant area with data from noisy areas removed.

lated apparent conductivity at 10-m depth intervals between 10 and 290 m for each of the four survey blocks (figure 23). There is a small, positive correlation between power-line noise and conductivity at shallow depths that corresponds to the small, positive correlation observed at early times in the *x*-axis data. This correlation was determined using all airborne TDEM data and served as the rationale for deleting locations with large power-line noise values from apparent conductivity maps and depth slices.

## CDT Comparison with Ground TDEM Models

Preliminary modeling and field measurements using ground-based instruments produced models of apparent conductivity changes with depth at several locations (figure 15) that can be compared with CDT profiles calculated from airborne data acquired at the same location. Using the series of ground measurements along the southeast boundary of the Pantex Plant as an example (TDEM 1, 6, 5, 7, and 10 from south to north), we extracted all airborne sounding locations within 50 m of the ground-based sounding and plotted the apparent conductivity profiles on the same depth and conductivity scale (figure 24). The ground-based profiles consist of two to four discrete conductivity layers that were shown to be influenced by changes in thickness of the FGZ and perched aquifer but could not resolve the FGZ (Paine, 2000). The CDTs derived from airborne data are only generally similar to depth profiles obtained from ground-based data but may more accurately represent smoother conductivity changes with depth that are apparent from borehole logs.

Plots of CDT profiles near ground-based soundings also help determine the exploration depth achieved by the airborne instruments. In most areas, CDTs derived from locations within a few tens of meters of each other should depict similar profiles, given the large sampling footprint of the airborne system. CDTs from locations near TDEM 1 have similar apparent conductivity values at all depths (figure 24a), as do those from locations near TDEM 10 (figure 24e). Profiles near TDEM 6 diverge at depths greater than 180 m (figure 24c), suggesting that apparent conductivity data deeper than 180 m at this location are unreliable. CDTs near TDEM 5 begin to diverge below 100 m, becoming strongly divergent below 250 m depth (figure 24b). CDTs near TDEM 7 show increasing divergence at depths

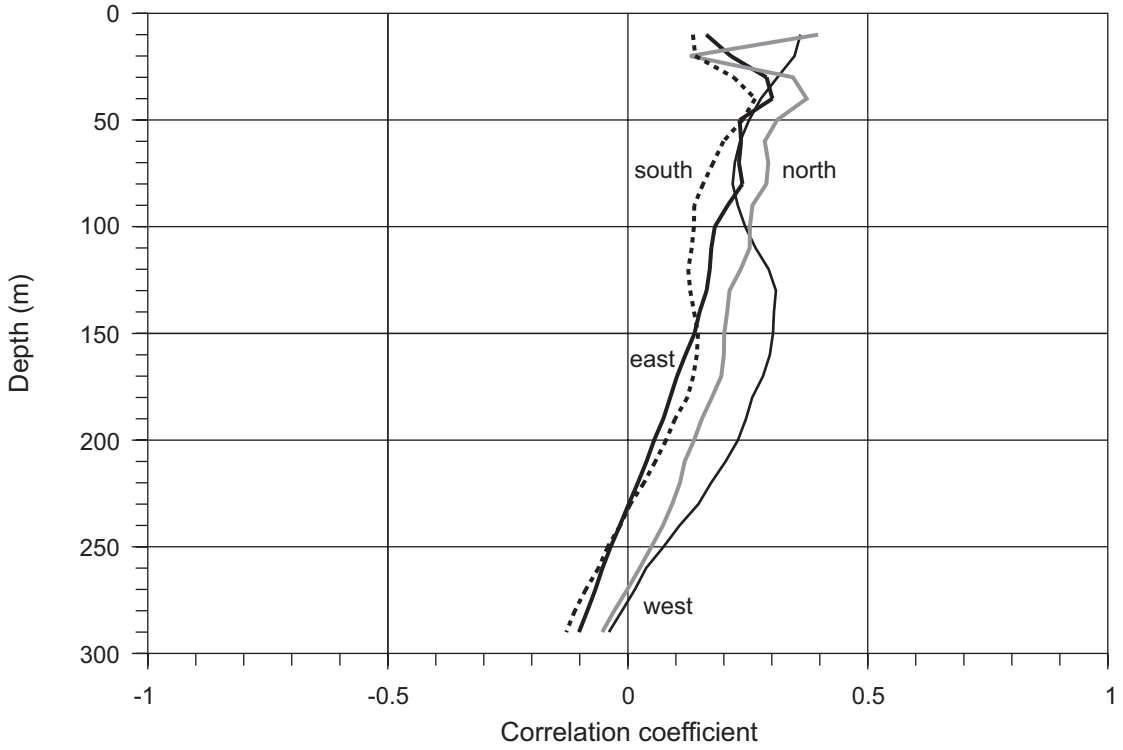


Figure 23. Correlation coefficient between power-line noise and calculated apparent conductivity at specific depths in the north, east, south, and west airborne geophysical survey blocks.

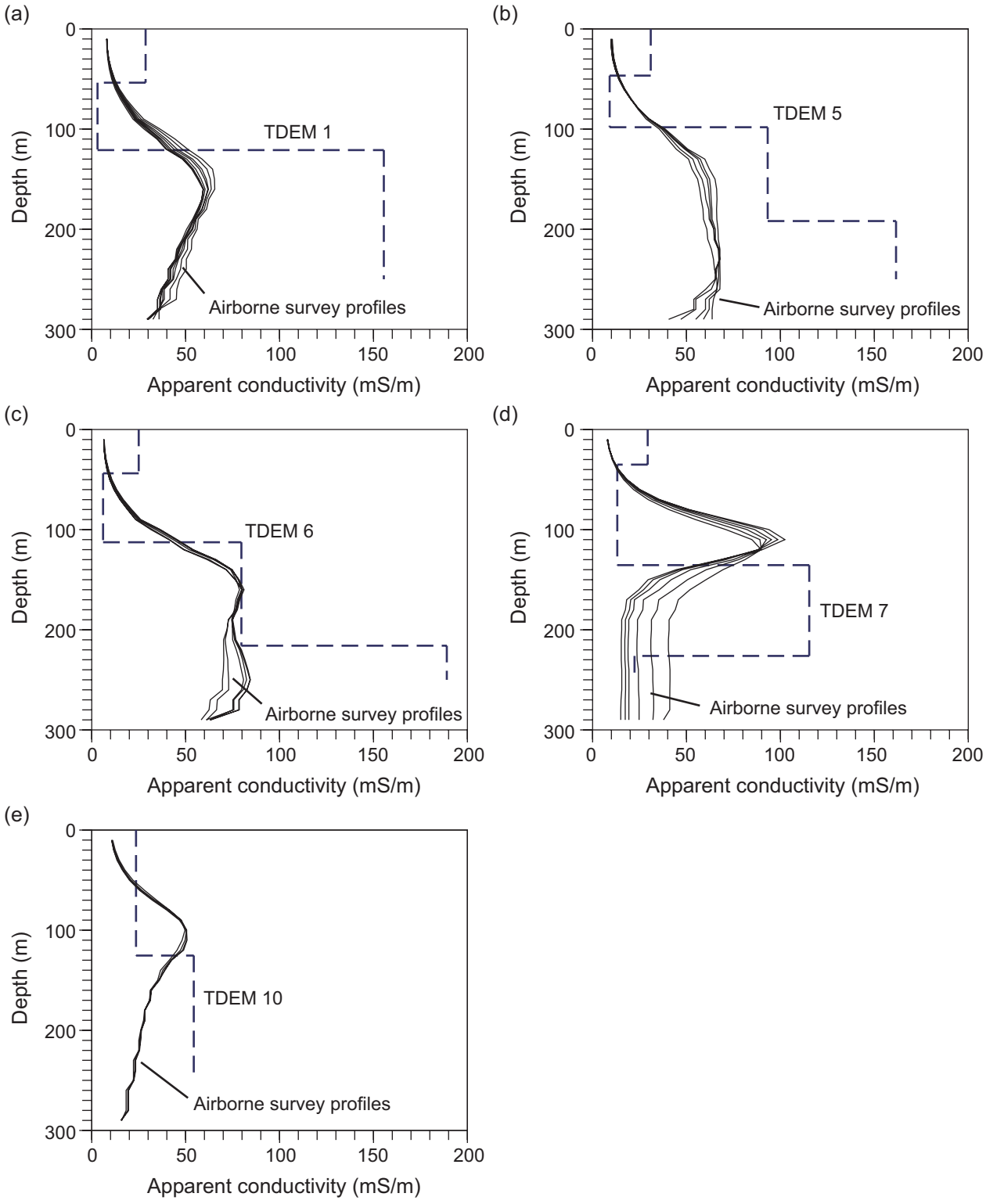


Figure 24. Comparisons between apparent conductivity profiles derived from airborne and ground-based TDEM instruments in the Pantex Southeast area at (a) TDEM 1, (b) TDEM 5, (c) TDEM 6, (d) TDEM 7, and (e) TDEM 10. Locations shown on figure 15. Airborne profiles are those from all sites within 50 m of the location of the ground-based sounding.

greater than 140 m. Possible reasons for divergence include differing transmitter and receiver geometries, power-line noise, and signal strength.

## CDT Correlation with Perched Aquifer and FGZ Thickness

Modeling and ground-based measurements indicated that the TDEM signal could respond to changes in thickness of the FGZ and perched aquifer if other stratigraphic and hydrologic change is minimal. We examined the relationship among these parameters and CDTs derived from airborne data by identifying boreholes with reported perched or FGZ thicknesses within the airborne survey area (appendix A), extracting the CDTs nearest those boreholes, and calculating correlations between thicknesses and apparent conductivities at various depths.

The saturated thickness of the perched aquifer is well known where it is penetrated by boreholes (table 1, appendix A). Within the airborne survey blocks, there are 194 well-CDT "pairs" associating a known perched aquifer saturated thickness with apparent conductivities from nearby CDTs. Of these pairs, 120 have nonzero saturated thickness. One way to examine whether the saturated thickness influences the airborne EM data is to calculate the correlation coefficient between apparent conductivity and measured saturated thickness for these data pairs (figure 25). Because cultural noise degrades the CDTs at Pantex, we also examined how the correlation changes with differing noise thresholds (figure 25). There are too few pairs remaining at the lowest noise levels (less than 5 mV) to produce a meaningful relationship. At a slightly higher noise level (less than 9 mV), there are 38 data pairs that show a reasonably strong positive correlation at depths of 80 to 130 m, peaking at 110 m. The relatively broad depth ranges for this positive correlation most likely reflects variable depths to the perched aquifer and changes in saturated thickness. The positive correlation is similar to that observed between perched saturated thickness and ground-based TDEM measurements in the Pantex Southeast area (figure 13), suggesting that (1) saturated thickness of the perched aquifer is a primary influence on airborne EM data and (2) increases in apparent conductivity at appropriate depths correlate with increases in perched aquifer saturated thickness (figure 26). The extended depth range may also imply

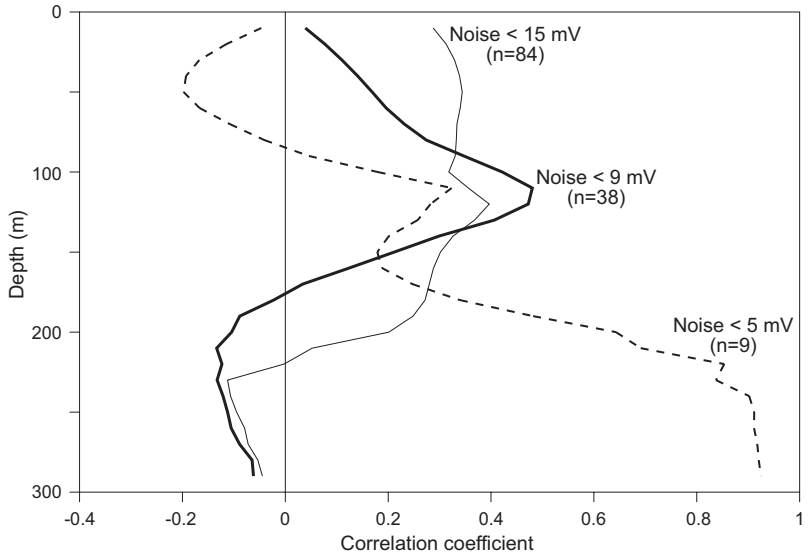


Figure 25. Correlation between reported saturated thickness of the perched aquifer and apparent conductivity at 10-m depth intervals on CDT profiles having noise levels below 5, 9, and 15 mV.

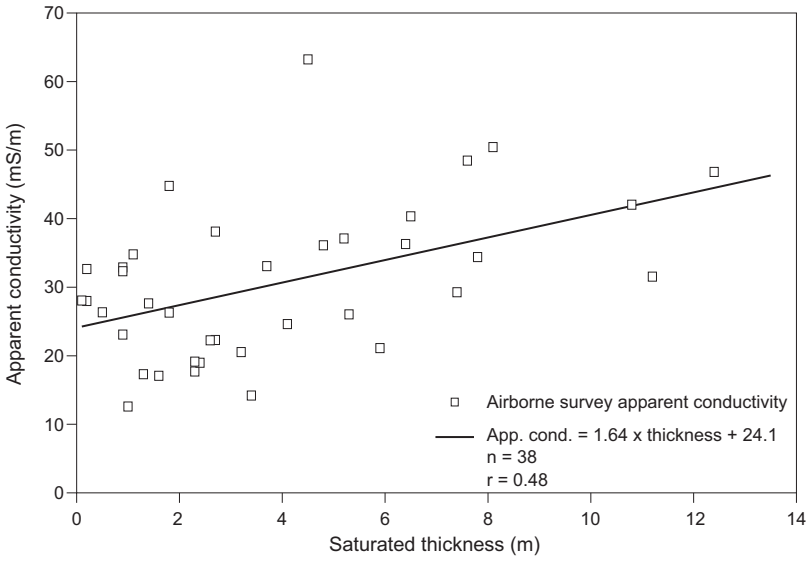


Figure 26. Relationship between reported saturated thickness of the perched aquifer and apparent conductivity at 110-m depth from airborne survey data with noise levels below 9 mV. Well data from BWXT Pantex.

that where the perched saturated zone thickens, the moisture content in the underlying FGZ increases. Where there is no perched aquifer, the FGZ may remain relatively dry and poorly conductive.

Depth to the base of the perched aquifer, defined as the top of the FGZ, is also well known from many boreholes (table 1, appendix A), but the thickness of the FGZ is much less certain. Many boreholes extend no deeper than the top of the FGZ; those few that do penetrate the FGZ may not penetrate it completely. Further, most estimates of FGZ thickness rely on subjective drillers' descriptions of strata encountered while drilling deeper wells, rather than on rigorous geological descriptions or borehole geophysical logs. Nevertheless, there are 85 well-CDT pairs that can be used to associate a reported FGZ thickness with apparent conductivity. There is no obvious positive correlation between reported FGZ thickness and apparent conductivity at any depth or noise threshold (figure 27). At low noise levels (below 9 mV), there is a tendency toward a negative correlation peaking at 120- to 130-m depth, suggesting that apparent conductivity at these depths decreases with increasing FGZ thickness (figure 28). While recognizing that FGZ thickness reported for boreholes is relatively uncertain, we are unable to document a rigorous relationship between apparent conductivity measured during the airborne survey and reported FGZ thickness. As noted for the relationship between apparent conductivity and saturated thickness, it may be that we can detect an effect related to FGZ thickness where the perched aquifer exists and increases the moisture content (and conductivity) of the underlying FGZ.

## Apparent Conductivity-Depth Slices from CDTs

Once excessively noisy data have been removed from the airborne TDEM data set, the remaining CDTs can be combined to form a pseudo-three-dimensional apparent conductivity model for the survey area that consists of individual apparent conductivity values at 10-m depth intervals at each CDT location. Although the vertical resolution of TDEM data is limited, the abundance and close spacing of measurements acquired during the airborne survey allow the conductivity volume to be sliced horizontally to produce images depicting apparent conductivity variations across the survey area at specific depths. These values are unlikely to be the true electrical conductivity of the ground at a particular

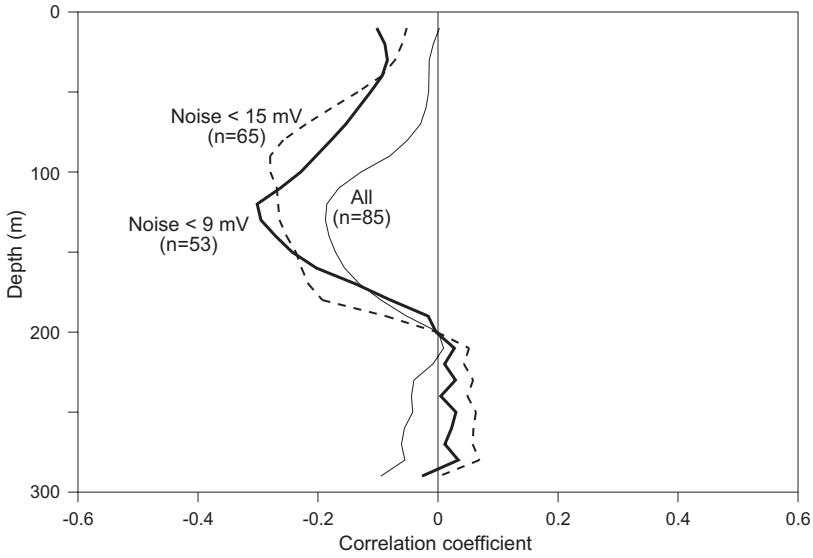


Figure 27. Correlation between reported FGZ thickness and apparent conductivity at 10-m depth intervals on CDT profiles having noise levels below 9 and 15 mV.

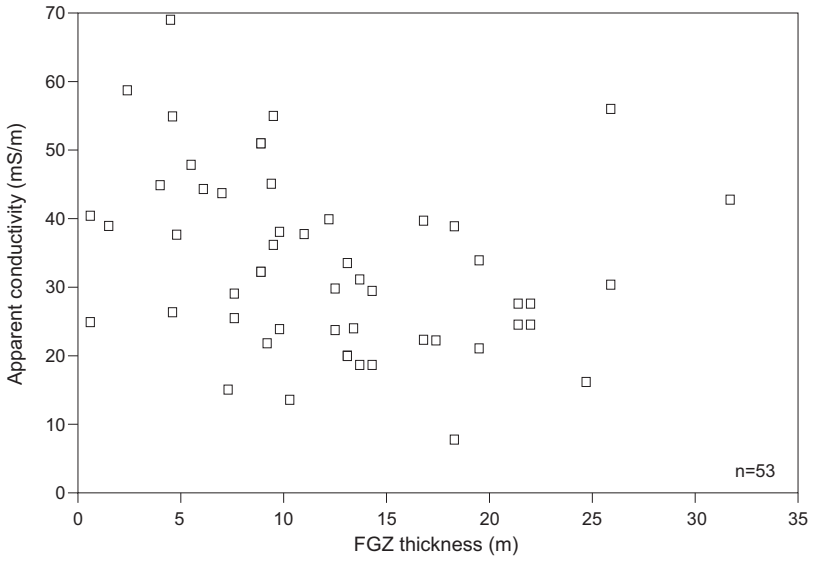


Figure 28. Relationship between reported Ogallala FGZ thickness and apparent conductivity at 120-m depth from airborne survey data with noise levels below 9 mV. Well data from BWXT Pantex.

location and depth; rather, they depict relative and semiquantitative values that should be consistent with surrounding values at the same depths. These images can be helpful in identifying geologic and hydrologic features associated with conductivity changes related to differing clay and water content. Features of special interest in the Pantex Plant area include the unsaturated zone above the perched aquifer, the FGZ and perched aquifer, the unsaturated zone between the FGZ and the main Ogallala aquifer, the Ogallala aquifer, the base of the Ogallala Formation, and playas as preferential Ogallala recharge features.

We combined CDT profiles from the four survey blocks after deleting profiles with power-line noise above the 15-mV threshold. We produced pseudo-depth slices at 10-m intervals between 10- and 200-m depth (appendix C) that show relative apparent conductivity changes across the survey area. Areas where power-line noise is high or where no data were acquired are shown in black.

### Blackwater Draw and Upper Ogallala Formations

Water migrating from the ground surface to the perched or main Ogallala aquifers must pass through tens of meters of soil and sediment forming the Blackwater Draw and upper Ogallala Formations. Conductivity-depth slices between 10 and 70 m (figures C1 to C7) are all above the average depth to the perched water at about 80 m (table 1). We chose the 20- and 40-m depth slices (figures 29 and 30) to illustrate shallow apparent conductivity patterns reflecting variations in water content and sediment texture that influence infiltration.

Superimposed on the 20-m depth slice are reported depths to the Ogallala caprock caliche (figure 29), the formal boundary between the Blackwater Draw and Ogallala Formations. The 20-m slice is at or above this level, showing apparent conductivity patterns in the lower Blackwater Draw. The 40-m slice (figure 30) depicts apparent conductivity in the uppermost Ogallala Formation.

Elevated apparent conductivity is found at both depths surrounding all surveyed playas, including Playa 3 (area G, figures 29 and 30), Playa 2 (area I), Playa 4 (area J), Pratt playa (area B), and two unnamed playas east of the plant (areas C and D). Playa 1 was not surveyed owing to flight restrictions,

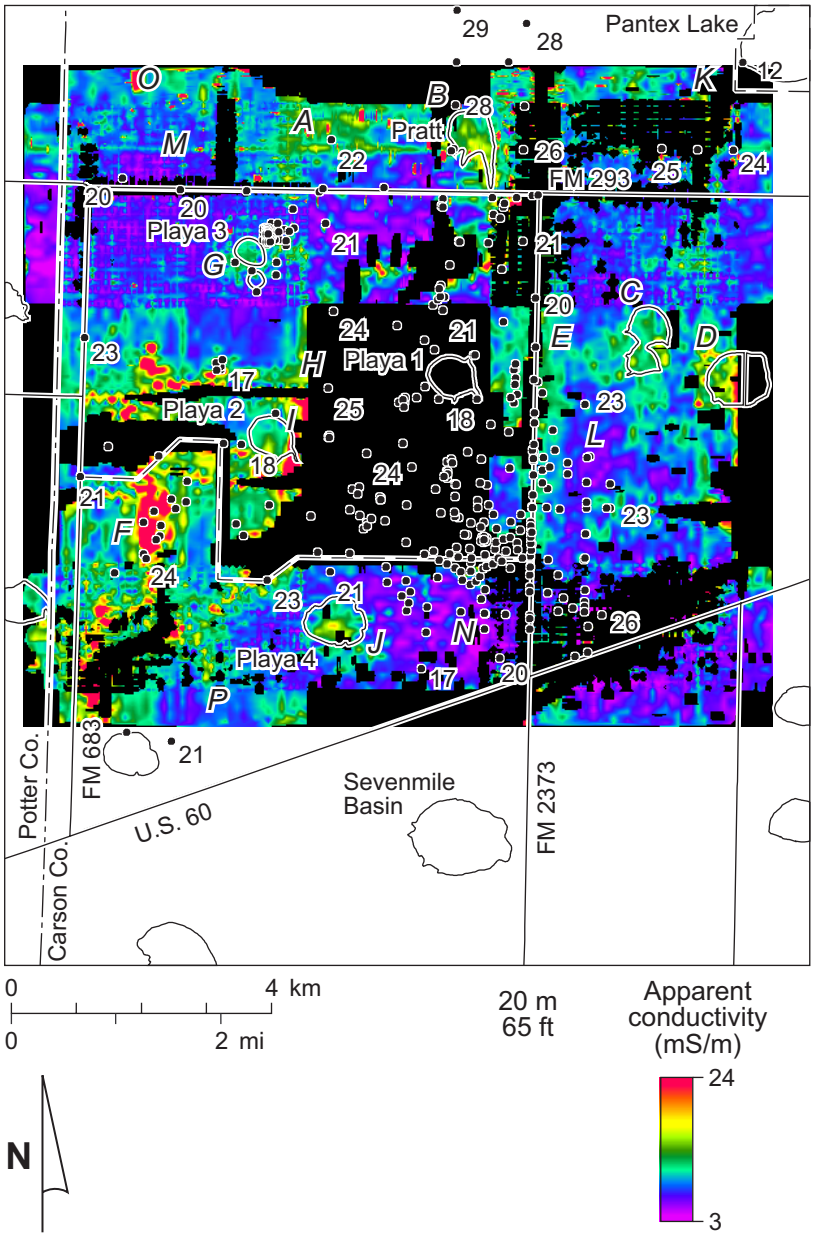


Figure 29. Apparent conductivity at 20-m depth and reported depths to the Ogallala caprock caliche. Well data from BWXT Pantex.

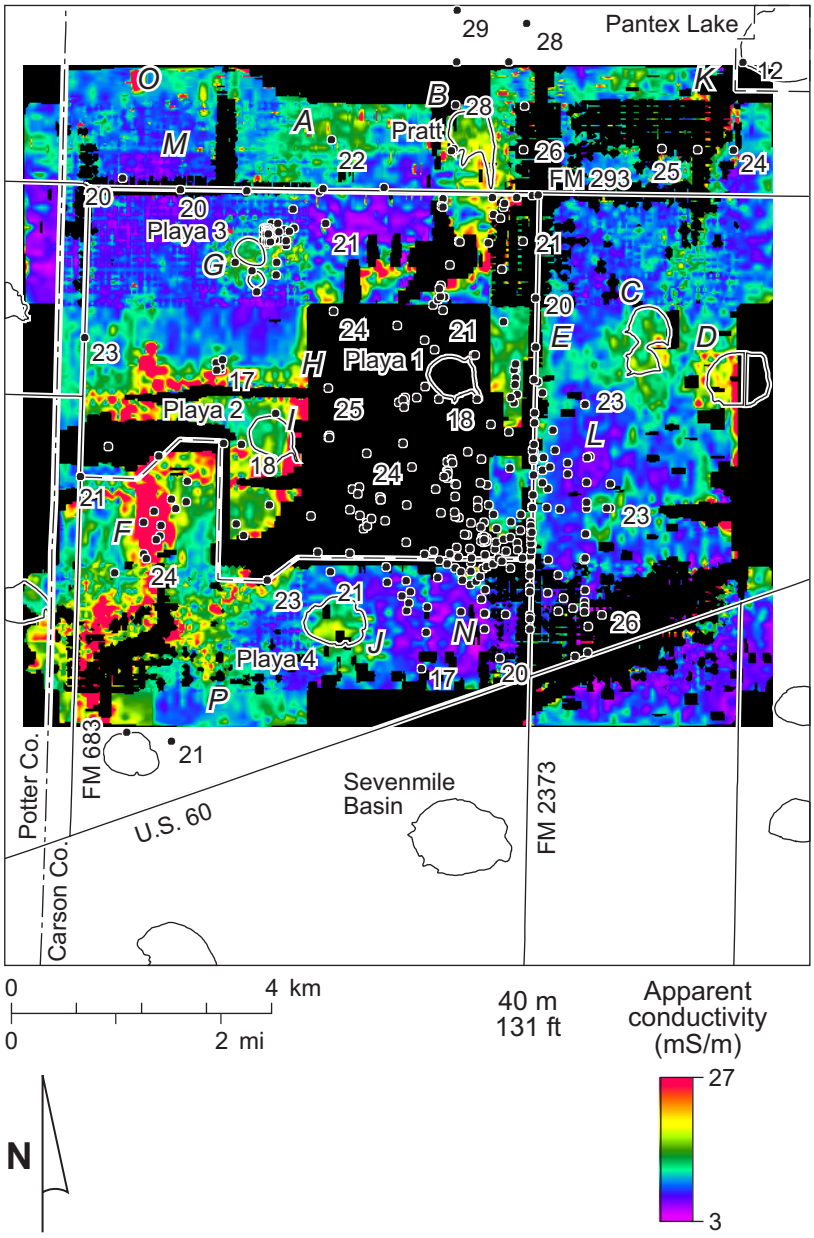


Figure 30. Apparent conductivity at 40-m depth and reported depths to the Ogallala caprock caliche. Well data from BWXT Pantex.

but elevated conductivities are found east of it (area E). Elevated conductivities at and near the playas are most likely related to elevated clay and water content in near-surface strata relative to surrounding interplaya strata at equivalent depths. This situation is consistent with a model of playas as significant groundwater recharge points.

Elevated apparent conductivities are also found outside playas, including area A north of FM 293 and area F southwest of the plant. World War II-era infrastructure and an abandoned hide-tanning facility are the likely cause of elevated shallow conductivities in area F. Area A coincides with the headward margin of a topographic low that deepens to the northeast beyond the survey area, suggesting that higher conductivities here reflect higher moisture and clay content consistent with the topographic setting.

### Middle Ogallala Perched Aquifer and FGZ

The principal objective of the airborne geophysical survey was to assess the extent of the middle Ogallala perched aquifer and the integrity of the underlying FGZ. Average depth to the perched aquifer is 80 m and its thickness averages about 5 m (table 1). Average depth to the FGZ is about 84 m and its average reported thickness is 14 m. The combined thickness of the FGZ and perched aquifer averages 17 m in the few boreholes where both are reported. Conductivity-depth slices that are relevant to the perched aquifer extent and thickness are those between 80 and 120 m (figures C8 to C12). We illustrate surveywide conductivity relationships by superimposing borehole data on selected depth slices at 80 and 100 m.

The 80-m depth slice (figure 31) depicts apparent conductivity at a depth at or near the top of the saturated zone or the base of the unsaturated zone above the perched aquifer where it is present. Many playas remain associated with broad areas of elevated apparent conductivity at this depth, including Playa 3 (area G, figure 31), Playa 4 (area J), two unnamed playas east of FM 2373 (areas C and D), and part of Pratt playa (area B). Unsurveyed Playa 1 is rimmed by elevated conductivities to the southeast, east, and northeast (area E). The survey did not include Pantex Lake, but an area of elevated

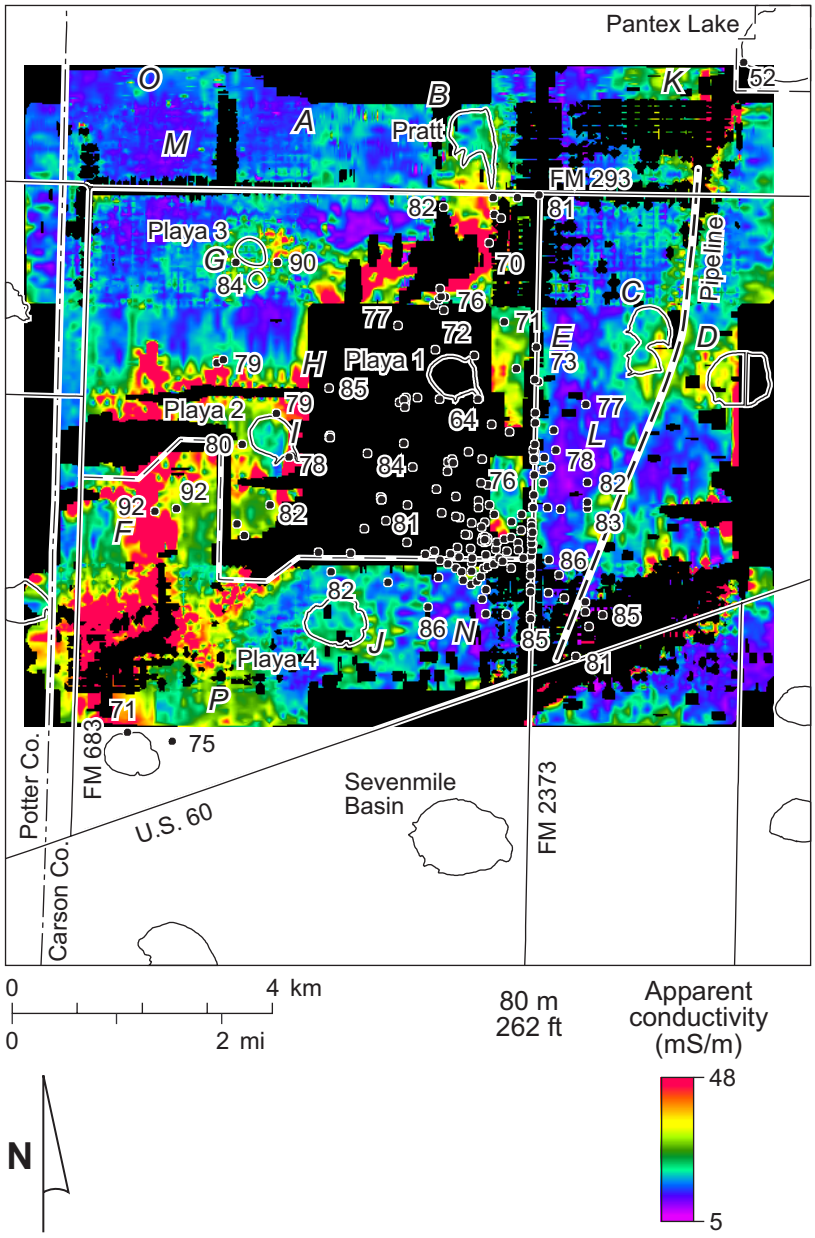


Figure 31. Apparent conductivity at 80-m depth and reported depths to the perched aquifer. Well data from BWXT Pantex.

conductivity rims that playa as well (area K). Elevated conductivity associated with each of these features is consistent with the presence of strata with higher water content, and perhaps higher clay content, than is present in surrounding strata at the same depth. Elevated conductivity extending 1 km or more from the margins of Playa 1 is consistent with the presence of a perched aquifer mound associated with that playa, as well as the relatively shallow depths (less than 76 m) to the perched water table near the playa.

Despite the attempt to remove CDTs contaminated with cultural noise, artifacts of that noise are prominent in the data set. Notable are a curvilinear apparent conductivity high that corresponds to a cathodically protected pipeline that trends northeast across the eastern part of the survey area and extremely high apparent conductivities associated with infrastructure west and southwest (area F) and north of the plant (area H).

We chose the 100-m depth slice to compare with recent BWXT Pantex models of perched aquifer extent and saturated thickness on the basis of borehole data (figure 32) because that depth both is near the known depth of the perched aquifer and shows relatively high correlation between apparent conductivity and saturated thickness (figure 25). The thickest parts of the perched aquifer, such as that near Playa 1, are mostly within unsurveyed areas, but significant saturated thicknesses have been reported within the surveyed area near Playa 2, at the northeast corner of the plant, and in the Pantex Southeast area.

In general, the modeled extent of the perched aquifer encloses areas with elevated apparent conductivity that are not associated with cultural contamination (figure 32). Further, in most areas where the saturated zone is relatively thick, apparent conductivities are relatively high, supporting the statistical correlation noted between perched saturated thickness and apparent conductivity at depths of 80 to 130 m. In some areas, the modeled extent of the perched aquifer matches apparent conductivity trends (such as area E east of Playa 1). In other areas, such as where the perched aquifer thins as it extends eastward across FM 2373, the aquifer appears to extend beyond the zone of elevated apparent conductivity associated with thicker parts of the perched aquifer.

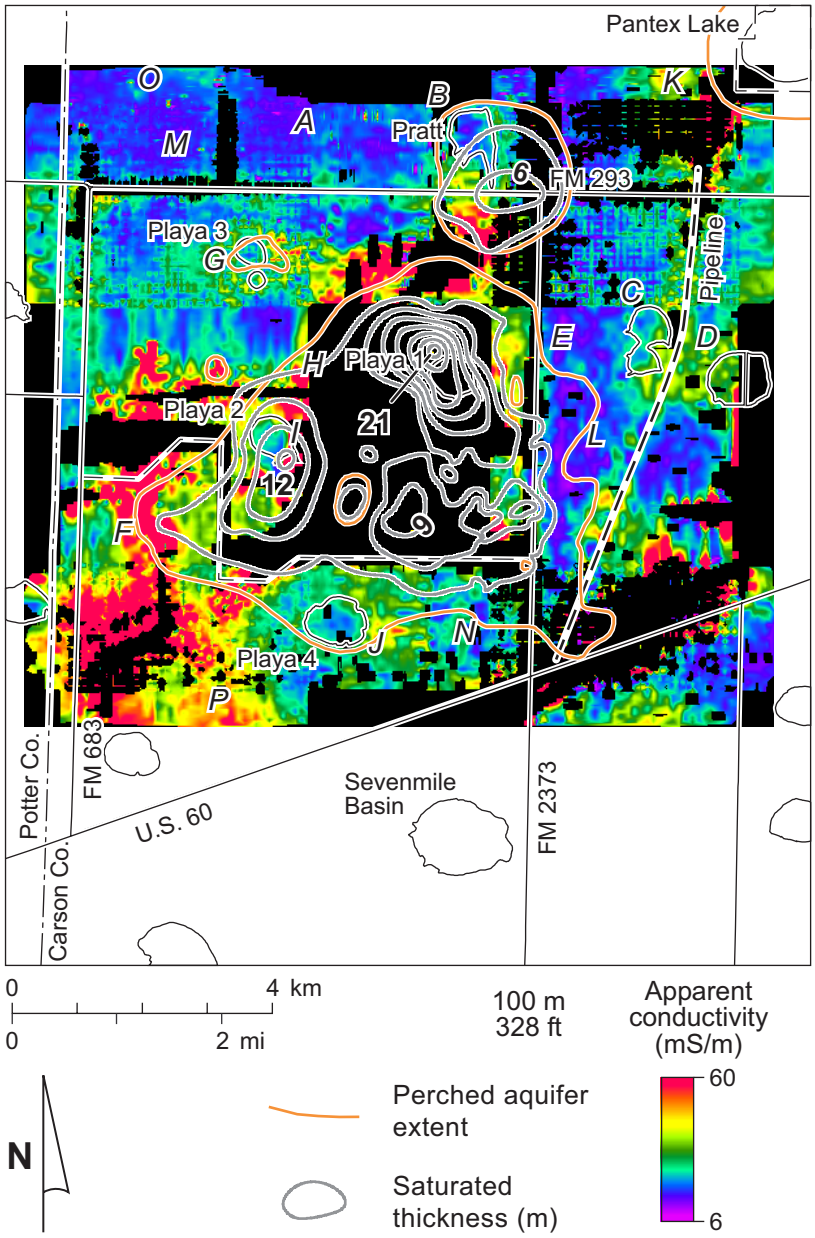


Figure 32. Apparent conductivity at 100-m depth and modeled extent and thickness of the perched aquifer. Perched aquifer data from BWXT Pantex.

Unlike at shallower depths, most playas coincide with low apparent conductivity (compare figures 29 and 32). Low apparent conductivity relative to surrounding environments is found at Playa 3 (area G), Pratt playa (area B), an unnamed playa east of FM 2373 (area C), Playa 4 (area J), and Playa 2 (area I). These local lows may be caused by real decreases in apparent conductivity at depth beneath the playas, possibly as a result of decreased clay content or water saturation, or they might be processing artifacts related to underestimating apparent conductivity beneath shallow conductive layers (Hunter and Macnae, 2001), such as those observed at survey-area playas.

We were unable to demonstrate a statistical relationship between reported FGZ thickness and apparent conductivity (figures 27 and 28). Apparent conductivity at 100 m bears little relationship to reported FGZ thickness (figure 33) perhaps because no relationship exists between FGZ thickness and apparent conductivity or FGZ thickness values are inaccurate or inconsistent. Reported FGZ thicknesses can vary greatly in boreholes that are near each other, suggesting inconsistent lithologic data or interpretation. Rather than exclude the possibility that EM data respond to changes in FGZ thickness, we can assume that if there is a relationship, we expect apparent conductivity to increase with increasing FGZ thickness and clay content. Areas with relatively low apparent conductivity are more likely to represent FGZ deposits that are relatively thin, dry, and less clayey. Relatively conductive areas are more likely to represent FGZ deposits that are relatively thick, wet, or more clayey. Thin, dry, or silty FGZ deposits are more likely within broad, low-conductivity areas east of FM 2373 (area L, figure 33), south of the Pantex Plant (area N), and northwest of the plant (area M).

### Main Ogallala Aquifer and Bedrock

Average depth to the main Ogallala saturated zone is 136 m in the survey area (table 1) but increases from near 100 m south of the plant to near 150 m north of the plant (figure 34). Conductivity slices at depths of 140 to 200 m (figures C14 to C20) image strata that include the Ogallala saturated zone and, in some areas, older Permian or Triassic bedrock. We chose depth slices at 140 m to repre-

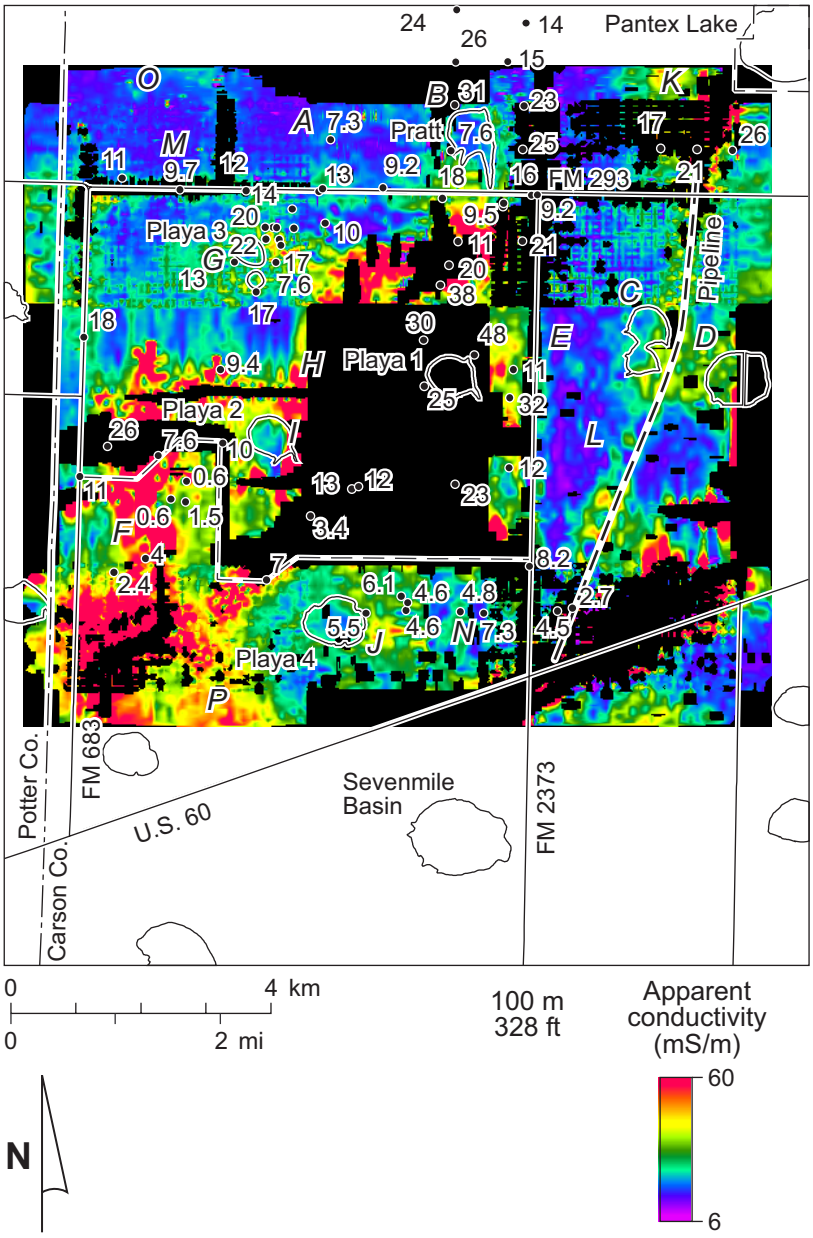


Figure 33. Apparent conductivity at 100-m depth and reported FGZ thickness. Well data from BWXT Pantex.

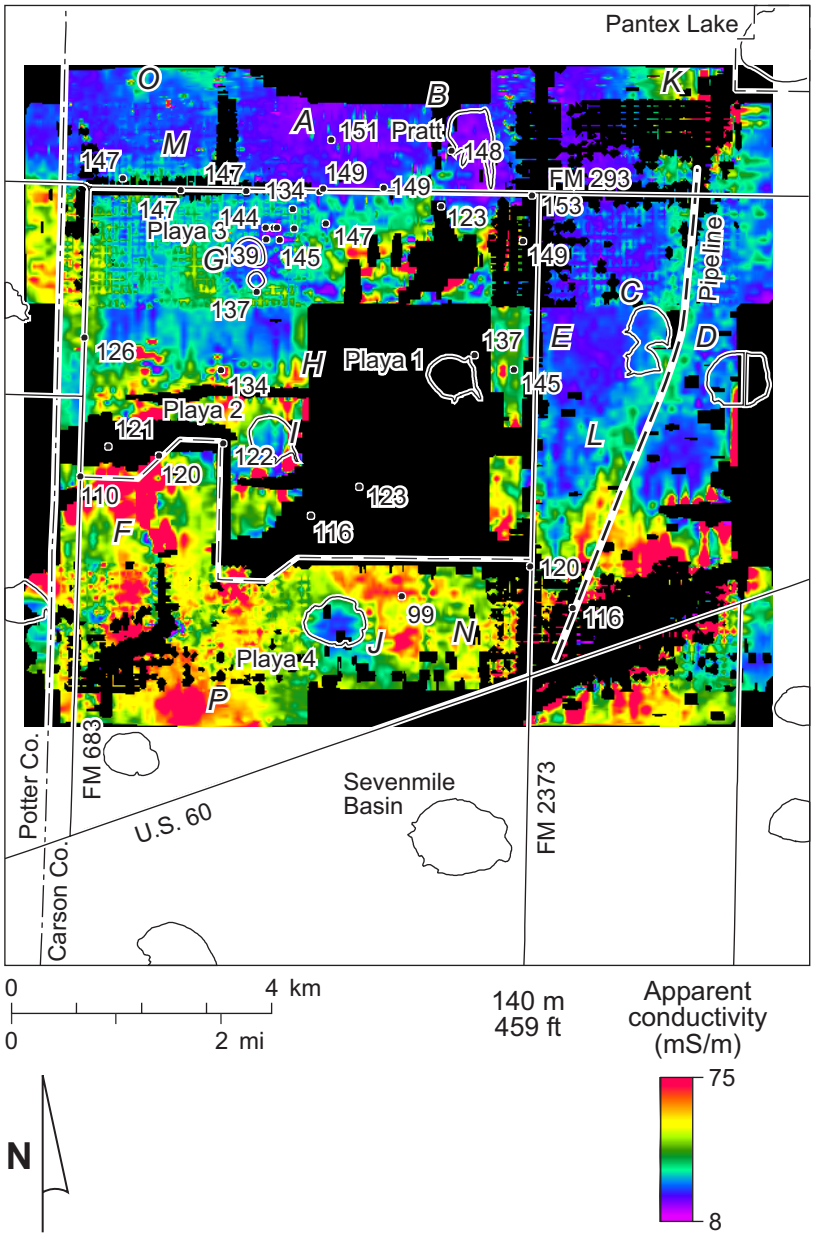


Figure 34. Apparent conductivity at 140-m depth and reported depths to the Ogallala water table. Well data from BWXT Pantex.

sent the top of the saturated zone and at 200 m to depict the deeper part of the Ogallala Formation and underlying bedrock.

The 140-m depth slice depicts high apparent conductivity in the southern part of the survey area and lower apparent conductivity in the northern part (figure 34). To the north, the low conductivities reflect dominantly coarse Ogallala sediments at or near the water table. To the south, elevated conductivities probably delineate areas where the Ogallala thins and more conductive bedrock is being sensed. Notable conductivity lows are found locally at Playa 2 and Playa 4, suggesting possible local deepening of bedrock beneath these playas.

Depth to the base of the Ogallala (Permian or Triassic bedrock) also increases northward across the survey area from near 110 m to more than 250 m (table 1, figure 35). Apparent conductivity depicted on the 200-m depth slice correlates well with bedrock depth. Where bedrock is shallower than 200 m, such as in most of the southern part of the survey area, apparent conductivity is high. Where bedrock is deeper, such as beneath much of the northern part of the survey area, apparent conductivity is low. High apparent conductivity is expected for pre-Ogallala bedrock that borehole logs show to be more conductive than overlying Ogallala deposits; low apparent conductivity is consistent with coarse Ogallala deposits within the saturated zone. The area of low conductivity delineates a paleovalley that trends generally west-northwest to east-southeast beneath the northern part of the survey area. Elevated apparent conductivity at area O and near Pantex Lake may represent local bedrock highs within the paleovalley. Low apparent conductivity near area P may indicate a change in bedrock lithology or a return to deeper bedrock.

## FOCUS AREAS AND CROSS SECTIONS

In addition to the surveywide analysis, we have examined several areas in more detail by producing limited-area conductivity-depth images or vertical cross sections from the CDTs. These include Pantex Southeast (figure 36), north and east of Playa 1, and several individual playas including Playa 3, Playa 4, and Pratt playa.

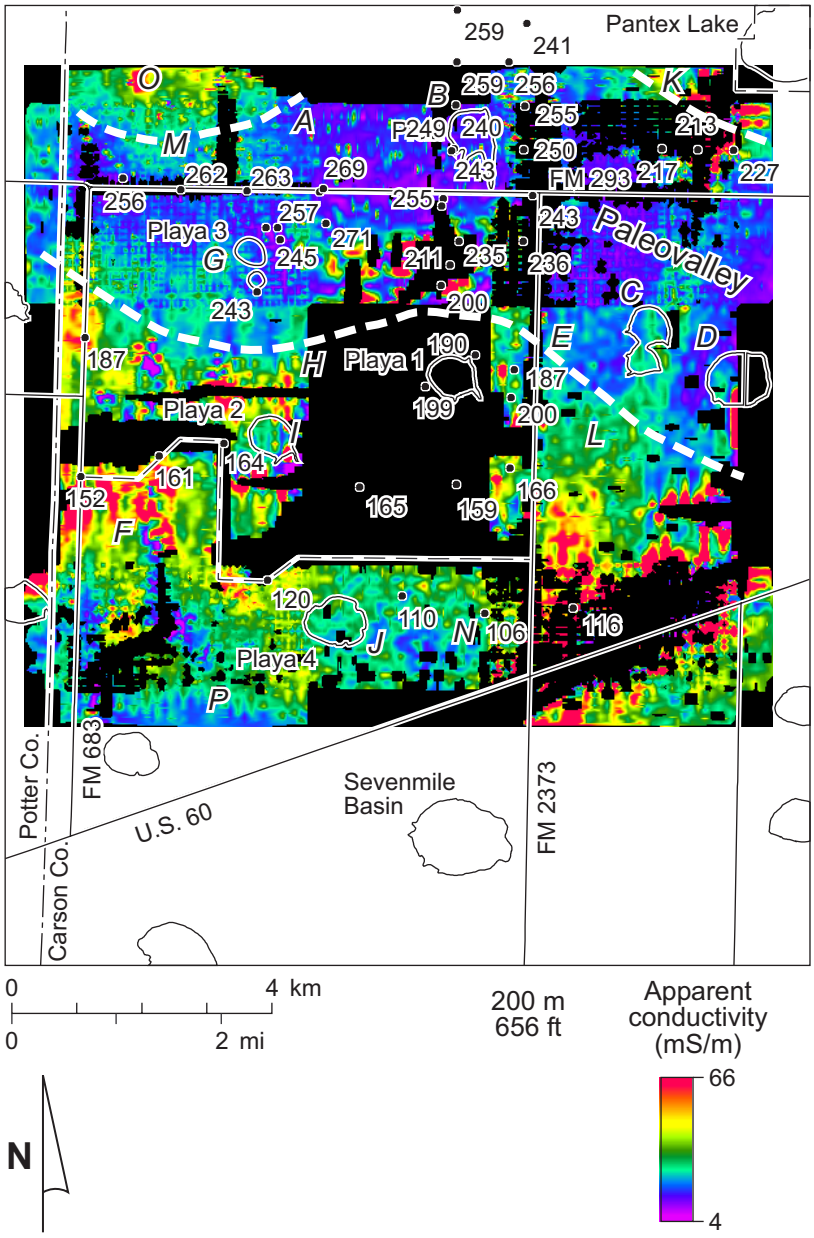


Figure 35. Apparent conductivity at 200-m depth and reported depths to the base of the Ogallala Formation. Well data from BWXT Pantex.

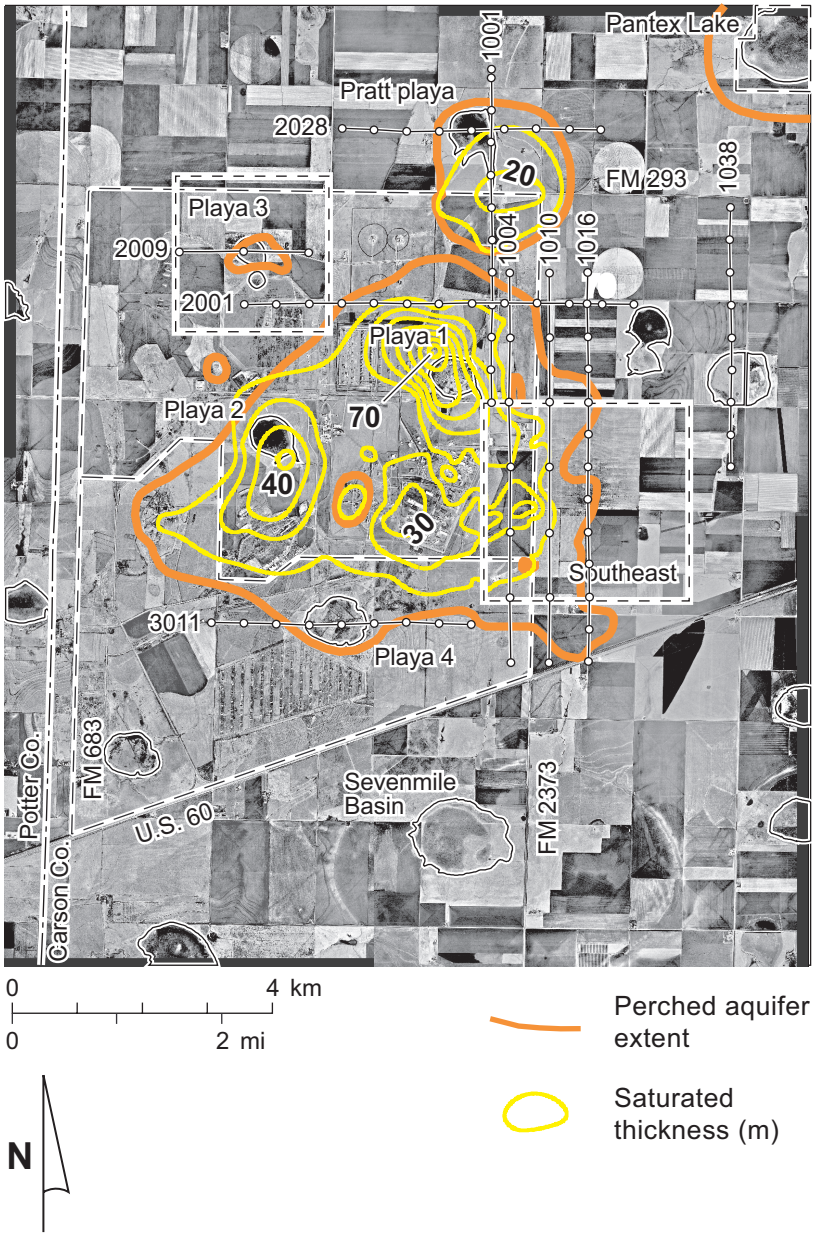


Figure 36. Location focus areas and cross sections constructed from airborne survey CDTs. Also shown is the extent and thickness of the perched aquifer based on borehole data (from BWXT Pantex).

## Pantex Southeast

Thickness of the FGZ and saturated thickness of the perched aquifer are important issues related to lateral and vertical migration of contaminants in the perched aquifer at Pantex, particularly in the Southeast focus area (figure 36). The Pantex Southeast focus area, measuring 3.2 km east-west and 3 km north-south, encompasses numerous borings and wells (figure 37). North-south flight lines in the east block cover the entire focus area; east-west flight lines in the south block give double coverage along the south edge (figures 15 and 23).

Cultural noise is a major problem in this area. EM noise generated by power lines is strong along FM 2373, the Pantex east gate entrance road, the southern boundary of the Pantex Plant, and U.S. 60 near the southeast corner of the focus area (figure 19). Power-line noise exceeds the 15-mV threshold along all of these features, significantly reducing the number of CDTs available to produce conductivity-depth slices. Additionally, a pipeline crosses from southwest to northeast (figure 37) and is clearly visible on depth slices deeper than about 50 m (appendix C). Pump-and-treat infrastructure, including well-heads, metallic pipes, structures, and electrical lines may also contribute to cultural contamination of the EM signal.

Despite these difficulties, apparent conductivity trends are visible on depth slices of the Pantex Southeast area. Above the FGZ and perched aquifer, maps of apparent conductivity at 40-m depth depict mostly low values east of FM 2373 (figure 38), consistent with relatively coarse and unsaturated upper Ogallala Formation fluvial deposits. Higher apparent conductivities are found locally along the northeast-trending pipeline that are probably cultural artifacts. At the approximate depth of the perched aquifer and FGZ at 80 m (figure 39), apparent conductivities remain low within the concentration of wells and borings east of FM 2373, suggesting thin, dry, or less clayey FGZ deposits. Elevated apparent conductivities in the northwest corner of the focus area appear to be related to the elevated conductivities surrounding Playa 1 (figure 31), reflecting a thickened FGZ and perched aquifer. Apparent conductivities are also elevated along and southwest of a line joining wells PTX06-1003 and PTX06-EW-07 (figure 39). This zone of elevated apparent conductivity extends southeastward across FM

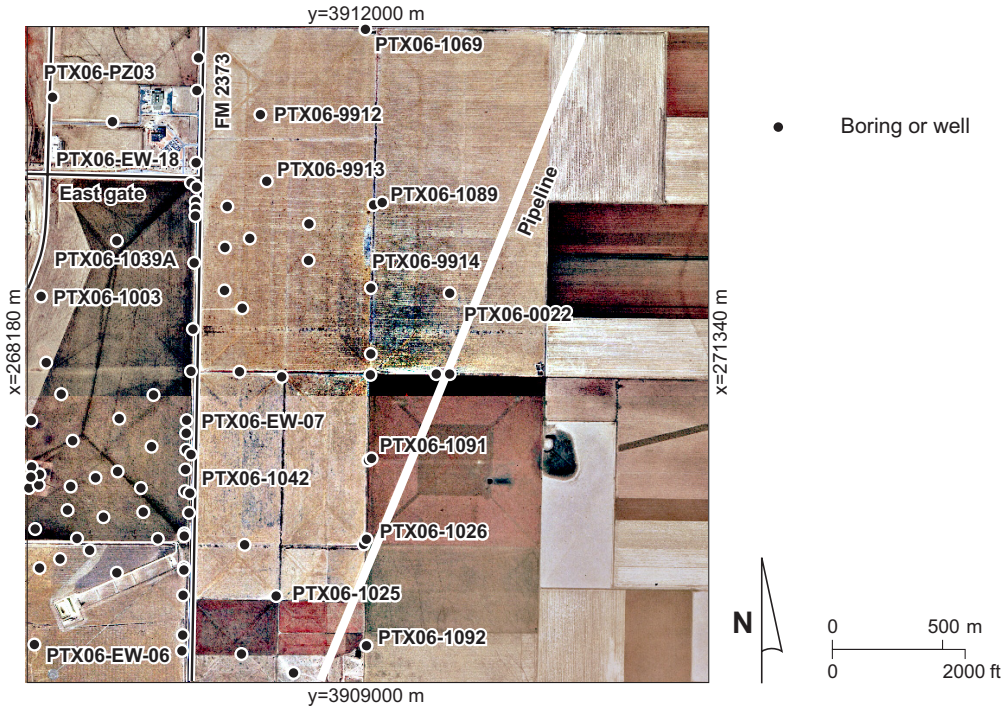


Figure 37. Aerial photograph of Pantex Southeast focus area. Also shown are well and boring locations.

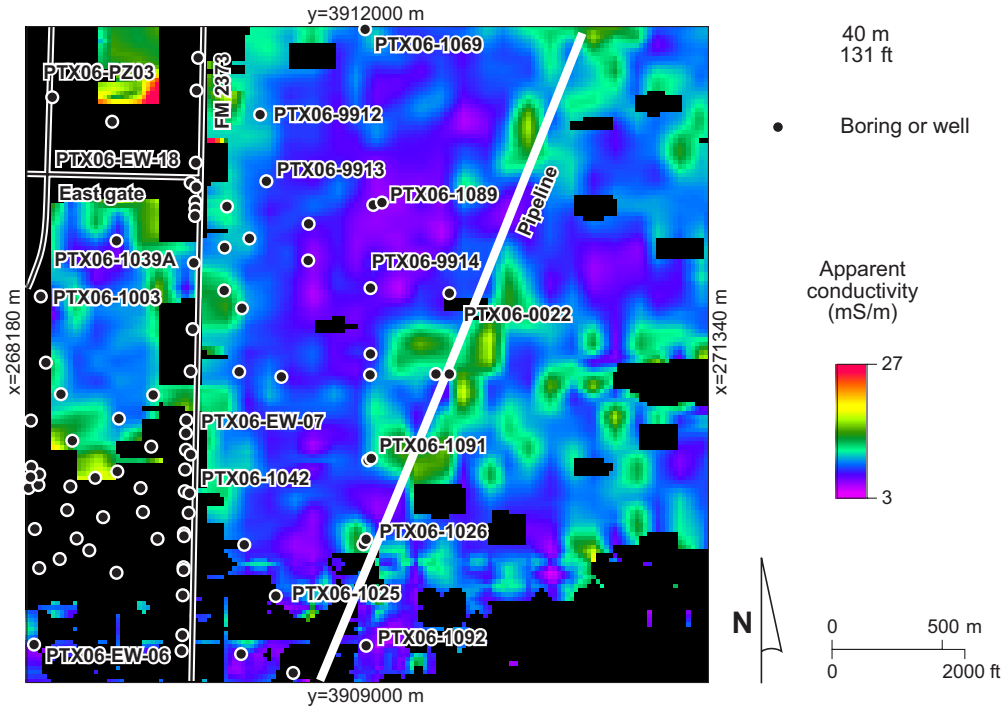


Figure 38. Apparent conductivity at 40-m depth in the Pantex Southeast focus area.

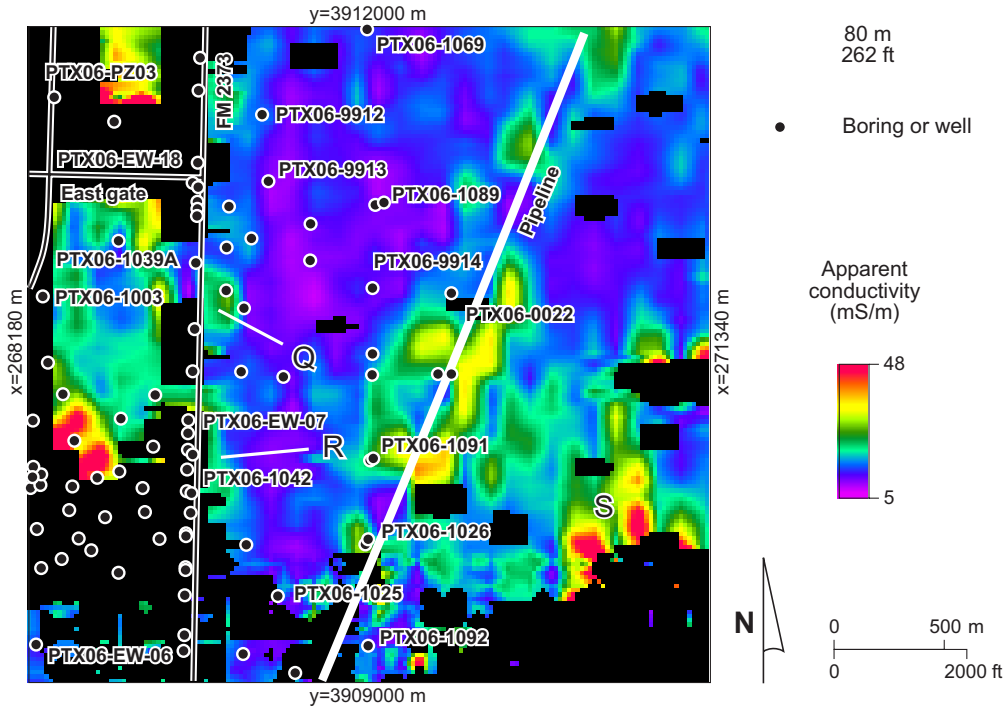


Figure 39. Apparent conductivity at 80-m depth in the Pantex Southeast focus area.

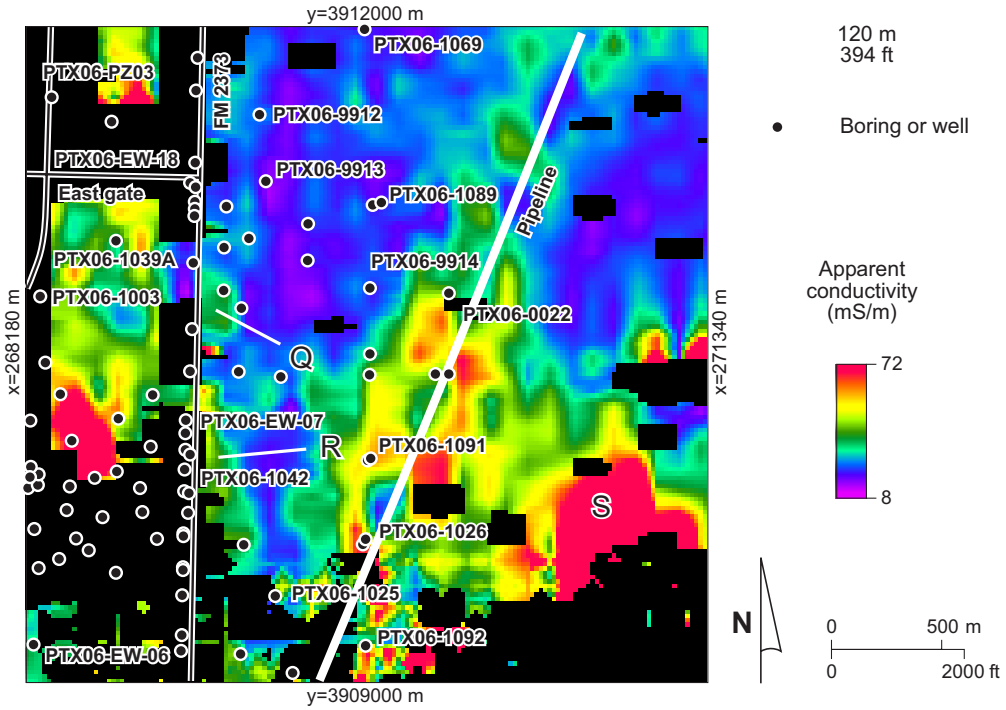


Figure 40. Apparent conductivity at 120-m depth in the Pantex Southeast focus area.

2373 a short distance. Elevated conductivities at this depth are likely to be caused by increases in FGZ thickness or perched aquifer saturated thickness. The low apparent conductivities east of FM 2373 suggest a thin or less clayey FGZ and thin or dry perched aquifer.

At a depth of 120 m, situated within the Ogallala Formation below the FGZ and above the Ogallala water level, apparent conductivities are generally higher than they are at shallower depths (figure 40). Elevated apparent conductivities persist and expand in areal coverage at the Pantex Plant and extend a short distance east of FM 2373 in some places (areas Q and R, figure 40). Because the effect of noise increases as EM signal strength decreases with depth, these elevated apparent conductivities could be an artifact of cultural noise. If real, it could be that Ogallala strata beneath the FGZ have higher clay or water content beneath the perched aquifer. Elevated conductivity to the southeast (area S, figure 40), where not contaminated by power-line- or pipeline-related noise, coincides with relatively shallow depths to the Ogallala water table (figure 34) and probably is an effect of shallow conductive bedrock or higher water content in the main Ogallala aquifer.

We used CDTs from segments of three north–south flight lines to create vertical cross sections depicting changes in apparent conductivity across the Pantex Southeast area (lines 1004, 1010, and 1016, figure 36). These lines extend 6 km from UTM northing coordinates 3908000 to 3914000 m, extending beyond the southern (3909000 m) and northern (3912000 m) boundaries of the focus area. The cross sections are useful in depicting gross vertical structure and in emphasizing the limited vertical resolution and noise contamination of EM data.

Line 1004 (figure 41) is the westernmost segment, crossing the southeast perched aquifer plume west of FM 2373 (figure 36). The conductivity structure along this and other segments consists of a resistive surface layer roughly corresponding to the unsaturated Blackwater Draw and upper Ogallala sediments, a conductive middle zone that generally corresponds to the perched aquifer and FGZ, and a variably conductive lower zone that represents the lower Ogallala in some areas and bedrock in others. Modeling and ground-based EM data showed that the conductive middle zone is influenced by changes in FGZ and perched aquifer saturated thickness. Areas of vertical smearing on this and other cross sections are processing artifacts from likely local cultural noise contamination.

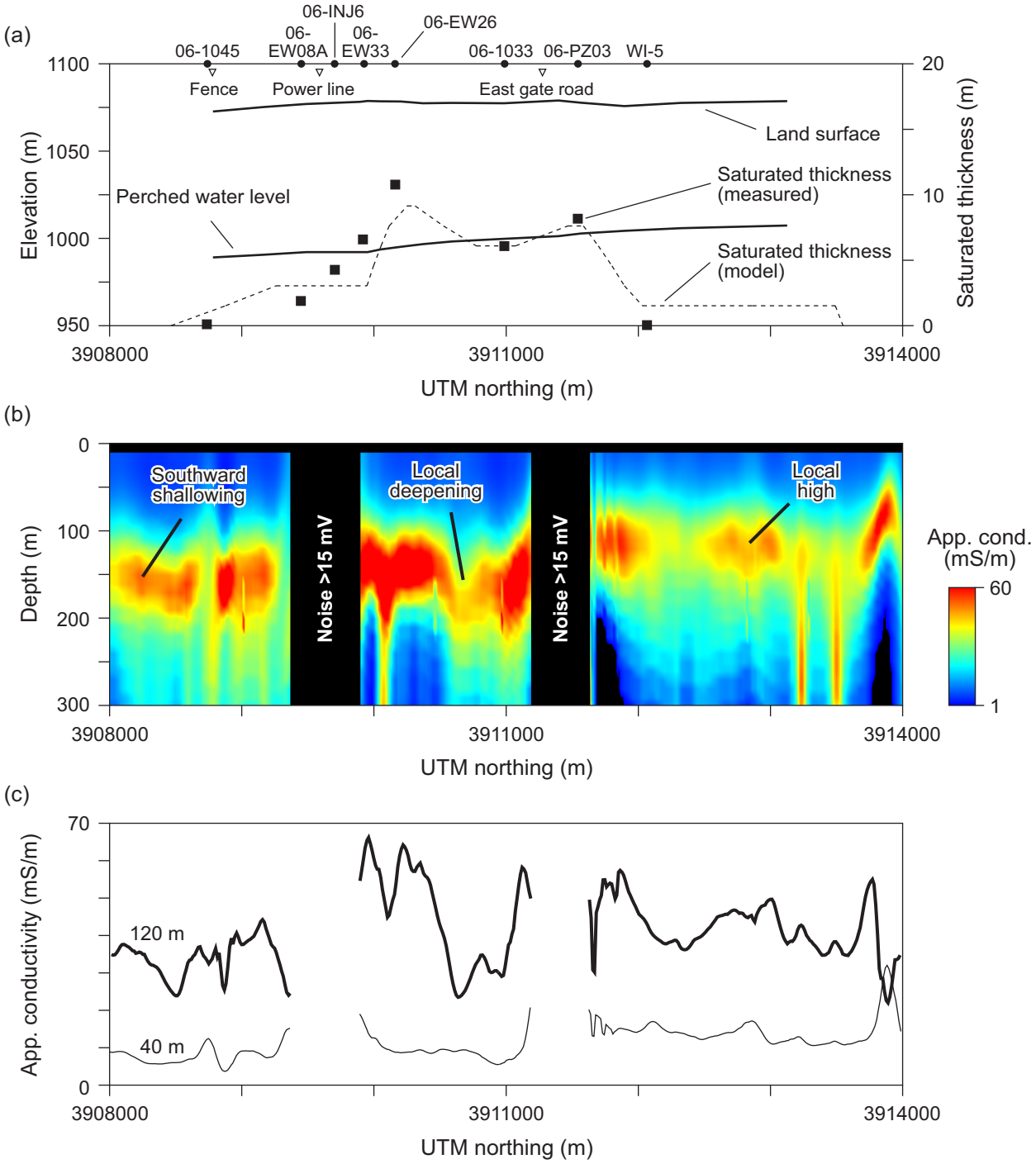


Figure 41. Cross section along east block line 1004 in the Pantex Southeast area (figure 36). (a) Feature and well locations, surface elevation, measured and modeled saturated thickness of the perched aquifer, and modeled perched aquifer water table; (b) vertical apparent conductivity image constructed from airborne survey CDTs with noisy profiles removed; and (c) sample apparent conductivities at 40- and 120-m depth.

Apparent conductivity data along line 1004 show reasonable agreement with borehole and perched aquifer model data. Depth to the middle conductive zone increases from north to south, matching the perched water-level trend (figure 41a, b). Apparent conductivity in the middle conductive interval increases where the perched saturated zone thickens near 3910000 m and 3911500 m (figure 41a, b). A zone of relatively high conductivity that shallows southward near the west end of the line is most likely related either to perched groundwater from Sevenmile Basin or to shallowing depths to the main Ogallala aquifer and underlying bedrock. Deepening of the conductive zone near 3911000 m coincides with a local low in perched aquifer saturated thickness. Lower conductivity and deeper depths to the conductive zone here might delineate a preferential path for downward migration of perched groundwater. The middle conductive zone has lower apparent conductivity north of 3912000 m and deepens slightly to the north, suggesting both thin or absent perched groundwater and a northward increase in depth to the perched aquifer and FGZ. A local increase in apparent conductivity near 3913000 (figure 41b) is near an area where the saturated thickness increases in the perched aquifer model (figure 36). The conductive area is interpreted to delineate where the saturated zone is thickest.

Line 1010 is about 600 m east of line 1004, crossing the perched groundwater plume just east of FM 2373, where borehole data indicate a thinner saturated zone. Depth to the middle conductive zone generally increases southward, mimicking the increase in depth to the perched water level (figure 42). Apparent conductivity in the middle conductive zone is low compared with that of line 1004, corroborating the reduced thickness of the perched water level (figure 42) documented in boreholes. Conductivity increases where the saturated zone is thicker (figure 42a, b). An increase in saturated thickness near the south end of the section (3909000 m) corresponds to a highly conductive zone that appears to shallow southward, suggesting a southerly source of groundwater, such as Sevenmile Basin. Local deepening and diminishing apparent conductivity are associated with a local saturated thickness minimum between about 3910500 and 3911000 m, indicating an area of potential downward infiltration of perched groundwater.

Line 1016 is 600 m farther east, near the mapped eastern limits of perched aquifer saturation (figure 36). Power-line and pipeline noise severely affects this section south of 3911000 m (figure 43).

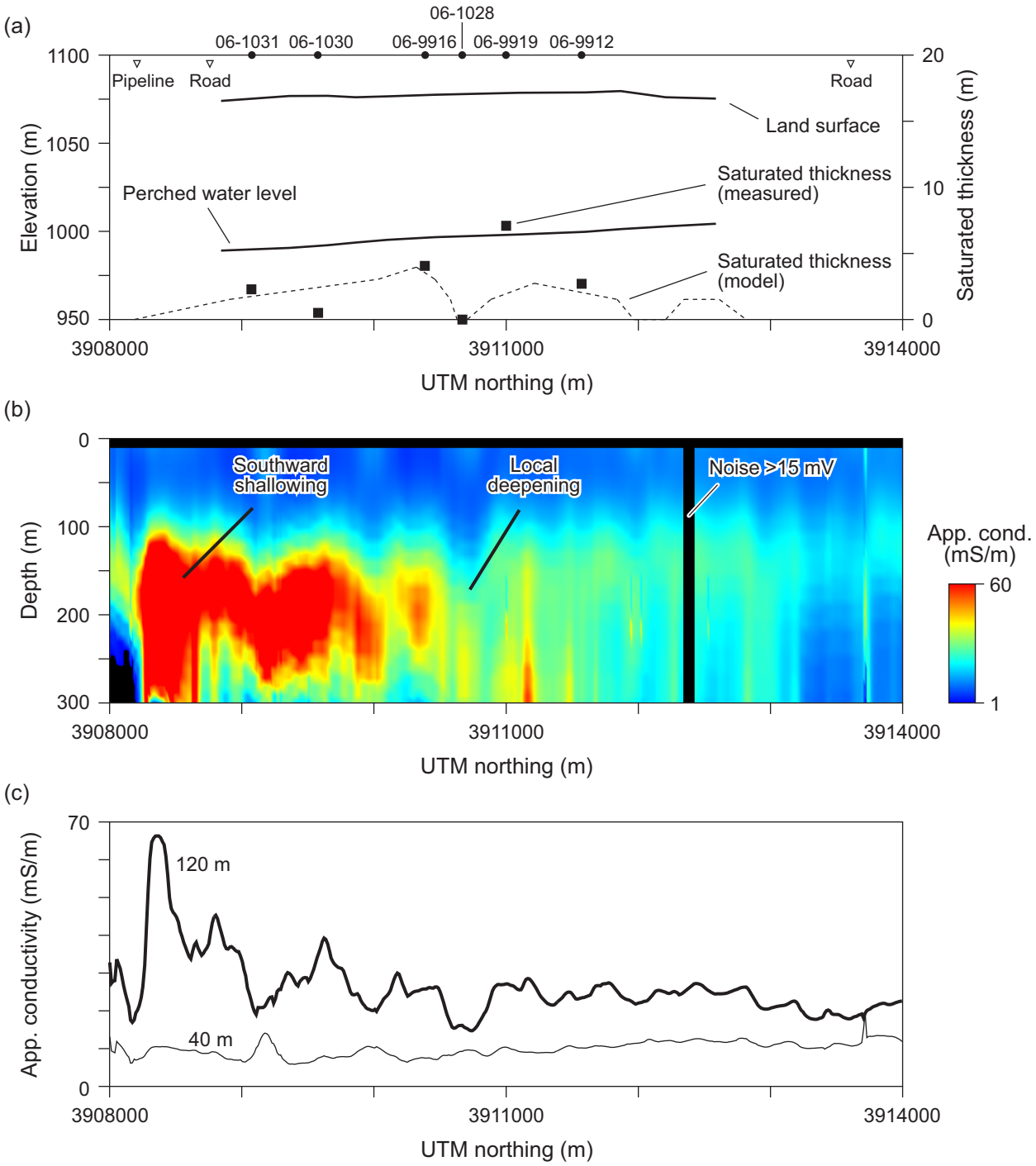


Figure 42. Cross section along east block line 1010 in the Pantex Southeast area (figure 36). (a) Feature and well locations, surface elevation, measured and modeled saturated thickness of the perched aquifer, and modeled perched aquifer water table; (b) vertical apparent conductivity image constructed from airborne survey CDTs with noisy profiles removed; and (c) sample apparent conductivities at 40- and 120-m depth.

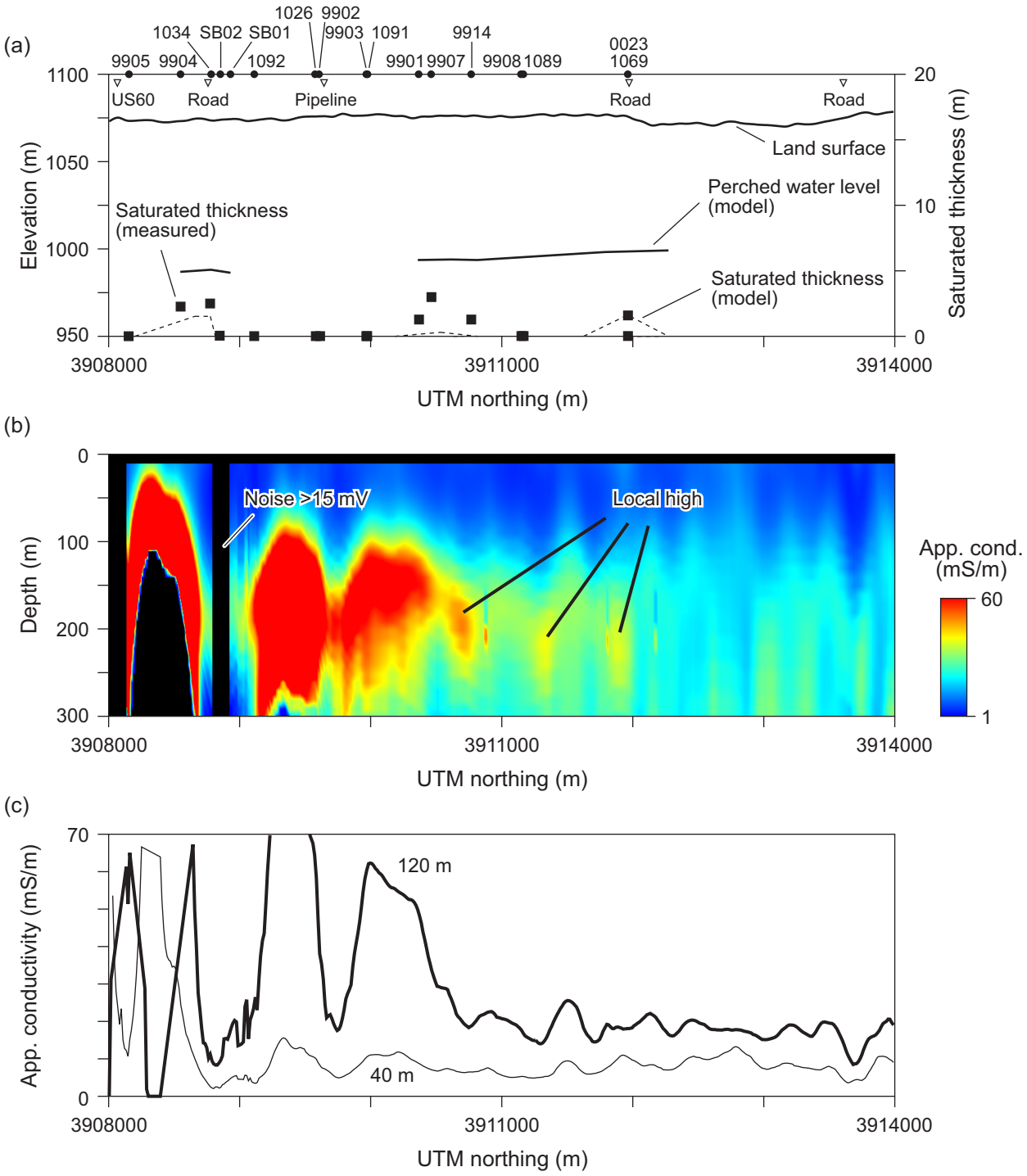


Figure 43. Cross section along east block line 1016 in the Pantex Southeast area (figure 36). (a) Feature and well locations, surface elevation, measured and modeled saturated thickness of the perched aquifer, and modeled perched aquifer water table; (b) vertical apparent conductivity image constructed from airborne survey CDTs with noisy profiles removed; and (c) sample apparent conductivities at 40- and 120-m depth. All well numbers in a have PTX-06 prefixes except SB borings.

North of that point, the middle conductive zone depicts locally increased apparent conductivity that is most likely related to accumulations of perched groundwater. Very low conductivities are measured north of 3912000 m, suggesting thin or dry perched aquifer and thin or less clayey FGZ.

## Playa 3

The Playa 3 focus area (figures 36 and 44) is a 2.4- × 2.4-km area northwest of the Pantex Plant that encompasses Playa 3, its enclosing basin, and the Burning Grounds. Numerous wells and borings have been drilled, although none penetrate the playa floor. Most of the focus area falls within both the west and north airborne survey blocks (figures 1 and 15), resulting in coverage along north–south and east–west flight lines. Seismic data were acquired across this playa in 1993 that showed there was evidence of playa formation by dissolution-induced subsidence (Paine, 1995). Reconnaissance, ground-based TDEM soundings acquired in 2000 showed that strata beneath the playa floor are more conductive at shallow depths and less conductive at greater depths than strata at similar depths outside the playa basin (Paine, 2000), consistent with a collapse model of playa formation.

Detailed ground elevation data from the airborne geophysical survey clearly show the low basin adjacent to the Burning Grounds that encloses Playa 3 and its southerly subplaya (figure 45). Elevation ranges from 1080 to 1096 m; there is 10 m or more of surface relief between the playa floor and the surrounding interplaya surface. The playa itself covers a relatively small part of the larger playa basin.

Selected conductivity-depth slices at Playa 3 are consistent with the results of the ground TDEM measurements and seismic data. At a depth of 40 m, which represents upper Ogallala Formation deposits in interplaya areas and is above the perched aquifer and FGZ (table 1), the apparent conductivity image depicts highest conductivities beneath the basin enclosing Playa 3 (figure 46). Areas of low apparent conductivity surround the basin. High apparent conductivities are also shown at the Burning Grounds, but the presence of several individual peaks suggests that the elevated conductivities here are at least partly an artifact of metallic structures or perhaps power lines. Elevated conductivities beneath the playa basin are consistent with higher clay and water content of lacustrine deposits filling the basin.

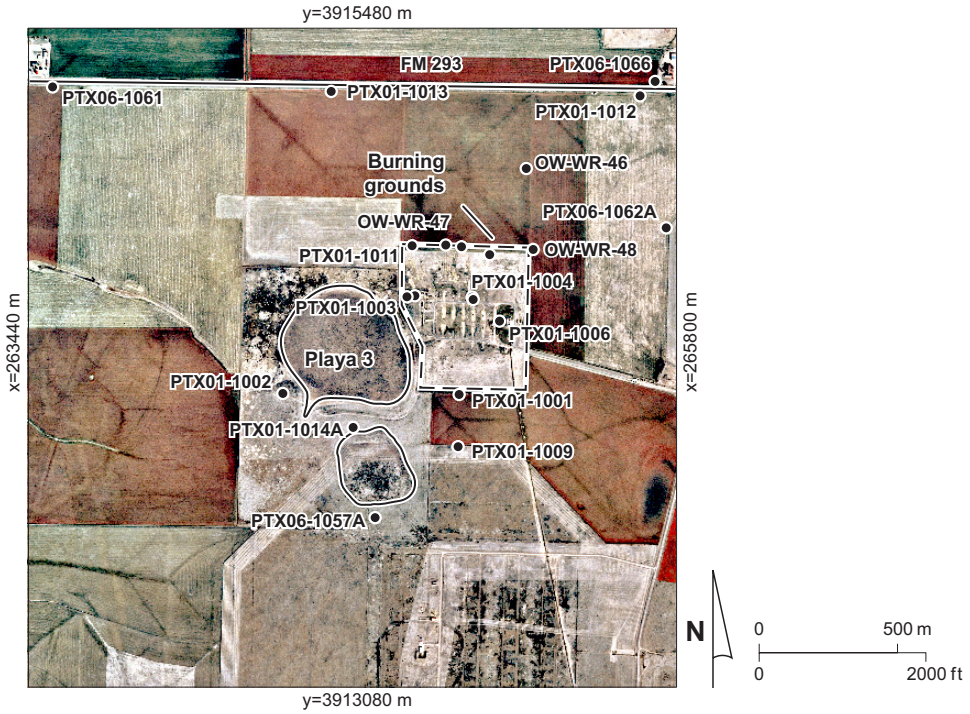


Figure 44. Aerial photograph of Playa 3 and the Burning Grounds. Also shown are well and boring locations.

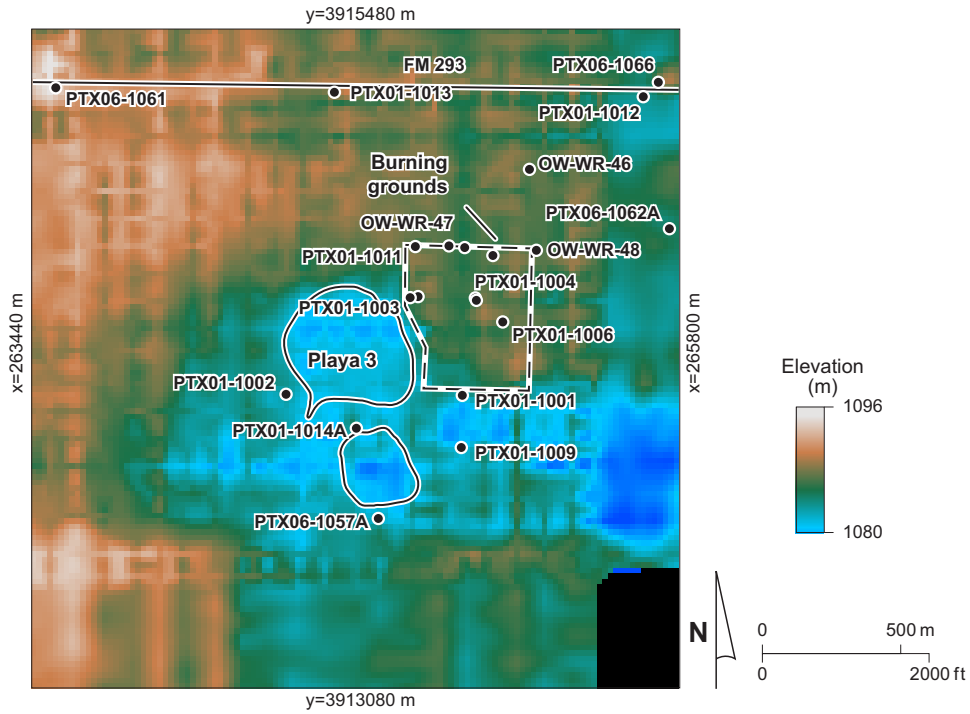


Figure 45. Terrain map of Playa 3 and the Burning Grounds. Also shown are well and boring locations.

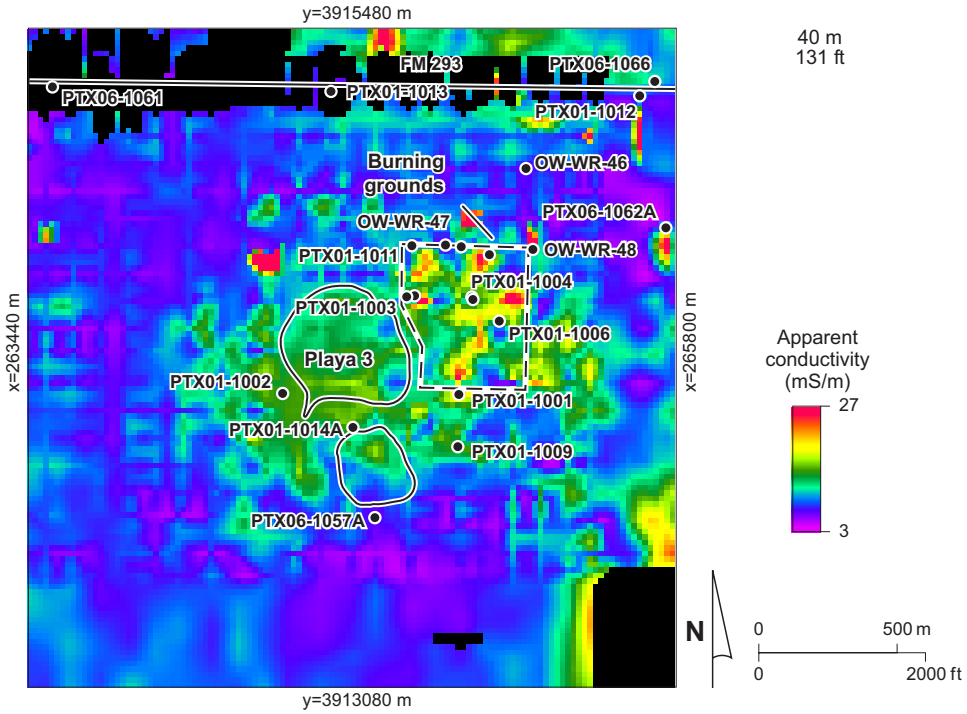


Figure 46. Apparent conductivity at 40-m depth in the Playa 3 focus area.

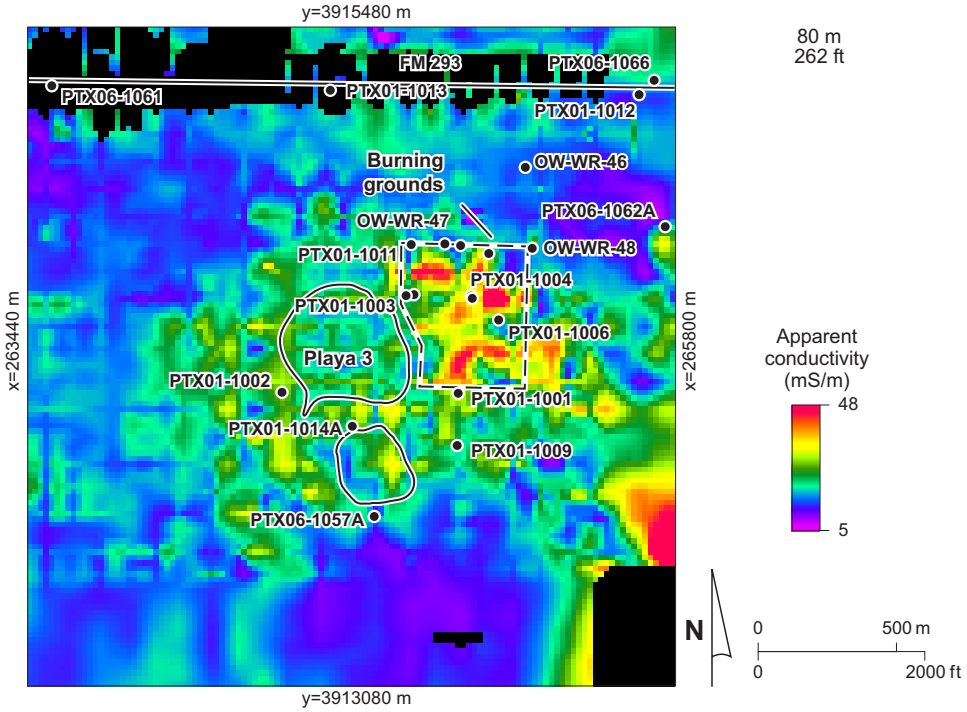


Figure 47. Apparent conductivity at 80-m depth in the Playa 3 focus area.

Outside the basin, lower apparent conductivities are consistent with the presence of coarser and drier upper Ogallala fluvial deposits described in nearby wells and borings.

Apparent conductivities remain elevated beneath the playa basin at 80-m depth (figure 47) but are less pronounced and cover a slightly larger area around the playa. This is the approximate depth of the perched aquifer and FGZ in other parts of the plant (table 1). Prominent conductivity lows northeast of the Burning Grounds and south of Playa 3 are separated by a zone of elevated apparent conductivity that trends east-southeast from Playa 3. These elevated conductivities may delineate areas of thicker FGZ development or higher water content.

The depth slice at 120 m depicts apparent conductivity within the middle to lower Ogallala Formation, below the FGZ and above the Ogallala water level (figure 48). The most prominent feature is the pronounced conductivity low that coincides with Playa 3; higher apparent conductivities surround the playa beneath the interplaya surface. Depth slices between 80 and 120 m (figures C8 to C12) depict a gradual change from conductivities beneath the playa that are similar to those at the same depth within a radius of about 1 km around the playa, to conductivities beneath the playa that are lower than those within the 1-km radius around the playa. Beyond that radius, conductivities are similar to those directly beneath the playa but lower than those within the annular region around the playa. Low apparent conductivities at depth beneath the playa are consistent with an interpretation of the playa as a subsidence and collapse feature. At this depth, lower conductivities could be caused by higher porosity developed through collapse and brecciation. Higher conductivities may imply downward and outward annular infiltration of groundwater above and below the FGZ from playa recharge.

A 2-km-long cross section constructed from CDTs acquired along flight-line 2009 (figures 36 and 49) extends across the playa within the focus area. This section depicts a middle conductive interval (roughly correlative to the perched aquifer and FGZ) that deepens from east to west, becoming less conductive and more diffuse directly beneath Playa 3 (figure 49b). Shallower than about 60 m on the section, apparent conductivities tend to be higher beneath the playa than they are farther from it, supporting an interpretation of higher clay and water content in shallow lacustrine deposits directly beneath the playa. In the middle conductive interval, apparent conductivities are lower beneath the playa than

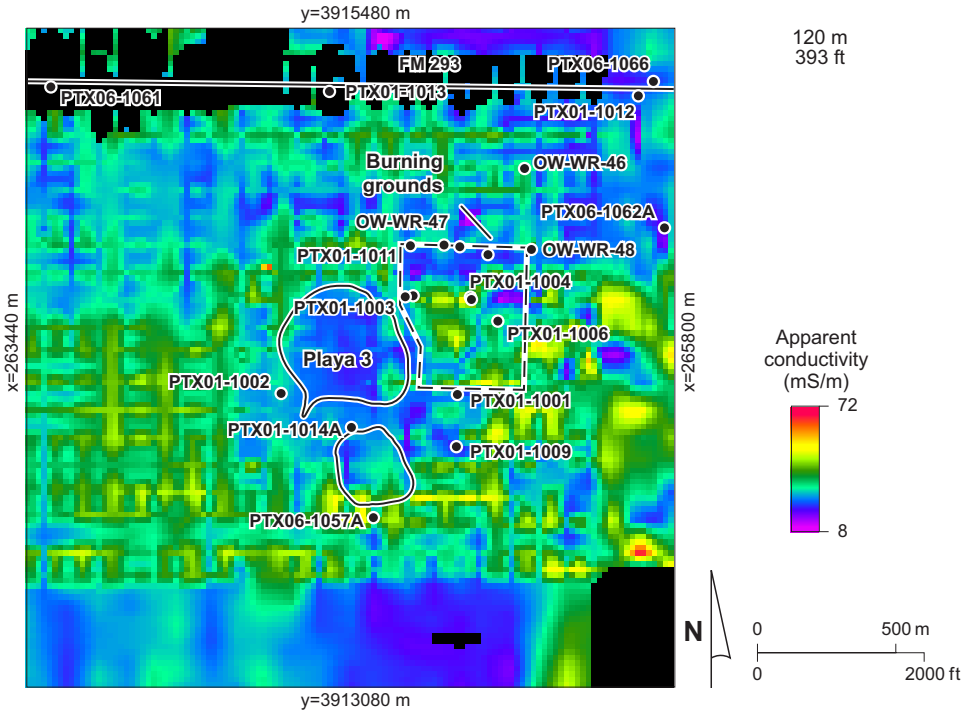


Figure 48. Apparent conductivity at 120-m depth in the Playa 3 focus area.

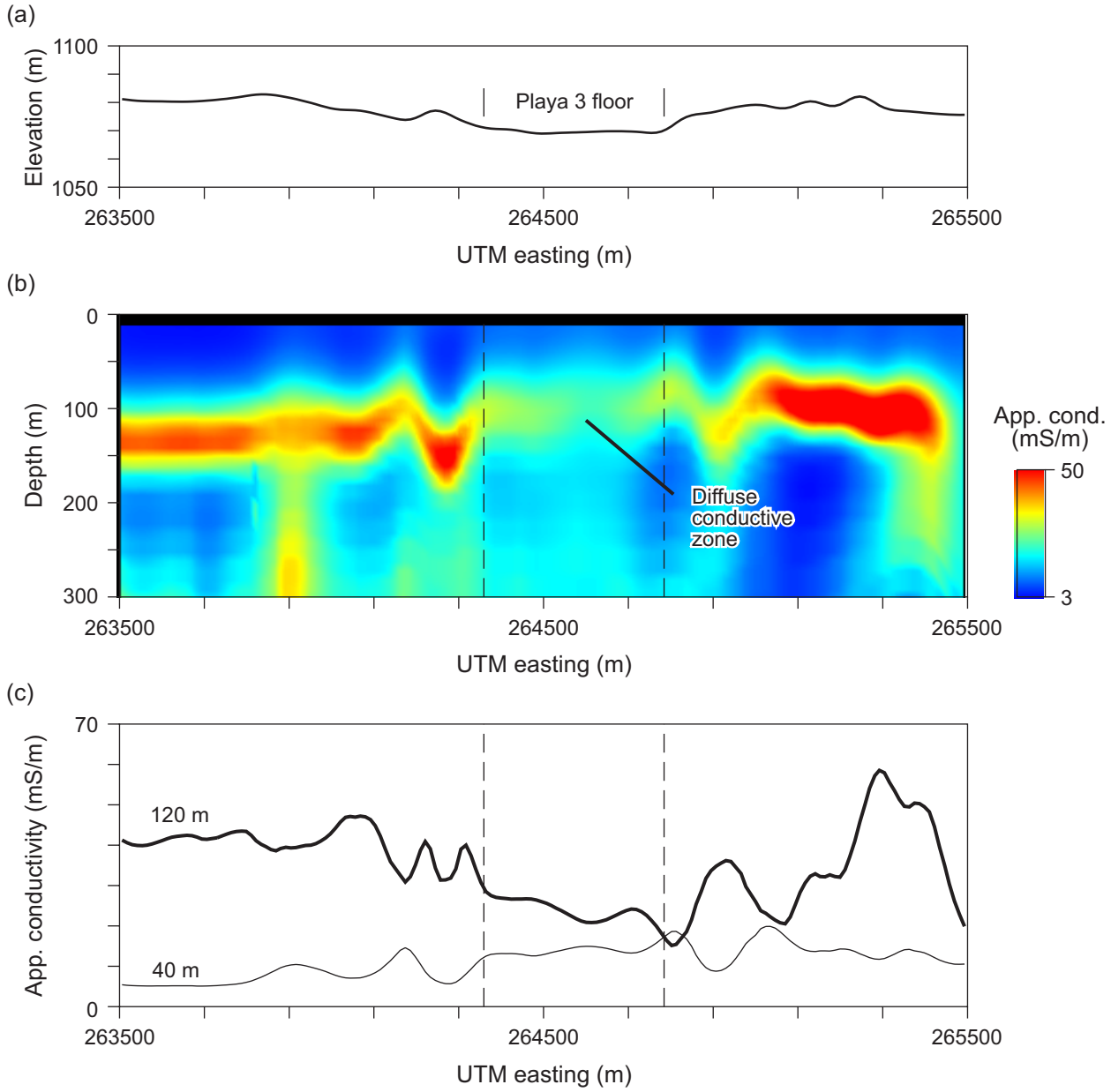


Figure 49. Cross section along north block line 2009 across Playa 3 (figure 36). (a) Feature locations and surface elevation; (b) vertical apparent conductivity image constructed from airborne survey CDTs; and (c) sample apparent conductivities at 40- and 120-m depth.

they are in immediately surrounding areas, implying lower water or clay content beneath the playa than in adjacent deposits at or below the perched aquifer and FGZ.

## Playa 1

Flight restrictions precluded acquiring data over Playa 1, but boundaries for the east and north blocks (figure 1) were placed as close as possible to this important hydrogeologic feature. Depth slices as shallow as 30 m to as deep as 140 m or more (figures 31, 32, and C3 to C14) depict an apparent conductivity halo around Playa 1 that extends more than 1 km southeast, east, and north of the playa. The most likely cause of the elevated conductivity is relatively high water content associated with downward and outward migrating groundwater that has infiltrated at Playa 1.

In addition to the depth slices, we constructed cross sections from CDTs acquired along flight-line segments in the east (line 1001) and north (line 2001) blocks that pass closest to the playa (figure 36). Line 1001, a 6-km-long segment extending northward near Pratt playa, passes about 250 m east of Playa 1. Line 2001 begins south of Playa 3, extending eastward and passing about 800 m north of Playa 1.

Line 1001 (figure 50) depicts apparent conductivity changes that correspond well to known and modeled perched aquifer saturated thickness. The middle conductive interval, roughly correlative to the perched aquifer and FGZ interval, shows elevated apparent conductivities increasing as saturated thickness increases southward from 3914000 m toward Playa 1 (figure 50). In addition, the depth to the conductive zone decreases toward the playa, apparently following the decreasing depth to water in the perched groundwater mound associated with Playa 1.

A northward increase in the perched aquifer saturated thickness has also been identified between 3914000 and 3915000 m that corresponds to a northward-shallowing, moderately conductive zone on line 1001. Conductivities in the middle conductive zone diminish abruptly north of about 3915200 m, which suggests that the perched saturated zone thins abruptly here as well. Two local, minor zones of

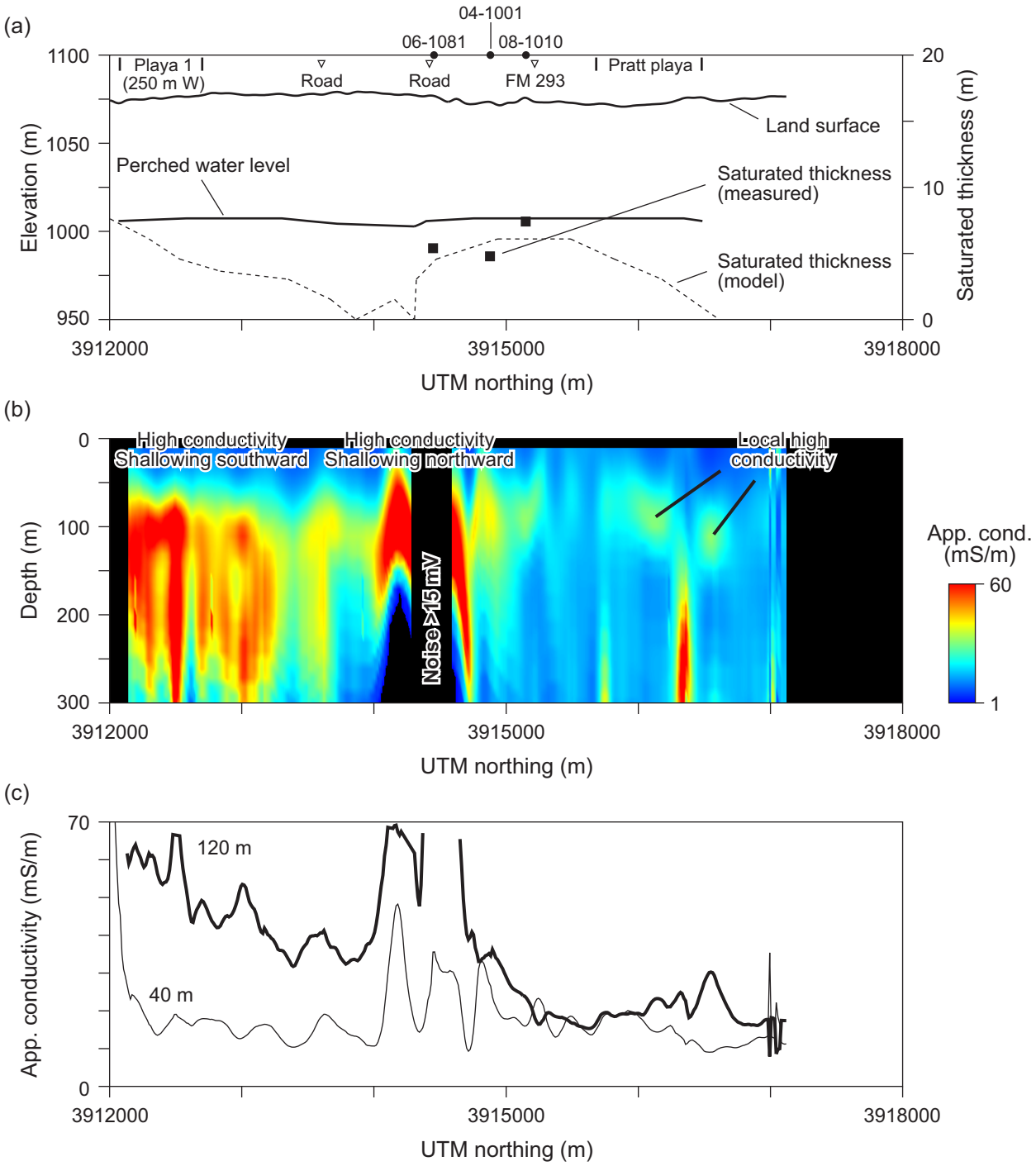


Figure 50. Cross section along east block line 1001 near Playa 1 and Pratt playa (figure 36). (a) Feature and well locations, surface elevation, measured and modeled saturated thickness of the perched aquifer, and modeled perched aquifer water table; (b) vertical apparent conductivity image constructed from airborne survey CDTs with noisy profiles removed; and (c) sample apparent conductivities at 40- and 120-m depth.

elevated apparent conductivity between 3916000 and 3917000 m may indicate local minor areas of perched water saturation near Pratt playa.

Although noisy and more distant from Playa 1, line 2001 also correlates reasonably well with measured and modeled perched aquifer data (figure 51). Elevated apparent conductivities in the middle conductive zone correspond roughly to relatively thick perched aquifer saturation between 265500 and 267500 m and from 268000 m, a short distance eastward. Relatively low apparent conductivities in the middle conductive interval at the east end of the line suggest a relatively thin perched saturated zone. A distinct depression in the middle conductive interval is evident at the west end of the line between 264500 and 265500 m. This depression is on the part of the segment that is nearest Playa 3 and may represent a local deepening of the FGZ, perhaps associated with the formation of Playa 3.

## Playa 4

Playa 4 is instructive because it is a medium-sized playa in a relatively unaltered area that has little cultural noise nearby to contaminate the EM data. Like other playas, depth slices depict elevated apparent conductivities coincident with the playa at shallow depths (most likely caused by lacustrine deposits with higher clay and water content than surrounding strata at equivalent depth) and lower apparent conductivities at greater depths beneath the playa than are measured surrounding the playa. At Playa 4, depth slices from 10 to 80 m have elevated conductivities; slices at 90 m and deeper depict lower apparent conductivity. Relatively low apparent conductivity at and below 90-m depth beneath this playa is clearer here than at other playas, partly because noise levels are low and perhaps partly because depth to Permian or Triassic bedrock is shallower here (figure 35; bedrock is reported at 110 to 120 m in nearby boreholes).

The middle conductive interval is well defined on an apparent conductivity cross section (line 3011) that extends 4 km across Playa 4 (figures 36 and 52). Depth to the conductive zone shallows at the west end of the line and generally deepens slightly to the east. Apparent conductivity is relatively high within this interval, with values similar to those measured elsewhere in the survey area where there was a

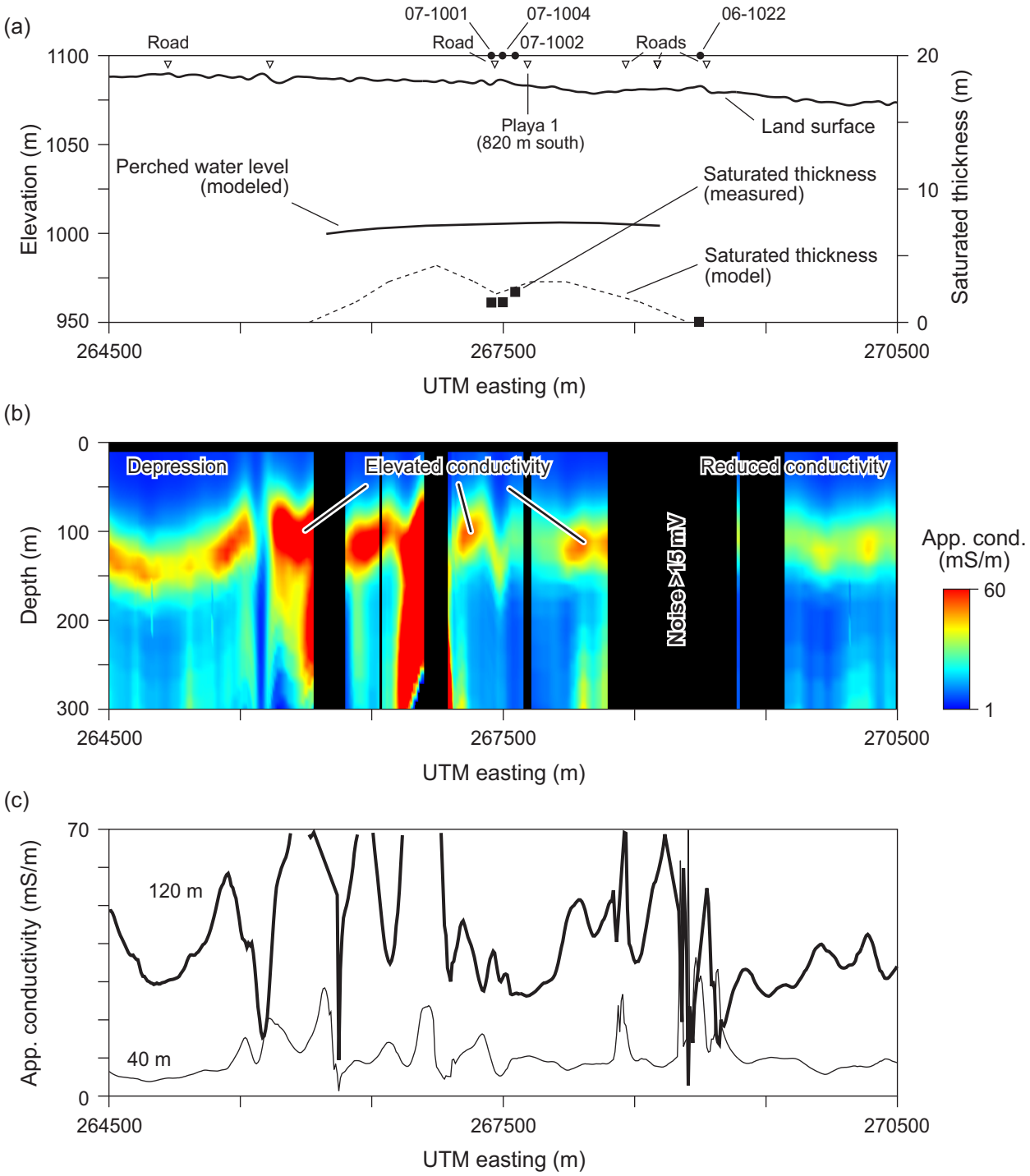


Figure 51. Cross section along north block line 2001 north of Playa 1 (figure 36). (a) Feature and well locations, surface elevation, measured and modeled saturated thickness of the perched aquifer, and modeled perched aquifer water table; (b) vertical apparent conductivity image constructed from airborne survey CDTs with noisy profiles removed; and (c) sample apparent conductivities at 40- and 120-m depth.

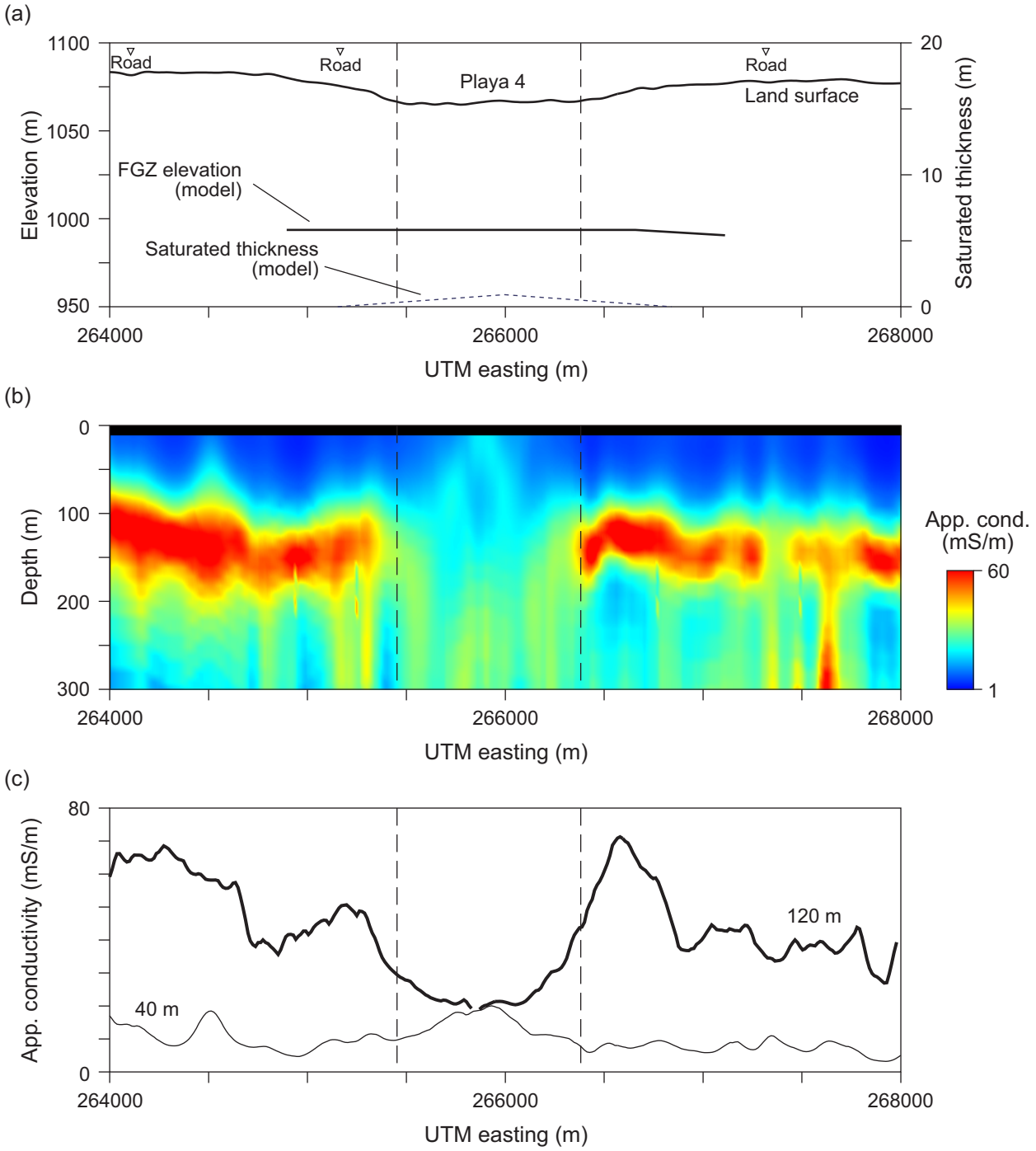


Figure 52. Cross section along south block line 3011 across Playa 4 (figure 36). (a) Feature locations, surface elevation, modeled saturated thickness of the perched aquifer, and modeled perched aquifer water table; (b) vertical apparent conductivity image constructed from airborne survey CDTs; and (c) sample apparent conductivities at 40- and 120-m depth.

substantial perched aquifer saturated thickness. The saturated zone of the perched aquifer is modeled to be very thin or absent at Playa 4, somewhat inconsistent with the apparent conductivity values. An explanation more likely than a substantial perched saturated thickness causing elevated conductivity along line 3011 is that both bedrock (figure 35) and the saturated zone of the main Ogallala aquifer (figure 34) are within depth range of the elevated conductivity interval. In this area, the EM instrument is most likely mapping the relatively high conductivity of bedrock.

There is a striking reduction in measured apparent conductivity directly beneath Playa 4 (figure 52). The presence of shallow bedrock surrounding the playa and the absence of a correlative conductive interval beneath the playa are strong evidence supporting the formation of this playa basin by subsidence related to evaporite dissolution at depth.

## CONCLUSIONS

This report summarizes results of the airborne geophysical survey of the Pantex Plant area completed in March 2003, which was used to assess the perched aquifer, FGZ, and deeper hydrogeologic horizons at and near the Pantex Plant. High-resolution airborne geophysical data, including TDEM and magnetic field data, were acquired over four survey blocks surrounding the Pantex Plant and were processed to produce models of apparent conductivity changes with depth. We achieved exploration depths to the lower Ogallala Formation and to pre-Ogallala strata, where the Ogallala is relatively thin. Analysis of power-line and other cultural noise related to pipelines and structures resulted in the removal of about 20 percent of the 104,880 measurement locations from the final TDEM data set. Comparisons of apparent conductivity profiles derived from ground and airborne instruments showed general agreement in magnitude and shape; smoothly varying profiles derived from airborne data are more realistic approximations of the actual electrical conductivity of the ground. We constructed conductivity-depth slices depicting apparent electrical conductivity across the survey area from the remaining measurement locations at 10-m intervals between depths of 10 and 200 m below the ground surface. We analyzed

these images to interpret geologic and hydrologic features related to the perched aquifer, FGZ, and the Ogallala aquifer.

Conductivity-depth images for strata above the perched aquifer, at the approximate depth of the perched aquifer and FGZ, between the FGZ and Ogallala aquifer, and below the Ogallala water table reveal patterns that can be used to interpret changes in clay and water content that are relevant to groundwater flow. Elevated apparent conductivities on depth slices above the perched aquifer appear to identify areas with higher water and clay content, particularly at playas where wet, clayey lacustrine deposits are tens of meters thick. At perched aquifer depths, apparent conductivity images show elevated conductivities that correlate reasonably well with increases in perched aquifer saturated thickness, allowing these images to be used to identify likely changes in saturated thickness where borehole data have not been acquired. We found a positive correlation between perched aquifer saturated thickness and measured electrical conductivity but found no relationship between FGZ thickness and measured conductivity. This relationship either does not exist or is obscured by sparse and inconsistent borehole data on FGZ thickness.

Deeper depth slices appear to depict the configuration of bedrock forming the base of the Ogallala aquifer. We interpreted approximate boundaries of the deep paleovalley north of the Pantex Plant on the basis of borehole data and apparent conductivity images and identified probable local dissolution features beneath several playas.

Depth slices and cross sections constructed from airborne TDEM data and combined with abundant borehole data provide a semiquantitative means of interpolating perched aquifer saturated thickness and likely FGZ integrity between boreholes and extrapolating beyond them. Although the method's statistical success in mapping FGZ thickness remains ambiguous until better data on actual FGZ thickness are obtained for comparison, spatial correlations between saturated thickness and apparent conductivity demonstrate that the method is useful in examining perched aquifer saturated thickness that are a function of recharge rates and FGZ integrity. Data from the airborne survey should find future use

in providing better lateral context for point-specific borehole data and can serve as a guide to ongoing and future hydrogeological characterization and remediation activities.

## ACKNOWLEDGMENTS

This project was funded by BWXT Pantex under contract number 00026424 between The University of Texas at Austin and BWXT Pantex. S. Todd Harris and Shane Currie of BWXT Pantex served as project managers. BWXT staff Todd Harris, Shane Currie, Tony Biggs, and Jeffrey Stovall provided geological and hydrological data. James Phelan and Carolyn Byrd of Sandia National Laboratories assisted in project justification and airborne survey approval. Fugro Airborne Surveys staff Darcy Wiens, Mark Williston, and Renko Constapel flew and maintained the aircraft, Dave Patzer operated onboard instruments, and Rick Williams and Brenda Sharp processed the data. We appreciate the management at Pantex, both DOE and BWXT, for their assistance in completing the project.

## REFERENCES

Frischknecht, F. C., Labson, V. F., Spies, B. R., and Anderson, W. L., 1991, Profiling using small sources, *in* Nabighian, M. N., ed., Electromagnetic methods in applied geophysics--applications, part A and part B: Tulsa, Society of Exploration Geophysicists, p. 105-270.

Fugro Airborne Surveys, 2003, Logistics and processing report: airborne magnetic and GEOTEM survey, Pantex survey area, Amarillo, Texas, USA: Fugro Airborne Surveys, Ottawa, Ontario, Canada, Job No. 03428, 73 p.

Geonics Limited, 1992, Protem 47 operating manual: Mississauga, Ontario, variously paginated.

Gustavson, T. C., Bebout, D. G., Bennett, P. C., Fish, E. B., Fryar, A. E., Hovorka, S. D., Hua, Hsiao-Peng, Kirschenmann, Kyle, Laun, Scot, Minehardt, T. J., Mullican, W. F., III, Nicot, Jean-Philippe, Paine, J. G., Pezzolesi, T. P., Rainwater, Ken, Ramsey, Heyward, Reedüer, Alan, Romanak, K. D., Scanlon, B. R., Thompson, David, Xiang, Jiannan, and Zartman, R. E., 1995,

Summary hydrogeologic assessment, U.S. Department of Energy Pantex Plant, Carson County, Texas: The University of Texas at Austin, Bureau of Economic Geology, contract report prepared for the U.S. Department of Energy, 127 p.

Hunter, Don, and Macnae, James, 2001, Subsurface conductivity structure as approximated by conductivity-depth transforms: Australian Society of Exploration Geophysicists, Extended Abstracts, Brisbane, 4 p.

Kaufman, A. A., and Keller, G. V., 1983, Frequency and transient soundings: Elsevier, Amsterdam, Methods in Geochemistry and Geophysics, No. 16, 685 p.

Paine, J. G., 1995, Shallow-seismic evidence for playa basin development by dissolution-induced subsidence on the Southern High Plains, Texas: The University of Texas at Austin, Bureau of Economic Geology Report of Investigations No. 233, 47 p.

Paine, J. G., 2000, Seismic evaluation and reconnaissance TDEM survey of the Southeast and Playa 3 areas of the Pantex Plant, Carson County, Texas: The University of Texas at Austin, Bureau of Economic Geology, report prepared for the Innovative Treatment Remediation Demonstration Program, Sandia National Laboratories under P.O. document no. 12236, 51 p.

Pantex Plant Environmental Restoration Department, 2000, Groundwater program management action process: final report prepared for the U.S. Department of Energy under subcontract 16189, June 2000, not consecutively paginated.

Parasnis, D. S., 1973, Mining geophysics: Amsterdam, Elsevier, 395 p.

Parasnis, D. S., 1986, Principles of applied geophysics: Chapman and Hall, 402 p.

Smith, R. S., and Annan, A. P., 2000, Using an induction coil sensor to indirectly measure the B-field response in the bandwidth of the transient electromagnetic method: Geophysics, v. 65, no. 5, p. 1489-1494.

Spies, B. R., and Frischknecht, F. C., 1991, Electromagnetic sounding: *in* Nabighian, M. N., ed., Electromagnetic methods in applied geophysics--applications, part A and part B: Tulsa, Society of Exploration Geophysicists, p. 285-386.

U.S. Army Corps of Engineers, Tulsa District, 1992, U.S. Department of Energy Pantex Plant: Amarillo, Texas, hydrogeological assessment, variously paginated.

Stoller, 2004, Pantex Plant Groundwater Final RCRA Facility Investigation Report, BWXT Pantex, L.L.C., not consecutively paginated.

U.S. Department of Energy, Technical Assistance Team, 2000, Protecting the Ogallala aquifer II: recommendations for characterization and remediation of the southeastern plume at the Pantex Plant: final report, July 7, 2000, 21 p.

West, G. F., and Macnae, J. C., 1991, Physics of the electromagnetic induction exploration method, *in* Nabighian, M. N., ed., Electromagnetic methods in applied geophysics--applications, part A and part B: Tulsa, Society of Exploration Geophysicists, p. 5-45.

Wolfgram, Peter, and Karlik, Gulcin, 1995, Conductivity-depth transform of GEOTEM data: Exploration Geophysics, v. 26, p. 179-185.

*Page intentionally blank*

# APPENDIX A. WELLS AND BORINGS

Reported depths to Ogallala caprock, fine-grained zone, base of the Ogallala Formation, and perched or main Ogallala water table and saturated thickness from wells and borings greater than 40 m deep within the airborne survey area. Locations are in meters in the Universal Transverse Mercator projection, zone 14 north, 1983 North American Datum. Data from BWXT Pantex, October 2003.

| Well/boring | Aquifer | UTM coordinates x (m) | UTM coordinates y (m) | Elev. (m) | Well Depth (m) | Caprock Top (m) | Caprock Bottom (m) | Fine-grained zone Top (m) | Fine-grained zone Bottom (m) | Fine-grained zone Thick. (m) | Ogallala Base (m) | Water Level (m) | Saturated Thick. (m) |
|---|---|---|---|---|---|---|---|---|---|---|---|---|---|
| 06-44-204 | Ogallala | 267732 | 3915897 | - | 223.1 | 21.9 | 25.0 | 63.4 | - | - | 248.9 | - | - |
| 06-44-205 | Ogallala | 267760 | 3916570 | - | 251.5 | 28.0 | 31.1 | 70.1 | 100.6 | 30.5 | 240.2 | - | - |
| 06-44-206 | Ogallala | 268823 | 3916555 | - | 251.5 | 24.4 | 30.5 | 74.1 | 96.9 | 22.8 | 254.5 | - | - |
| 06-44-207 | Ogallala | 268804 | 3915885 | - | 247.5 | 25.9 | 29.0 | 74.7 | 99.4 | 24.7 | 249.9 | - | - |
| 06-44-304 | Ogallala | 270929 | 3915899 | - | 215.8 | 25.0 | 28.0 | 68.6 | 85.3 | 16.7 | 216.7 | - | - |
| 06-44-305 | Ogallala | 271484 | 3915882 | - | 204.5 | 24.4 | 27.4 | 61.0 | 82.3 | 21.3 | 213.4 | - | - |
| 06-44-308 | Ogallala | 272032 | 3915871 | - | 226.5 | 24.4 | 27.4 | 59.4 | 85.3 | 25.9 | 226.5 | - | - |
| 15-05 | Ogallala | 267566 | 3915133 | 1075.8 | 234.4 | 21.9 | 25.0 | 79.2 | 97.5 | 18.3 | 255.1 | - | - |
| 15-06 | Ogallala | 267536 | 3913793 | 1080.8 | 197.8 | 24.7 | 30.5 | 86.0 | 123.7 | 37.7 | 199.6 | - | - |
| 15-11 | Ogallala | 268407 | 3913601 | 1077.2 | - | - | - | - | - | - | - | - | - |
| 15-16 | Ogallala | 268498 | 3915003 | 1074.5 | 233.2 | 21.3 | 24.4 | 77.7 | 87.2 | 9.5 | - | - | - |
| 15-17 | Ogallala | 267541 | 3915014 | 1076.6 | 274.3 | 27.4 | 29.3 | 86.6 | - | - | 255.1 | 122.5 | 132.6 |
| 15-20 | Ogallala | 268458 | 3914028 | 1077.9 | 220.1 | - | - | - | - | - | - | - | - |
| 15-26 | Ogallala | 267807 | 3914470 | 1079.4 | 240.2 | 23.8 | 25.0 | 83.8 | 94.8 | 11.0 | 234.7 | - | - |
| 15-32 | Ogallala | 268798 | 3914474 | 1077.4 | 240.2 | 20.7 | 23.8 | 74.7 | 95.4 | 20.7 | 236.2 | 149.4 | 86.9 |
| CW-SB01 | Perched | 269745 | 3908931 | 1073.4 | 94.5 | 18.6 | 20.7 | 84.1 | - | - | - | 86.9 | -2.7 |
| CW-SB02 | Perched | 269742 | 3908854 | 1073.0 | 94.5 | 18.0 | 20.1 | 85.6 | - | - | - | - | 0.0 |
| FPOP-BG-MW13 | Perched | 267001 | 3909256 | - | 87.5 | 18.3 | 21.3 | 84.4 | - | - | - | - | - |
| FPOP-BG-MW14 | Perched | 267065 | 3909081 | - | 85.3 | 18.3 | 21.3 | 81.1 | - | - | - | - | - |
| FPOP-CB-MW-08 | Ogallala | 267007 | 3908795 | 1074.1 | 111.3 | 18.3 | 19.5 | 83.8 | 88.4 | 4.6 | - | - | - |
| FPOP-CB-MW15 | Ogallala | 267036 | 3908913 | - | 112.8 | 18.3 | 21.3 | 81.7 | 86.3 | 4.6 | 0.0 | - | - |
| FPOP-LF-MW-07 | Ogallala | 266390 | 3908750 | 1066.2 | 106.1 | - | 24.7 | 71.6 | 77.1 | 5.5 | - | - | - |
| FPOP-Z9-MW-01 | Perched | 262957 | 3909661 | - | 86.0 | 21.3 | 24.4 | - | - | - | - | - | - |
| FPOP-Z9-MW-01A | Perched | 262958 | 3909667 | 1082.8 | 97.5 | 21.3 | 24.4 | 87.8 | - | - | - | - | - |
| FPOP-Z9-MW-02 | Perched | 263119 | 3910323 | 1084.0 | 97.5 | 26.2 | 29.0 | 94.8 | - | - | - | 92.2 | - |
| FPOP-Z9-MW-03 | Perched | 263455 | 3910361 | 1083.6 | 99.1 | 26.8 | 29.0 | 94.5 | - | - | - | 91.7 | - |

| | | | | | | | | | | | | | |
|---|---|---|---|---|---|---|---|---|---|---|---|---|---|
| FPOP-Z9-MW-04 | Perched | 262961 | 3910149 | 1082.8 | 93.0 | 25.0 | 27.4 | 92.4 | - | - | - | - | - |
| FPOP-Z9-MW-05 | Perched | 263212 | 3909941 | 1082.0 | 93.0 | 25.0 | 27.4 | 92.4 | - | - | - | - | - |
| FPOP-Z9-MW-06 | Perched | 263230 | 3910103 | 1082.0 | 93.0 | 24.4 | 27.4 | 93.0 | - | - | - | - | - |
| FPOP-Z9-MW-07 | Perched | 263156 | 3909885 | 1081.7 | 93.0 | 24.4 | 27.4 | 92.0 | - | - | - | - | - |
| FPOP-Z9-MW-08 | Ogallala | 262999 | 3909594 | 1081.9 | 111.3 | 24.4 | 27.4 | 92.0 | 96.0 | 4.0 | - | - | - |
| FPOP-Z9-MW-09 | Ogallala | 263633 | 3910780 | 1083.0 | 111.3 | 25.9 | 29.0 | 93.9 | 94.5 | 0.6 | - | - | - |
| FPOP-Z9-MW10 | Ogallala | 263614 | 3910466 | - | 110.3 | 27.4 | 30.5 | 95.4 | 96.9 | 1.5 | - | - | - |
| FPOP-Z9-MW11 | Ogallala | 263390 | 3910504 | - | 107.3 | 25.9 | 29.0 | 98.5 | 99.1 | 0.6 | - | - | - |
| FPOP-Z9-MW12 | Ogallala | 262511 | 3909377 | - | 104.5 | 21.3 | 24.4 | 86.0 | 88.4 | 2.4 | - | - | - |
| OW-WR-46 | Ogallala | 265254 | 3914967 | 1089.0 | 151.5 | 23.2 | 24.7 | 75.3 | 88.4 | 13.1 | - | 134.1 | - |
| OW-WR-47 | Ogallala | 264961 | 3914686 | 1088.7 | 151.5 | 22.6 | 24.1 | 77.7 | 92.0 | 14.3 | - | 149.0 | - |
| OW-WR-48 | Ogallala | 265277 | 3914672 | 1088.7 | 151.5 | 21.9 | 23.8 | 76.8 | 86.6 | 9.8 | - | 140.2 | - |
| OW-WR-52 | Ogallala | 268509 | 3915057 | 1074.9 | 139.0 | 21.6 | 24.7 | 77.7 | 87.2 | 9.5 | - | - | - |
| OW-WR-54 | Perched | 267236 | 3907902 | 1073.5 | 98.8 | 17.1 | 20.1 | 75.6 | - | - | - | - | 0.0 |
| PTX01-1001 | Perched | 265007 | 3914146 | 1087.0 | 91.2 | 29.6 | 31.4 | 90.2 | 97.8 | 7.6 | - | 90.1 | 0.2 |
| PTX01-1002 | Perched | 264368 | 3914148 | 1085.1 | 85.3 | 25.9 | 26.5 | 84.1 | 96.6 | 12.5 | - | 83.5 | 0.9 |
| PTX01-1003 | Ogallala | 264846 | 3914505 | 1087.7 | 152.4 | 26.2 | 29.0 | 85.0 | 106.4 | 21.4 | - | 139.3 | 0.0 |
| PTX01-1004 | Perched | 265058 | 3914488 | 1088.6 | 84.3 | 22.9 | 24.4 | 84.1 | 93.0 | 8.9 | - | - | 0.0 |
| PTX01-1005 | Ogallala | 265057 | 3914498 | 1088.5 | 249.3 | 22.9 | 24.4 | 84.1 | 93.0 | 8.9 | 245.1 | 145.4 | 99.7 |
| PTX01-1006 | Perched | 265156 | 3914412 | 1088.3 | 89.9 | 22.6 | 23.8 | 88.4 | - | - | - | - | 0.0 |
| PTX01-1007 | Perched | 265119 | 3914653 | 1088.8 | 79.6 | 22.9 | 24.4 | 77.7 | - | - | - | - | 0.0 |
| PTX01-1008 | Perched | 264818 | 3914499 | 1087.1 | 85.3 | 26.2 | 27.7 | 84.1 | - | - | - | - | 0.0 |
| PTX01-1009 | Perched | 265003 | 3913956 | 1087.1 | 88.1 | 29.6 | 31.4 | 87.5 | - | - | - | - | 0.0 |
| PTX01-1010 | Ogallala | 265016 | 3914681 | 1090.0 | 259.1 | 21.9 | 24.1 | 78.3 | 92.0 | 13.7 | 256.6 | 145.5 | 111.2 |
| PTX01-1011 | Ogallala | 264836 | 3914686 | 1089.0 | 243.2 | 23.8 | 25.6 | 79.9 | 99.4 | 19.5 | 239.6 | 144.2 | 95.3 |
| PTX01-1012 | Ogallala | 265667 | 3915234 | 1088.8 | 275.2 | 22.9 | 24.4 | 73.8 | 87.2 | 13.4 | 271.0 | 150.1 | 120.9 |
| PTX01-1013 | Ogallala | 264542 | 3915248 | 1091.8 | 272.8 | 21.3 | 27.4 | 74.7 | 86.9 | 12.2 | 263.0 | 147.3 | 115.8 |
| PTX01-1014A | Perched | 264623 | 3914023 | 1085.3 | 92.0 | 22.9 | 24.7 | 79.9 | - | - | - | - | 0.0 |
| PTX01-1015 | NA | 264794 | 3914494 | 1086.3 | 82.9 | 24.4 | 25.9 | - | - | - | - | - | 0.0 |
| PTX01-1016 | NA | 264855 | 3914510 | 1087.9 | 84.1 | 26.5 | 28.7 | - | - | - | - | - | 0.0 |
| PTX01-1017 | NA | 264864 | 3914433 | 1087.3 | 84.4 | 25.3 | 27.7 | - | - | - | - | - | 0.0 |
| PTX01-1018 | NA | 264850 | 3914508 | 1087.8 | 141.7 | 24.4 | 28.0 | 84.7 | 106.7 | 22.0 | - | - | 0.0 |
| PTX01-1019 | NA | 264869 | 3914641 | 1088.4 | 84.1 | 22.3 | 23.8 | 82.3 | - | - | - | - | 0.0 |
| PTX01-1034 | NA | 264807 | 3914602 | 1088.4 | 84.1 | 25.0 | 25.6 | 79.2 | - | - | - | - | 0.0 |
| PTX01-1035 | NA | 264987 | 3914496 | 1088.4 | 84.4 | 22.6 | 24.5 | 83.5 | - | - | - | - | 0.0 |
| PTX01-1036 | NA | 264927 | 3914752 | 1088.5 | 78.3 | 22.9 | 23.6 | - | - | - | - | - | 0.0 |
| PTX01-2062 | NA | 265080 | 3914410 | 1088.1 | 143.1 | - | - | 79.2 | 96.0 | 16.8 | - | - | 0.0 |
| PTX04-1001 | Perched | 268340 | 3914883 | 1073.9 | 72.8 | 21.9 | 23.5 | 72.1 | - | - | - | 67.2 | 4.8 |
| PTX04-1002 | Perched | 268448 | 3914829 | 1075.0 | 74.0 | 23.8 | 25.9 | 72.8 | - | - | - | 68.4 | 4.5 |

| | | | | | | | | | | | | | |
|---|---|---|---|---|---|---|---|---|---|---|---|---|---|
| PTX06-0020 | Perched | 269018 | 3912315 | 1082.7 | 80.2 | 21.3 | 22.9 | 79.6 | - | - | - | 75.1 | 4.5 |
| PTX06-0021 | Perched | 268990 | 3912846 | 1078.5 | 81.4 | 19.8 | 20.7 | 74.4 | - | - | - | 73.4 | 1.0 |
| PTX06-0022 | Perched | 270141 | 3910742 | 1075.5 | 83.5 | 23.2 | 25.6 | 83.2 | - | - | - | - | 0.0 |
| PTX06-0023 | Perched | 269751 | 3911964 | 1076.0 | 78.6 | 22.6 | 24.4 | 78.6 | - | - | - | - | - |
| PTX06-1013 | Perched | 268963 | 3912348 | 1079.1 | 82.3 | 21.3 | 24.4 | 78.0 | - | - | - | 76.0 | 2.0 |
| PTX06-1014 | Perched | 268909 | 3909620 | 1075.8 | 88.4 | 22.9 | 24.4 | 85.2 | - | - | - | 82.5 | 2.9 |
| PTX06-1015 | Perched | 268899 | 3909160 | 1074.9 | 90.8 | 24.4 | 25.9 | 86.9 | - | - | - | 84.6 | 2.3 |
| PTX06-1017 | Perched | 268909 | 3909632 | 1075.8 | 86.6 | 22.9 | 24.4 | 85.3 | - | - | - | 81.9 | 3.5 |
| PTX06-1018 | Perched | 268936 | 3910385 | 1076.9 | 91.0 | 22.6 | 24.4 | 90.2 | - | - | - | 79.9 | 10.3 |
| PTX06-1019 | Perched | 268155 | 3908971 | 1074.5 | 89.9 | 18.3 | 20.4 | 86.3 | - | - | - | 83.7 | 2.6 |
| PTX06-1020 | Perched | 268440 | 3908061 | 1072.0 | 93.9 | 19.5 | 21.0 | 82.9 | - | - | - | - | 0.0 |
| PTX06-1021 | Perched | 265831 | 3909390 | 1076.4 | 83.8 | 20.7 | 22.6 | 82.6 | - | - | - | 81.5 | 1.1 |
| PTX06-1022 | Perched | 268990 | 3913600 | 1078.3 | 91.4 | 19.8 | 21.6 | 75.0 | - | - | - | - | 0.0 |
| PTX06-1023 | Perched | 268681 | 3912516 | 1079.0 | 82.1 | 20.1 | 23.2 | 77.7 | - | - | - | 74.1 | 7.8 |
| PTX06-1024 | Perched | 269361 | 3910355 | 1076.5 | 88.1 | 23.2 | 26.2 | 87.2 | - | - | - | 82.2 | 4.6 |
| PTX06-1025 | Perched | 269338 | 3909341 | 1074.8 | 91.1 | 21.3 | 24.4 | 88.4 | - | - | - | 85.0 | 3.4 |
| PTX06-1026 | Perched | 269737 | 3909579 | 1075.0 | 91.4 | 20.7 | 23.8 | 86.0 | - | - | - | - | 0.0 |
| PTX06-1027 | Perched | 269341 | 3908785 | 1073.2 | 91.4 | 27.4 | 29.6 | 86.9 | 91.4 | 4.5 | - | - | 0.0 |
| PTX06-1028 | Perched | 269179 | 3910672 | 1077.2 | 91.4 | 22.9 | 25.0 | 90.2 | - | - | - | - | 0.0 |
| PTX06-1029 | Perched | 269415 | 3908982 | 1073.8 | 88.1 | 20.1 | 22.9 | 87.0 | - | - | - | 85.2 | 1.8 |
| PTX06-1030 | Perched | 269186 | 3909577 | 1075.7 | 88.1 | 22.9 | 26.5 | 86.4 | - | - | - | 85.9 | 0.5 |
| PTX06-1031 | Perched | 269174 | 3909071 | 1074.4 | 90.8 | 20.1 | 22.6 | 87.2 | - | - | - | 84.8 | 2.3 |
| PTX06-1032 | Ogallala | 269567 | 3908831 | 1073.6 | 131.2 | 20.1 | 22.9 | 87.8 | 90.5 | 2.7 | 116.4 | 115.7 | 0.8 |
| PTX06-1033 | Ogallala | 268594 | 3910987 | 1078.5 | 169.5 | 22.6 | 24.4 | 85.3 | 97.5 | 12.2 | 166.1 | 79.2 | 6.1 |
| PTX06-1034 | Perched | 269741 | 3908778 | 1073.2 | 88.1 | 24.1 | 27.1 | 87.5 | - | - | - | 85.0 | 2.5 |
| PTX06-1036 | Perched | 267320 | 3908845 | 1076.1 | 88.1 | 18.9 | 20.7 | 86.9 | - | - | - | 86.0 | 0.9 |
| PTX06-1037 | Perched | 268213 | 3908743 | 1074.1 | 85.6 | 15.8 | 17.4 | 84.7 | - | - | - | 84.6 | 0.2 |
| PTX06-1038 | Perched | 268963 | 3911235 | 1078.4 | 86.0 | 22.3 | 23.8 | 85.5 | - | - | - | 79.0 | 6.5 |
| PTX06-1039A | Perched | 268956 | 3910883 | 1078.0 | 85.3 | 25.0 | 26.5 | 84.0 | - | - | - | 80.3 | 3.7 |
| PTX06-1040 | Perched | 268949 | 3910576 | 1077.7 | 87.2 | 24.7 | 26.8 | 86.3 | - | - | - | 80.7 | 5.5 |
| PTX06-1041 | Perched | 268942 | 3910381 | 1077.3 | 91.1 | 22.6 | 24.4 | 90.5 | - | - | - | 79.9 | 10.7 |
| PTX06-1042 | Perched | 268930 | 3909819 | 1076.3 | 87.0 | 25.3 | 27.1 | 85.6 | - | - | - | 80.5 | 5.2 |
| PTX06-1044 | Ogallala | 268660 | 3912497 | 1078.8 | 189.6 | 21.6 | 24.4 | 76.2 | 87.2 | 11.0 | 186.8 | 145.1 | 42.1 |
| PTX06-1045 | Perched | 268531 | 3908738 | 1074.1 | 86.3 | 16.8 | 19.8 | 85.6 | - | - | - | 85.3 | 0.1 |
| PTX06-1046 | Perched | 268898 | 3908719 | 1073.6 | 89.0 | 25.0 | 25.9 | 88.1 | - | - | - | 84.6 | 3.7 |
| PTX06-1047A | Perched | 268903 | 3908668 | 1073.7 | 87.2 | 25.9 | 27.4 | 86.3 | - | - | - | 84.9 | 1.4 |
| PTX06-1048A | Perched | 268495 | 3913239 | 1078.3 | 74.1 | 17.4 | 18.6 | 73.8 | - | - | - | 71.3 | 2.5 |
| PTX06-1051 | Perched | 267843 | 3908779 | 1075.9 | 96.3 | 19.5 | 21.3 | 86.0 | 90.8 | 4.8 | - | - | 0.0 |
| PTX06-1052 | Perched | 267480 | 3909300 | 1077.3 | 88.4 | 20.4 | 21.9 | 87.8 | - | - | - | 83.5 | 5.3 |

| | | | | | | | | | | | | | |
|---|---|---|---|---|---|---|---|---|---|---|---|---|---|
| PTX06-1053 | Perched | 266708 | 3909232 | 1072.0 | 79.2 | 20.7 | 22.9 | 77.7 | - | - | - | 76.0 | 2.7 |
| PTX06-1054 | Ogallala | 268205 | 3908752 | 1074.9 | 110.9 | 16.2 | 17.7 | 86.0 | 93.3 | 7.3 | 106.2 | - | 0.0 |
| PTX06-1056 | Ogallala | 268908 | 3909473 | 1076.1 | 152.4 | 18.9 | 21.9 | 83.5 | 91.7 | 8.2 | - | 120.1 | - |
| PTX06-1057A | Ogallala | 264702 | 3913696 | 1085.8 | 243.2 | 20.1 | 22.6 | 78.6 | 96.0 | 17.4 | 243.2 | 136.5 | 105.8 |
| PTX06-1058 | Ogallala | 263194 | 3911174 | 1086.7 | 162.5 | 25.9 | 27.4 | 83.8 | 91.4 | 7.6 | 160.9 | 120.2 | 41.6 |
| PTX06-1059 | Ogallala | 264186 | 3911366 | 1080.2 | 165.5 | 21.3 | 22.9 | 85.3 | 95.4 | 10.1 | 164.0 | 121.8 | 43.0 |
| PTX06-1060 | Ogallala | 261989 | 3910854 | 1087.8 | 161.5 | 21.3 | 24.4 | 85.3 | 96.0 | 10.7 | 152.4 | 109.5 | 44.5 |
| PTX06-1061 | Ogallala | 263528 | 3915264 | 1093.8 | 267.0 | 19.8 | 21.9 | 75.6 | 85.3 | 9.7 | 262.1 | 146.6 | 116.2 |
| PTX06-1062A | Ogallala | 265762 | 3914750 | 1087.8 | 275.8 | 21.3 | 22.7 | 73.8 | 84.1 | 10.3 | 271.3 | 147.1 | 127.9 |
| PTX06-1063A | Ogallala | 267696 | 3915865 | 1073.2 | 244.8 | 21.3 | 22.9 | 71.6 | 79.2 | 7.6 | 242.6 | 147.7 | 96.7 |
| PTX06-1064 | Ogallala | 266655 | 3915299 | 1085.2 | 241.4 | 19.8 | 21.3 | 77.7 | 86.9 | 9.2 | - | 149.4 | 91.7 |
| PTX06-1065 | Ogallala | 265849 | 3916032 | 1087.7 | 236.5 | 21.9 | 23.2 | 79.9 | 87.2 | 7.3 | - | 151.1 | 85.4 |
| PTX06-1066 | Ogallala | 265721 | 3915283 | 1088.2 | 268.8 | 23.2 | 24.7 | 73.8 | 86.9 | 13.1 | 268.8 | 148.6 | 120.0 |
| PTX06-1067 | Ogallala | 262637 | 3915443 | 1096.0 | 256.6 | 19.8 | 22.9 | 83.8 | 94.5 | 10.7 | 256.0 | 146.8 | 109.8 |
| PTX06-1068 | Ogallala | 268941 | 3915181 | 1077.1 | 245.4 | 23.8 | 26.8 | 75.3 | 91.4 | 16.1 | 242.6 | 152.9 | 89.7 |
| PTX06-1069 | Perched | 269748 | 3911964 | 1075.8 | 78.3 | 22.9 | 24.7 | 78.3 | - | - | - | 76.7 | 1.6 |
| PTX06-1070 | Perched | 268928 | 3909725 | 1075.6 | 85.3 | 22.6 | 24.4 | 86.3 | - | - | - | 81.6 | 4.6 |
| PTX06-1071 | Perched | 268695 | 3915144 | 1075.2 | 79.9 | 22.3 | 24.4 | 74.1 | - | - | - | 67.4 | 11.9 |
| PTX06-1074 | Ogallala | 262051 | 3912996 | 1089.2 | 201.2 | 22.9 | 25.9 | 88.4 | 106.7 | 18.3 | 187.1 | 125.8 | 0.0 |
| PTX06-1075 | Ogallala | 264860 | 3909264 | 1080.3 | 126.5 | 23.2 | 25.0 | 86.9 | 93.9 | 7.0 | 120.1 | - | - |
| PTX06-1076 | Ogallala | 266932 | 3909015 | 1074.6 | 113.1 | 20.1 | 21.6 | 80.8 | 86.9 | 6.1 | 110.3 | 99.4 | 11.0 |
| PTX06-1078 | Perched | 268475 | 3914047 | 1078.6 | 79.7 | 22.6 | 24.4 | 73.2 | - | - | - | - | 0.0 |
| PTX06-1079 | Perched | 267828 | 3914463 | 1079.3 | 84.4 | 23.8 | 25.0 | 83.8 | - | - | - | - | 0.0 |
| PTX06-1080 | Perched | 267563 | 3914997 | 1077.1 | 87.5 | 27.4 | 29.3 | 86.6 | - | - | - | 81.7 | 5.2 |
| PTX06-1081 | Perched | 268257 | 3914451 | 1076.3 | 75.1 | 20.7 | 22.9 | 74.4 | - | - | - | 69.6 | 5.4 |
| PTX06-1085 | Perched | 264469 | 3911346 | 1076.0 | 87.6 | 18.3 | 19.8 | 86.9 | - | - | - | 80.4 | 6.5 |
| PTX06-1086 | Perched | 265182 | 3911153 | 1073.6 | 91.1 | - | - | 90.8 | - | - | - | 77.5 | 13.3 |
| PTX06-1087 | Perched | 264991 | 3911828 | 1076.0 | 88.4 | 15.2 | 17.7 | 87.2 | - | - | - | 79.1 | 8.1 |
| PTX06-1089 | Perched | 269826 | 3911162 | 1076.9 | 84.7 | 23.2 | 25.0 | 82.3 | - | - | - | - | 0.0 |
| PTX06-1090 | Perched | 270138 | 3910369 | 1075.3 | 83.8 | 22.9 | 24.4 | 81.4 | - | - | - | - | 0.0 |
| PTX06-1091 | Perched | 269770 | 3909976 | 1076.0 | 86.9 | 26.5 | 28.0 | 81.7 | - | - | - | - | 0.0 |
| PTX06-1092 | Perched | 269752 | 3909109 | 1074.1 | 87.8 | 21.9 | 24.4 | 85.0 | - | - | - | - | 0.0 |
| PTX06-1093 | Perched | 269485 | 3911068 | 1077.6 | 83.2 | 18.9 | 21.3 | 79.2 | - | - | - | - | 0.0 |
| PTX06-1094 | Perched | 268898 | 3908513 | 1073.4 | 85.0 | 25.0 | 26.5 | 86.3 | - | - | - | - | 0.0 |
| PTX06-9901 | Perched | 269770 | 3910366 | 1075.9 | 85.2 | 25.0 | 27.1 | 83.8 | - | - | - | 82.5 | 1.3 |
| PTX06-9902 | Perched | 269753 | 3909601 | 1075.3 | 86.1 | 21.3 | 24.4 | 85.0 | - | - | - | - | 0.0 |
| PTX06-9903 | Perched | 269761 | 3909970 | 1075.8 | 85.8 | 26.5 | 28.0 | 81.7 | - | - | - | - | 0.0 |
| PTX06-9904 | Perched | 269802 | 3908548 | 1071.8 | 88.2 | 24.7 | 27.1 | 86.9 | - | - | - | 84.6 | 2.3 |
| PTX06-9905 | Perched | 269793 | 3908152 | 1070.2 | 83.4 | 24.4 | 27.4 | 82.6 | - | - | - | - | 0.0 |

| | | | | | | | | | | | | | |
|---|---|---|---|---|---|---|---|---|---|---|---|---|---|
| PTX06-9906 | Perched | 269599 | 3908085 | 1069.4 | 85.2 | 24.4 | 27.4 | 82.9 | - | - | - | 81.4 | 1.5 |
| PTX06-9907 | Perched | 269772 | 3910460 | 1075.8 | 85.5 | 24.7 | 26.8 | 85.0 | - | - | - | 81.9 | 3.0 |
| PTX06-9908 | Perched | 269786 | 3911151 | 1076.5 | 94.3 | 22.3 | 24.1 | 82.3 | - | - | - | - | 0.0 |
| PTX06-9909 | Perched | 269098 | 3910955 | 1077.6 | 84.1 | 20.7 | 23.2 | 82.3 | - | - | - | 79.1 | 3.2 |
| PTX06-9910 | Perched | 269109 | 3911147 | 1077.7 | 83.2 | 20.7 | 23.2 | 80.8 | - | - | - | 78.3 | 2.4 |
| PTX06-9911 | Perched | 269095 | 3910758 | 1077.4 | 88.8 | 21.9 | 24.1 | 86.0 | - | - | - | 79.6 | 6.4 |
| PTX06-9912 | Perched | 269259 | 3911570 | 1077.5 | 82.3 | 22.3 | 24.4 | 78.9 | - | - | - | 76.2 | 2.7 |
| PTX06-9913 | Perched | 269292 | 3911263 | 1077.6 | 79.7 | 22.3 | 24.4 | 78.9 | - | - | - | 77.9 | 1.0 |
| PTX06-9914 | Perched | 269773 | 3910768 | 1076.4 | 85.6 | 22.3 | 24.4 | 82.9 | - | - | - | 81.6 | 1.3 |
| PTX06-9915 | Perched | 270078 | 3910367 | 1074.9 | 83.2 | 22.9 | 25.9 | 81.7 | - | - | - | - | 0.0 |
| PTX06-9916 | Perched | 269162 | 3910380 | 1077.1 | 84.7 | 23.2 | 25.0 | 83.8 | - | - | - | 79.8 | 4.1 |
| PTX06-9917 | Perched | 269485 | 3910894 | 1077.0 | 79.9 | 21.3 | 23.2 | 78.6 | - | - | - | - | 0.0 |
| PTX06-9918 | Perched | 270005 | 3908731 | 1072.2 | 89.0 | 25.9 | 28.0 | 87.8 | - | - | - | 85.1 | 2.7 |
| PTX06-9919 | Perched | 269210 | 3910999 | 1077.4 | 88.2 | 20.7 | 22.3 | 86.3 | - | - | - | 79.1 | 7.1 |
| PTX06-B01 | Perched | 268678 | 3912365 | 1078.4 | 91.0 | 20.7 | 23.8 | 77.1 | - | - | - | - | 0.0 |
| PTX06-B02 | Perched | 268676 | 3912274 | 1077.9 | 90.7 | 21.0 | 24.1 | 84.0 | - | - | - | - | 0.0 |
| PTX06-B04 | Perched | 268710 | 3912119 | 1077.8 | 91.0 | 22.3 | 25.3 | 78.6 | - | - | - | - | 0.0 |
| PTX06-B05 | Perched | 268684 | 3912592 | 1079.2 | 90.7 | 20.1 | 23.2 | 77.7 | - | - | - | - | 0.0 |
| PTX06-B06 | Perched | 268657 | 3911991 | 1077.4 | 92.4 | 22.3 | 25.3 | 79.2 | - | - | - | - | 0.0 |
| PTX06-B07 | Perched | 269097 | 3912142 | 1078.1 | 90.1 | 22.9 | 25.9 | 78.0 | - | - | - | - | 0.0 |
| PTX06-EW-04 | Perched | 268918 | 3910016 | 1076.7 | 89.3 | 22.9 | 25.0 | 85.3 | - | - | - | 81.2 | 4.1 |
| PTX06-EW-05 | Perched | 268786 | 3909603 | 1076.0 | 89.0 | 20.7 | 23.2 | 88.4 | - | - | - | 82.8 | 0.7 |
| PTX06-EW-06 | Perched | 268210 | 3909112 | 1075.3 | - | 23.2 | 25.0 | 86.3 | - | - | - | 83.7 | 2.5 |
| PTX06-EW-07 | Perched | 268920 | 3910155 | 1077.0 | 63.7 | 21.3 | 23.8 | 86.0 | - | - | - | 80.7 | 4.7 |
| PTX06-EW-08A | Perched | 268597 | 3909447 | 1076.1 | 88.7 | 19.8 | 24.1 | 86.0 | - | - | - | 84.1 | 1.9 |
| PTX06-EW-11 | Perched | 268903 | 3909343 | 1075.4 | 88.7 | 24.4 | 28.0 | 87.2 | - | - | - | 84.9 | 2.3 |
| PTX06-EW-12 | Perched | 268913 | 3909824 | 1076.4 | 87.2 | 24.4 | 26.2 | 86.6 | - | - | - | 81.7 | 4.9 |
| PTX06-EW-13 | Perched | 268906 | 3909465 | 1075.6 | 89.9 | 18.9 | 20.4 | 83.8 | - | - | - | 83.8 | 0.0 |
| PTX06-EW-14 | Perched | 268898 | 3909084 | 1074.5 | 87.5 | 24.4 | 25.9 | 86.3 | - | - | - | 84.5 | 1.7 |
| PTX06-EW-16 | Perched | 268959 | 3911103 | 1078.2 | 86.3 | 20.7 | 21.9 | 85.3 | - | - | - | 78.8 | 6.2 |
| PTX06-EW-17 | Perched | 268961 | 3911166 | 1078.3 | 85.3 | 19.8 | 21.3 | 84.1 | - | - | - | 78.2 | 5.9 |
| PTX06-EW-18 | Perched | 268942 | 3911257 | 1078.3 | 85.6 | 20.7 | 22.6 | 85.3 | - | - | - | 78.5 | 6.8 |
| PTX06-EW-19 | Perched | 268964 | 3911346 | 1078.4 | 85.3 | 22.9 | 25.9 | 84.4 | - | - | - | 78.0 | 6.4 |
| PTX06-EW-22A | Perched | 268340 | 3910276 | 1077.1 | 90.8 | 22.6 | 25.0 | 90.2 | - | - | - | 77.8 | 12.4 |
| PTX06-EW-23A | Perched | 268765 | 3910269 | 1077.3 | 92.4 | 21.3 | 23.8 | 90.8 | - | - | - | 80.0 | 12.1 |
| PTX06-EW-26 | Perched | 268607 | 3910162 | 1077.2 | 91.1 | 21.3 | 23.5 | 91.1 | - | - | - | 80.3 | 10.8 |
| PTX06-EW-27 | Perched | 268918 | 3910094 | 1076.8 | 87.2 | 21.3 | 23.8 | 86.9 | - | - | - | 80.5 | 6.3 |
| PTX06-EW-30 | Perched | 268367 | 3909741 | 1076.3 | 89.9 | 23.5 | 24.4 | 88.7 | - | - | - | 81.1 | 7.6 |
| PTX06-EW-31 | Perched | 268386 | 3909847 | 1076.5 | 88.7 | 23.2 | 24.4 | 86.7 | - | - | - | 80.9 | 5.8 |

| | | | | | | | | | | | | | |
|---|---|---|---|---|---|---|---|---|---|---|---|---|---|
| PTX06-EW-32 | Perched | 268494 | 3909890 | 1076.6 | 90.2 | 22.6 | 24.4 | 86.9 | - | - | - | 80.9 | 6.0 |
| PTX06-EW-33 | Perched | 268601 | 3909917 | 1076.7 | 88.4 | 23.8 | 25.0 | 87.5 | - | - | - | 80.8 | 6.6 |
| PTX06-EW-34 | Perched | 268707 | 3909839 | 1076.6 | 87.8 | 21.9 | 23.8 | 86.3 | - | - | - | 81.1 | 6.7 |
| PTX06-EW-35 | Perched | 268914 | 3909926 | 1076.6 | 88.4 | 25.0 | 26.8 | 86.9 | - | - | - | 80.9 | 6.6 |
| PTX06-EW-37 | Perched | 267629 | 3909512 | 1077.0 | 91.4 | 24.7 | 25.6 | 90.8 | - | - | - | 82.0 | 5.8 |
| PTX06-EW-38C | Perched | 267754 | 3909444 | 1076.6 | 91.4 | 24.1 | 25.6 | 89.0 | - | - | - | 82.0 | 7.0 |
| PTX06-EW-39 | Perched | 267840 | 3909388 | 1076.1 | 89.0 | 23.5 | 25.6 | 87.5 | - | - | - | 82.4 | 5.1 |
| PTX06-EW-40 | Perched | 267867 | 3909262 | 1075.9 | 88.1 | 24.4 | 25.9 | 87.8 | - | - | - | 82.6 | 5.2 |
| PTX06-EW-41 | Perched | 267988 | 3909198 | 1075.6 | 87.8 | 21.0 | 23.8 | 86.9 | - | - | - | 83.2 | 3.7 |
| PTX06-EW-42A | Perched | 268074 | 3909242 | 1075.5 | 86.6 | 22.6 | 24.4 | 86.6 | - | - | - | 82.9 | 3.7 |
| PTX06-EW-43 | Perched | 268128 | 3909320 | 1075.7 | 87.8 | 23.8 | 25.0 | 87.8 | - | - | - | 82.2 | 5.0 |
| PTX06-EW-44 | Perched | 268178 | 3909440 | 1075.9 | 87.8 | 22.6 | 25.0 | 87.8 | - | - | - | 82.0 | 5.8 |
| PTX06-EW-45 | Perched | 268239 | 3909470 | 1075.8 | 86.6 | 21.9 | 23.8 | 86.6 | - | - | - | 82.2 | 4.3 |
| PTX06-EW-46 | Perched | 268332 | 3909512 | 1076.0 | 88.4 | 22.6 | 24.4 | 87.8 | - | - | - | 82.3 | 5.5 |
| PTX06-EW-47 | Perched | 268411 | 3909605 | 1076.2 | 86.6 | 22.9 | 24.4 | 85.6 | - | - | - | 81.7 | 3.8 |
| PTX06-EW-48 | Perched | 268718 | 3909731 | 1076.4 | 88.4 | 21.3 | 23.8 | 86.6 | - | - | - | 81.8 | 4.7 |
| PTX06-EW-49 | Perched | 268470 | 3909552 | 1076.2 | 88.7 | 22.3 | 24.4 | 88.1 | - | - | - | 82.3 | 5.8 |
| PTX06-INJ-3 | Perched | 268757 | 3910034 | 1076.9 | 90.8 | 22.6 | 25.0 | 89.3 | - | - | - | 80.8 | 8.5 |
| PTX06-INJ-6 | Perched | 268534 | 3909704 | 1076.4 | 88.4 | 22.9 | 24.4 | 86.0 | - | - | - | 81.7 | 4.3 |
| PTX06-INJ-7 | Perched | 267993 | 3909397 | 1075.9 | 88.4 | 22.6 | 24.4 | 88.1 | - | - | - | 82.3 | 5.8 |
| PTX06-INJ-9 | Perched | 268391 | 3910058 | 1076.8 | 91.4 | 22.6 | 25.0 | 88.7 | - | - | - | - | - |
| PTX06-PZ01 | Perched | 268970 | 3911682 | 1078.4 | 83.2 | 19.2 | 20.4 | 80.5 | - | - | - | 76.4 | 4.1 |
| PTX06-PZ02 | Perched | 268974 | 3911835 | 1078.5 | 80.2 | 19.5 | 20.1 | 78.3 | - | - | - | 76.5 | 1.8 |
| PTX06-PZ03 | Perched | 268576 | 3911540 | 1078.6 | 84.7 | 22.3 | 25.0 | 84.1 | - | - | - | 75.9 | 8.2 |
| PTX06-PZ04 | Perched | 268299 | 3911653 | 1074.3 | 81.1 | 19.2 | 22.6 | 78.6 | - | - | - | 72.5 | 6.1 |
| PTX06-PZ05 | Perched | 268960 | 3911134 | 1078.3 | 86.9 | 22.3 | 24.4 | 85.0 | - | - | - | 82.5 | 2.6 |
| PTX06-PZ06 | Perched | 268936 | 3909996 | 1076.8 | 86.6 | 20.7 | 23.2 | 85.3 | - | - | - | 76.7 | 8.4 |
| PTX07-1O01 | Perched | 267412 | 3913491 | 1081.5 | 79.2 | 21.3 | 23.8 | 78.0 | - | - | - | 76.6 | 1.5 |
| PTX07-1O02 | Perched | 267591 | 3913616 | 1081.0 | 79.2 | 21.3 | 25.3 | 78.0 | - | - | - | 75.7 | 2.3 |
| PTX07-1O04 | Perched | 267481 | 3913578 | 1081.5 | 78.9 | 20.7 | 23.8 | 77.7 | - | - | - | 75.3 | 1.5 |
| PTX07-1O05 | Perched | 267522 | 3913620 | 1081.4 | 79.2 | 21.3 | 24.4 | 77.7 | - | - | - | 75.1 | 2.7 |
| PTX07-1O06 | Perched | 267505 | 3913746 | 1081.7 | 80.8 | 23.2 | 24.4 | 80.2 | - | - | - | 78.2 | 2.0 |
| PTX07-1Q01 | Perched | 264499 | 3909948 | 1080.2 | 91.6 | 20.4 | 21.9 | 90.2 | - | - | - | 86.5 | 3.7 |
| PTX07-1Q02 | Perched | 264382 | 3910125 | 1081.4 | 96.3 | 19.8 | 21.9 | 95.1 | - | - | - | 87.5 | 7.6 |
| PTX07-1Q03 | Perched | 264898 | 3910417 | 1077.0 | 94.8 | 20.7 | 23.8 | 93.6 | - | - | - | 82.4 | 11.2 |
| PTX07-1R01 | Ogallala | 264149 | 3912495 | 1087.9 | 182.9 | 17.1 | 19.8 | 81.4 | 90.8 | 9.4 | - | 133.5 | 56.6 |
| PTX07-1R02 | Perched | 264145 | 3912544 | - | 79.7 | 18.3 | 21.3 | - | - | - | - | - | - |
| PTX07-1R03 | Perched | 264075 | 3912602 | 1088.0 | 79.7 | 18.0 | 20.1 | 78.0 | - | - | - | 77.6 | 0.4 |
| PTX07-1R04 | Perched | 264171 | 3912654 | 1088.0 | 79.7 | 18.3 | 21.3 | 78.6 | - | - | - | 79.2 | -0.5 |

| | | | | | | | | | | | | | |
|---|---|---|---|---|---|---|---|---|---|---|---|---|---|
| PTX07-1R05 | Perched | 264087 | 3912491 | 1087.7 | 83.4 | 17.1 | 19.8 | 81.7 | - | - | - | - | 0.0 |
| PTX08-1010 | Perched | 268329 | 3915149 | 1072.9 | 73.2 | 24.4 | 27.4 | 72.2 | - | - | - | 64.8 | 7.4 |
| PTX08-1011A | Ogallala | 262415 | 3911316 | 1089.5 | 135.5 | 25.0 | 28.0 | 98.1 | 124.4 | 26.3 | - | 120.6 | 14.9 |
| PTX12-1016 | NA | 266415 | 3914007 | 1082.2 | - | - | - | - | - | - | - | - | 0.0 |
| PTX-BEG-2 | Ogallala | 265537 | 3910248 | 1079.2 | 128.0 | 21.3 | 23.2 | 95.1 | 98.5 | 3.4 | - | 115.5 | 21.6 |
| PTX-BEG-3 | Perched | 269032 | 3915184 | 1077.8 | 132.3 | 20.1 | 21.6 | 77.4 | 86.6 | 9.2 | - | 80.5 | 13.9 |
| PXSB03 | Perched | 266694 | 3909464 | 1072.4 | 81.7 | 18.9 | 20.7 | 78.5 | - | - | - | - | 0.0 |
| SVE-I-11 | NA | 264885 | 3914631 | 1088.1 | 80.8 | 24.4 | 27.4 | 80.8 | - | - | - | - | 0.0 |
| SVE-I-16 | NA | 264920 | 3914537 | 1088.1 | 85.3 | 25.3 | 27.4 | 85.3 | - | - | - | - | 0.0 |
| SVE-I-21 | NA | 264882 | 3914501 | 1088.1 | 86.9 | 24.4 | 25.9 | 86.1 | - | - | - | - | 0.0 |
| SVE-I-26 | NA | 264845 | 3914467 | 1088.1 | 86.6 | 25.9 | 33.2 | 86.3 | - | - | - | - | 0.0 |
| SVE-I-29 | NA | 264910 | 3914465 | 1088.1 | 83.8 | 27.4 | 30.5 | 83.8 | - | - | - | - | 0.0 |
| SVE-I-6 | NA | 264844 | 3914675 | 1088.1 | 83.8 | 24.4 | 29.0 | 81.7 | - | - | - | - | 0.0 |
| SVE-S-13 | NA | 264847 | 3914539 | 1088.1 | 83.8 | 27.1 | 29.9 | 83.8 | - | - | - | - | 0.0 |
| TT-SB02 | Perched | 267306 | 3908464 | 1075.2 | 87.9 | 19.5 | 21.0 | 84.7 | - | - | - | - | 0.0 |
| TT-SB03 | Perched | 268204 | 3908510 | 1073.2 | 84.7 | 16.8 | 18.9 | 84.4 | - | - | - | - | 0.0 |
| WI-3 | UNK | 267667 | 3914106 | 1080.2 | 211.8 | 27.4 | 30.5 | 80.8 | 100.6 | 19.8 | 210.9 | - | - |
| WI-5 | UNK | 268608 | 3912068 | 1076.6 | 216.4 | 21.0 | 24.1 | 78.0 | 109.7 | 31.7 | 199.6 | - | - |

*Page intentionally blank*

## APPENDIX B: GROUND-BASED TDEM SOUNDINGS

Locations and best-fit models for ground-based TDEM soundings (Paine, 2000). Locations on figure 12. Location coordinates given in Universal Transverse Mercator projection, zone 14 north, North American Datum of 1983. Locations derived from differential GPS.

TDEM 1

Date: September 19, 2000
UTM coordinates: x = 268827.54 m, y = 3908688.90 m
Surface elevation: 1073.15 m MSL

Best-fit model (fitting error 3.8 %)

| Layer | Resistivity (ohm-m) | Thickness (m) | Conductivity (mS/m) | Top (m) | Base (m) | Top elev. (m) | Base elev. (m) |
|---|---|---|---|---|---|---|---|
| 1 | 34.9 | 53.7 | 28.7 | 0.0 | 53.7 | 1073.2 | 1019.4 |
| 2 | 324.4 | 67.3 | 3.1 | 53.7 | 121.0 | 1019.4 | 952.2 |
| 3 | 6.4 | 155.5 | 121.0 | | | 952.2 | |

TDEM 2

Date: September 19, 2000
UTM coordinates: x = 264595.60 m, y = 3914359.72 m
Surface elevation: 1083.19 m MSL

Best-fit model (fitting error 1.5 %)

| Layer | Resistivity (ohm-m) | Thickness (m) | Conductivity (mS/m) | Top (m) | Base (m) | Top elev. (m) | Base elev. (m) |
|---|---|---|---|---|---|---|---|
| 1 | 9.3 | 24.8 | 107.3 | 0.0 | 24.8 | 1083.2 | 1058.4 |
| 2 | 2374.3 | 96.8 | 0.4 | 24.8 | 121.6 | 1058.4 | 961.6 |
| 3 | 22.1 | 45.3 | 121.6 | | | 961.6 | |

TDEM 3

Date: September 19, 2000
UTM coordinates: x = 268185.43 m, y = 3908662.10 m
Surface elevation: 1073.86 m MSL

Best-fit model (fitting error 7.1 %)

| Layer | Resistivity (ohm-m) | Thickness (m) | Conductivity (mS/m) | Top (m) | Base (m) | Top elev. (m) | Base elev. (m) |
|---|---|---|---|---|---|---|---|
| 1 | 21.5 | 26.7 | 46.6 | 0.0 | 26.7 | 1073.2 | 1046.5 |
| 2 | 190.6 | 84.7 | 5.2 | 26.7 | 111.4 | 1046.5 | 961.8 |
| 3 | 15.6 | 64.0 | 111.4 | | | 961.8 | |

TDEM 4

Date: September 20, 2000
UTM coordinates: x = 267391.77 m, y = 3908891.22 m
Surface elevation: 1075.71 m MSL

Best-fit model (fitting error 7.9 %)

| Layer | Resistivity (ohm-m) | Thickness (m) | Conductivity (mS/m) | Top (m) | Base (m) | Top elev. (m) | Base elev. (m) |
|---|---|---|---|---|---|---|---|
| 1 | 18.3 | 19.1 | 54.6 | 0.0 | 19.1 | 1075.7 | 1056.6 |
| 2 | 208.1 | 97.0 | 4.8 | 19.1 | 116.1 | 1056.6 | 959.7 |
| 3 | 14.8 | 67.5 | 116.1 | | | 959.7 | |

TDEM 5

Date: September 20, 2000
UTM coordinates: x = 268842.06 m, y = 3909356.32 m
Surface elevation: 1075.25 m MSL

Best-fit model (fitting error 3.9 %)

| Layer | Resistivity (ohm-m) | Thickness (m) | Conductivity (mS/m) | Top (m) | Base (m) | Top elev. (m) | Base elev. (m) |
|---|---|---|---|---|---|---|---|
| 1 | 32.3 | 46.6 | 30.9 | 0.0 | 46.6 | 1073.2 | 1026.5 |
| 2 | 110.4 | 51.5 | 9.1 | 46.6 | 98.1 | 1026.5 | 975.0 |
| 3 | 10.7 | 93.7 | 93.2 | 98.1 | 191.8 | 975.0 | 881.3 |
| 4 | 6.2 | 161.6 | 191.8 | | | 881.3 | |

TDEM 6

Date: September 20, 2000
UTM coordinates: x = 268783.29 m, y = 3909032.86 m
Surface elevation: 1074.22 m MSL

Best-fit model (fitting error 3.2 %)

| Layer | Resistivity (ohm-m) | Thickness (m) | Conductivity (mS/m) | Top (m) | Base (m) | Top elev. (m) | Base elev. (m) |
|---|---|---|---|---|---|---|---|
| 1 | 40.0 | 43.8 | 25.0 | 0.0 | 43.8 | 1074.2 | 1030.4 |
| 2 | 165.5 | 68.9 | 6.0 | 43.8 | 112.7 | 1030.4 | 961.6 |
| 3 | 12.6 | 103.3 | 79.7 | 112.7 | 216.0 | 961.6 | 858.3 |
| 4 | 5.3 | 189.0 | 216.0 | | | 858.3 | |

TDEM 7

Date: September 20, 2000
UTM coordinates: x = 268436.07 m, y = 3910128.05 m
Surface elevation: 1076.71 m MSL

Best-fit model (fitting error 12.1 %)

| Layer | Resistivity (ohm-m) | Thickness (m) | Conductivity (mS/m) | Top (m) | Base (m) | Top elev. (m) | Base elev. (m) |
|---|---|---|---|---|---|---|---|
| 1 | 34.1 | 35.1 | 29.3 | 0.0 | 35.1 | 1076.7 | 1041.7 |
| 2 | 76.2 | 100.4 | 13.1 | 35.1 | 135.5 | 1041.7 | 941.3 |
| 3 | 8.7 | 90.6 | 115.3 | 135.5 | 226.1 | 941.3 | 850.6 |
| 4 | 44.8 | 22.3 | 226.1 | | | 850.6 | |

TDEM 8

Date: September 21, 2000
UTM coordinates: x = 265047.28 m, y = 3914231.26 m
Surface elevation: 1087.49 m MSL

Best-fit model (fitting error 1.9 %)

| Layer | Resistivity (ohm-m) | Thickness (m) | Conductivity (mS/m) | Top (m) | Base (m) | Top elev. (m) | Base elev. (m) |
|---|---|---|---|---|---|---|---|
| 1 | 36.5 | 52.9 | 27.4 | 0.0 | 52.9 | 1087.5 | 1034.6 |
| 2 | 329.7 | 38.8 | 3.0 | 52.9 | 91.7 | 1034.6 | 995.8 |
| 3 | 5.7 | 17.9 | 174.5 | 91.7 | 109.6 | 995.8 | 977.9 |
| 4 | 314.1 | 126.6 | 3.2 | 109.6 | 236.2 | 977.9 | 851.3 |
| 5 | 19.1 | 52.2 | 236.2 | | | 851.3 | |

TDEM 9

Date: September 21, 2000
UTM coordinates: x = 264289.55 m, y = 3913980.23 m
Surface elevation: 1086.05 m MSL

Best-fit model (fitting error 1.5 %)

| Layer | Resistivity (ohm-m) | Thickness (m) | Conductivity (mS/m) | Top (m) | Base (m) | Top elev. (m) | Base elev. (m) |
|---|---|---|---|---|---|---|---|
| 1 | 24.9 | 43.1 | 40.1 | 0.0 | 43.1 | 1086.1 | 1043.0 |
| 2 | 52.2 | 113.2 | 19.2 | 43.1 | 156.3 | 1043.0 | 929.8 |
| 3 | 16.1 | 62.3 | 156.3 | | | 929.8 | |

TDEM 10

Date: September 21, 2000
UTM coordinates: x = 268763.71 m, y = 3911187.08 m
Surface elevation: 1078.43 m MSL

Best-fit model (fitting error 4.0 %)

| Layer | Resistivity (ohm-m) | Thickness (m) | Conductivity (mS/m) | Top (m) | Base (m) | Top elev. (m) | Base elev. (m) |
|---|---|---|---|---|---|---|---|
| 1 | 42.4 | 125.3 | 23.6 | 0.0 | 125.3 | 1078.4 | 953.1 |
| 2 | 18.4 | 54.3 | 125.3 | | | 953.1 | |

# APPENDIX C: CONDUCTIVITY-DEPTH SLICES

*Page intentionally blank*

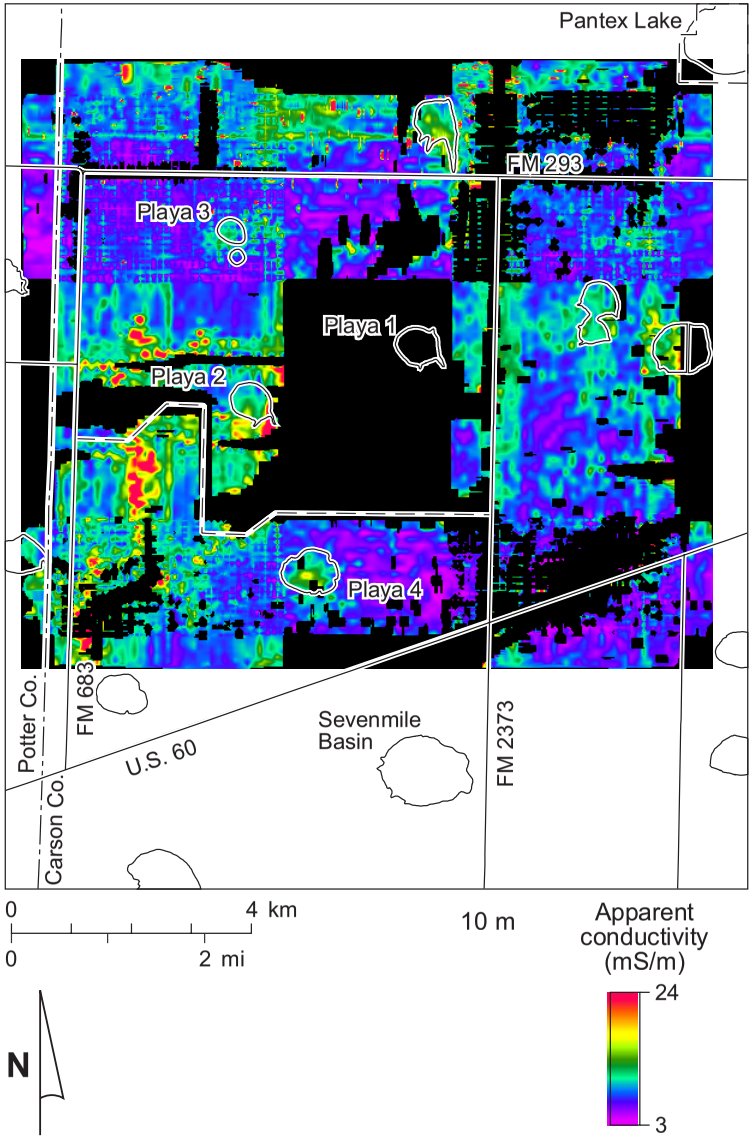


Figure C1. Apparent conductivity at a depth of 10 m.

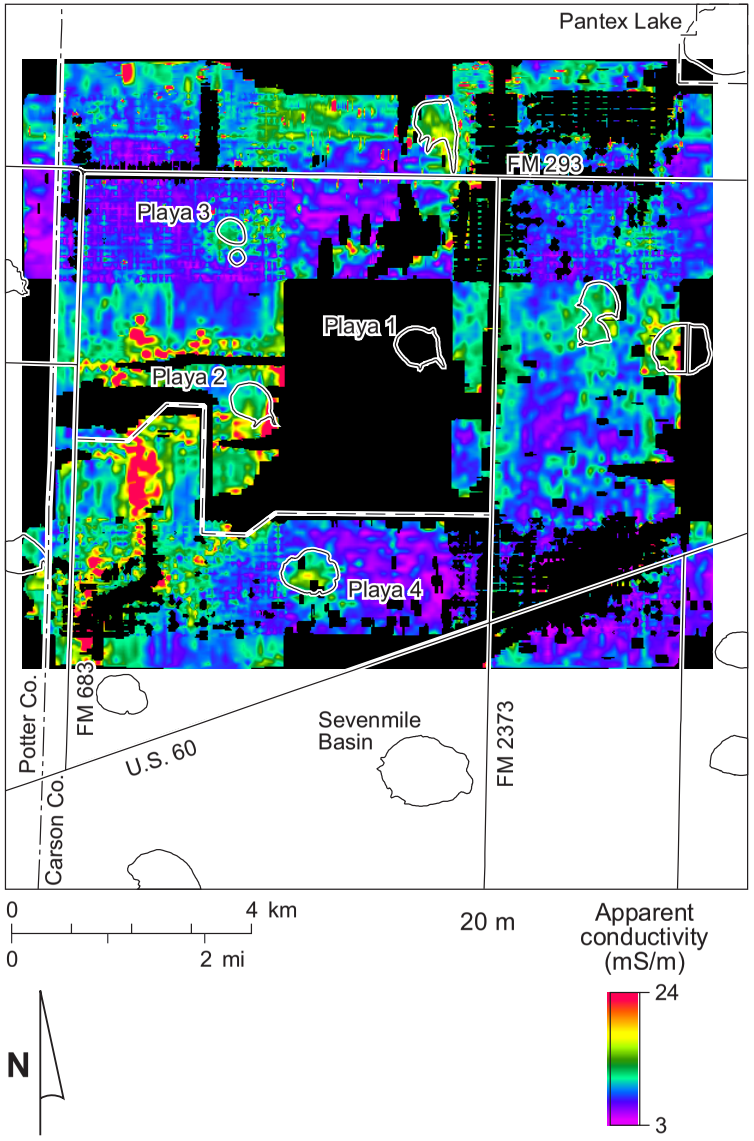


Figure C2. Apparent conductivity at a depth of 20 m.

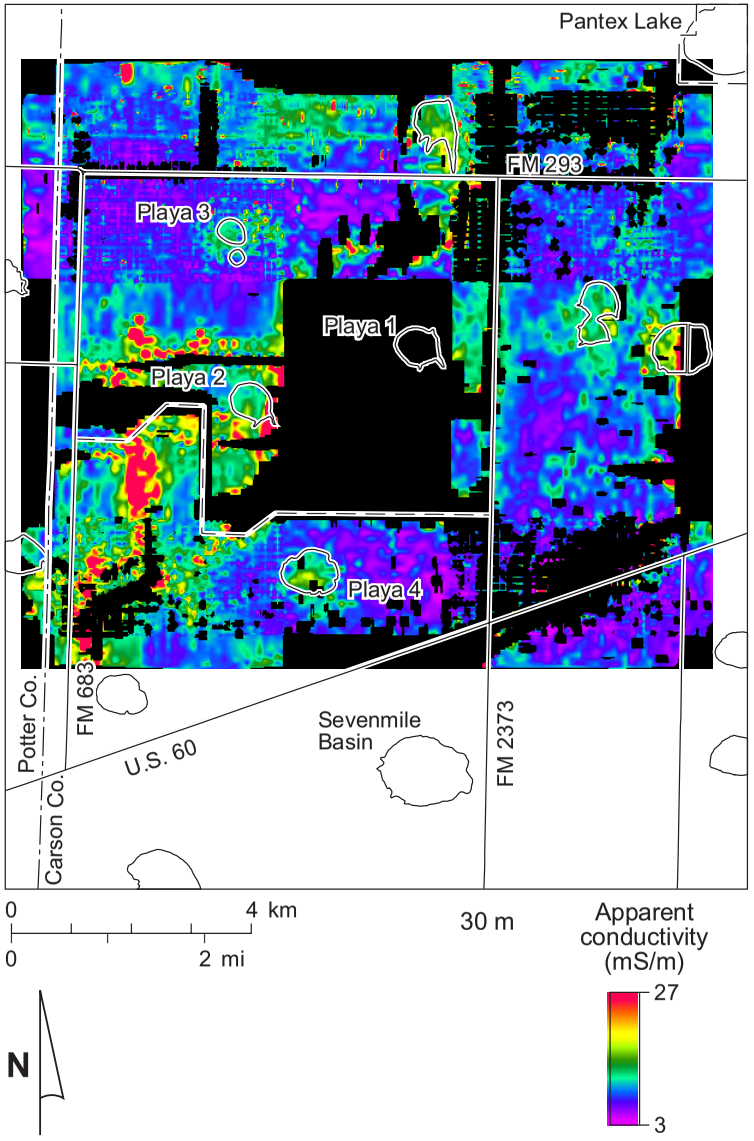


Figure C3. Apparent conductivity at a depth of 30 m.

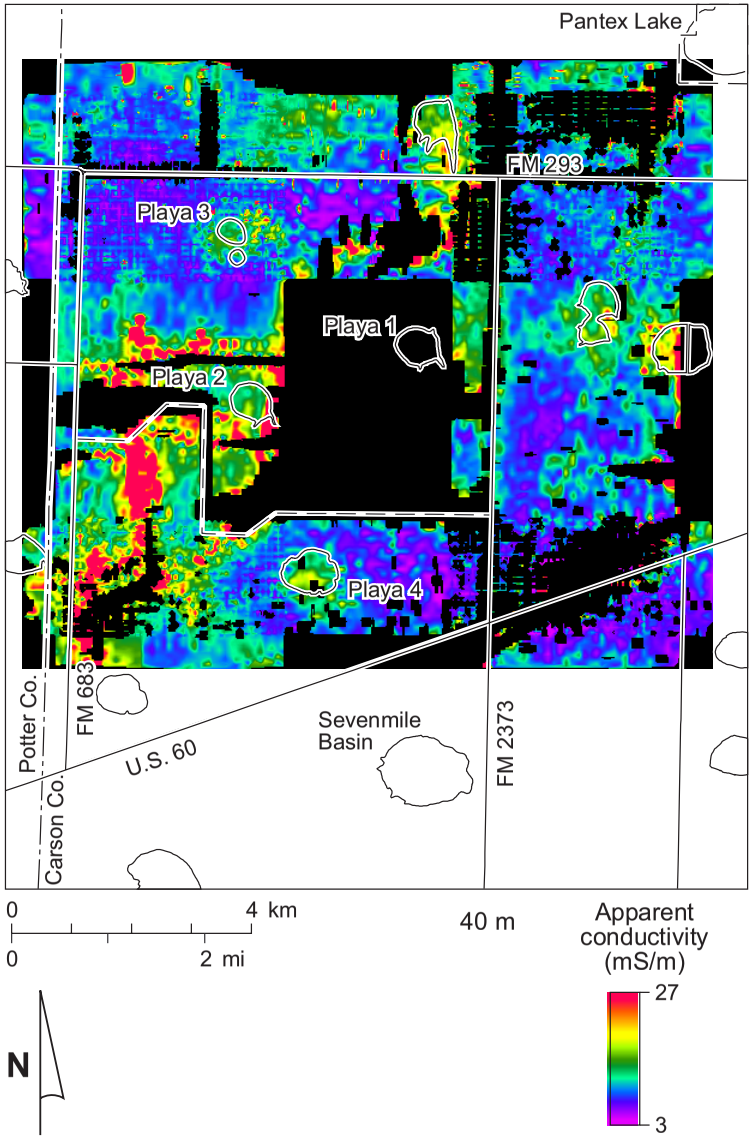


Figure C4. Apparent conductivity at a depth of 40 m.

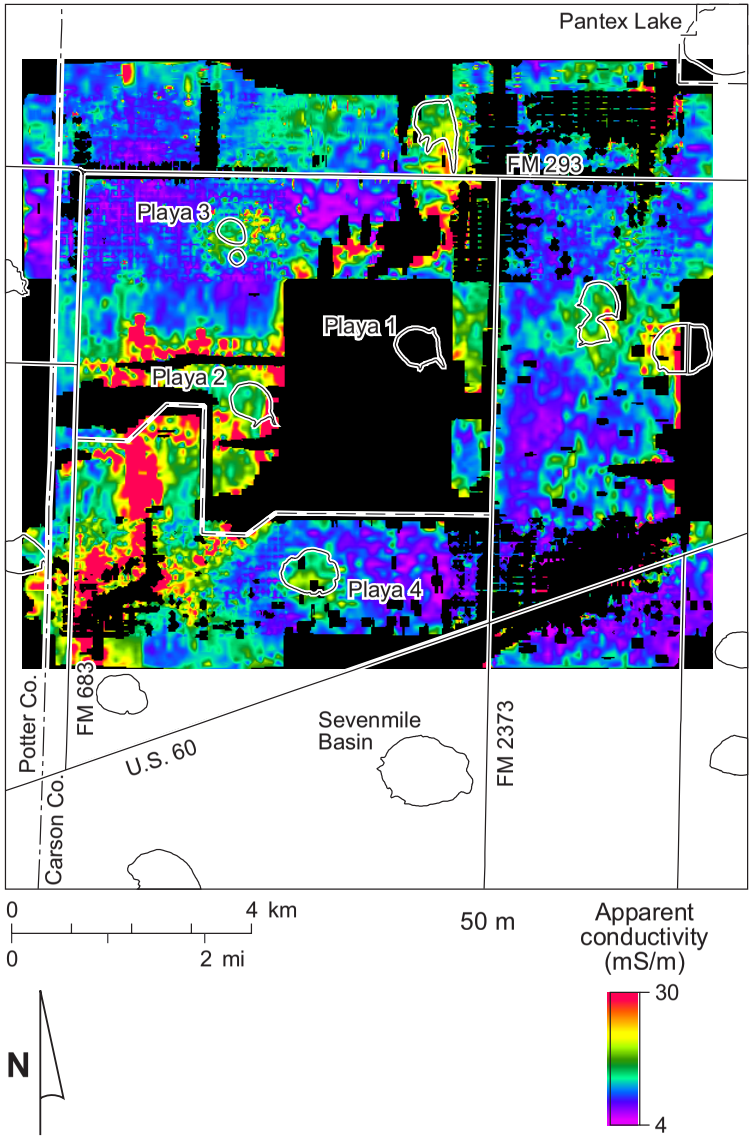


Figure C5. Apparent conductivity at a depth of 50 m.

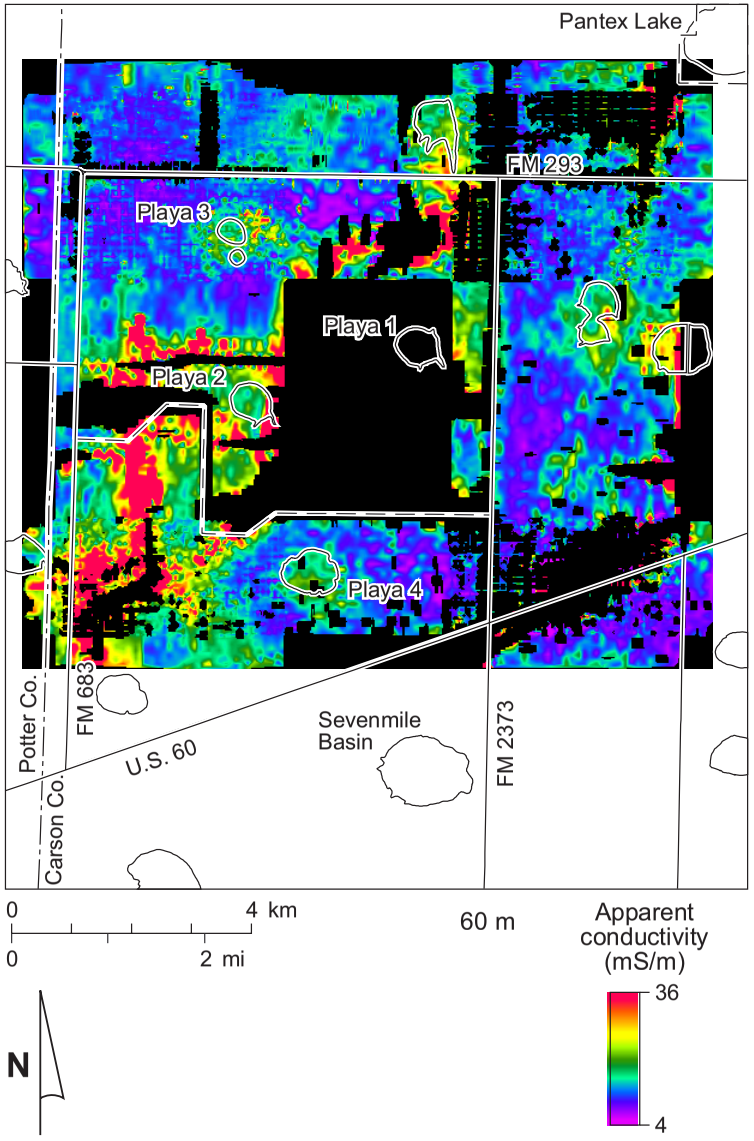


Figure C6. Apparent conductivity at a depth of 60 m.

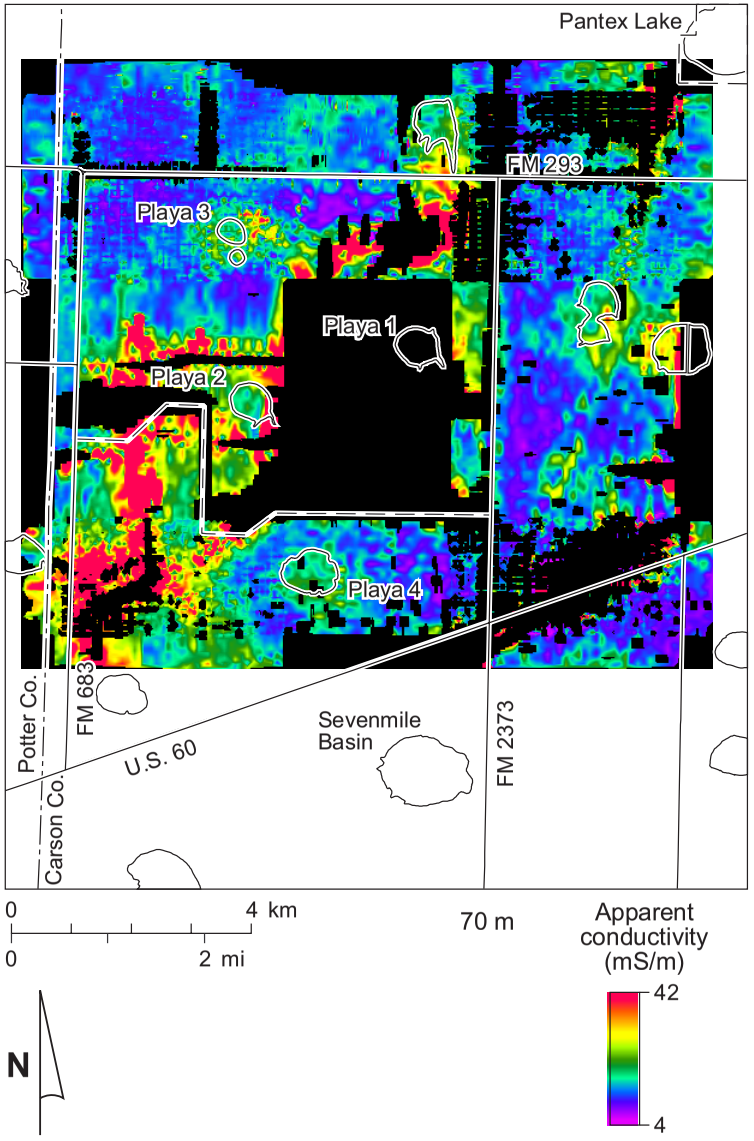


Figure C7. Apparent conductivity at a depth of 70 m.

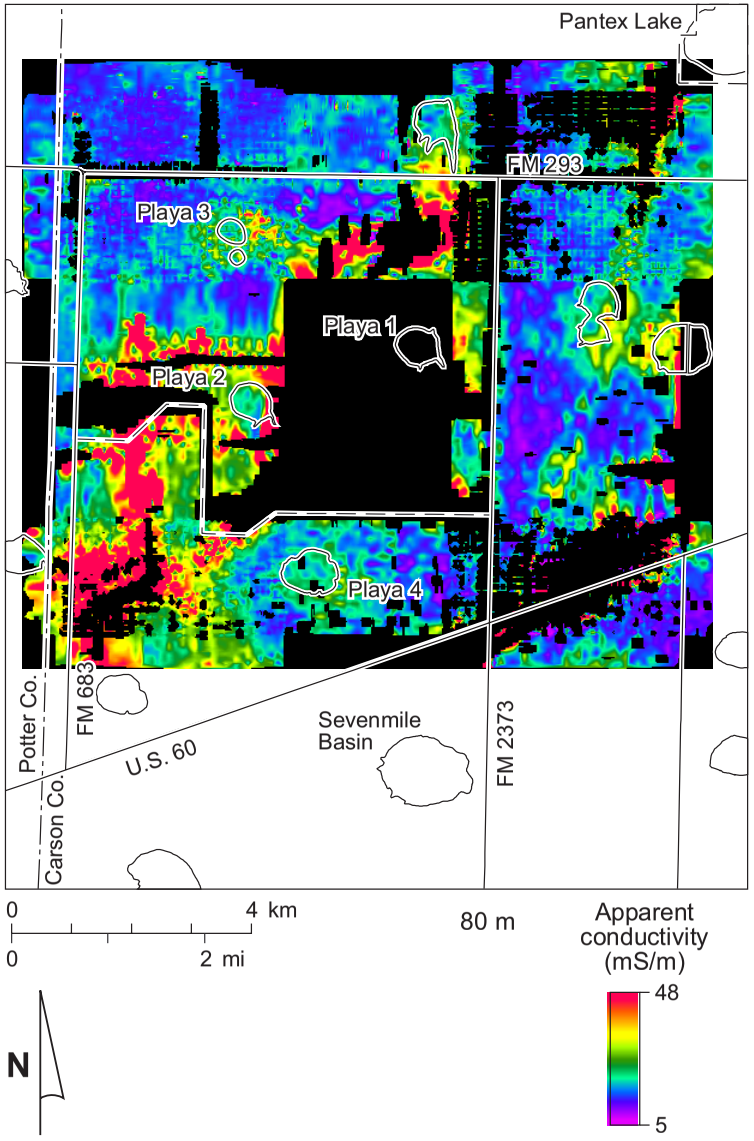


Figure C8. Apparent conductivity at a depth of 80 m

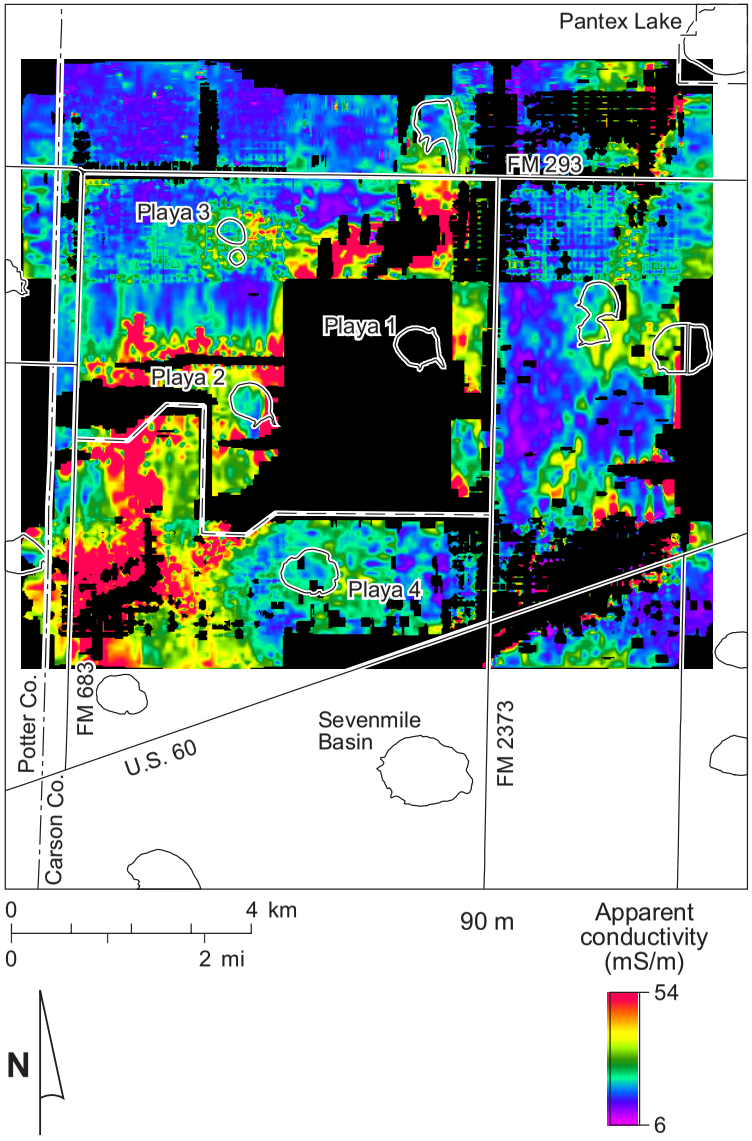


Figure C9. Apparent conductivity at a depth of 90 m.

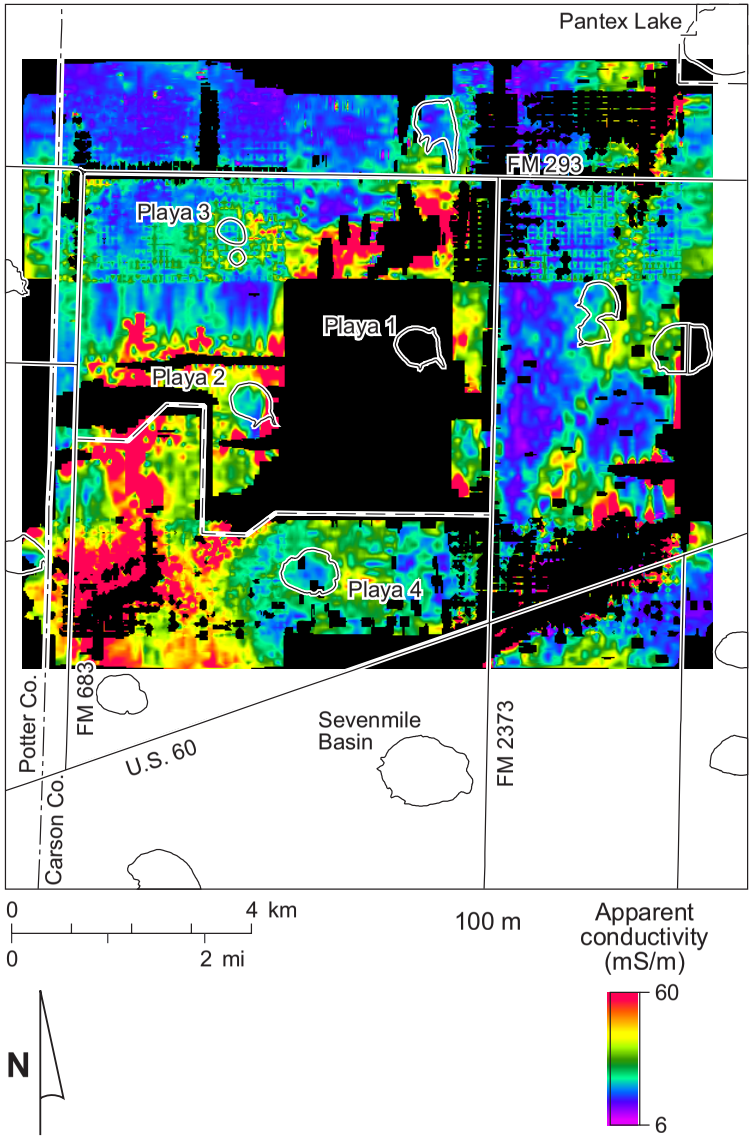


Figure C10. Apparent conductivity at a depth of 100 m.

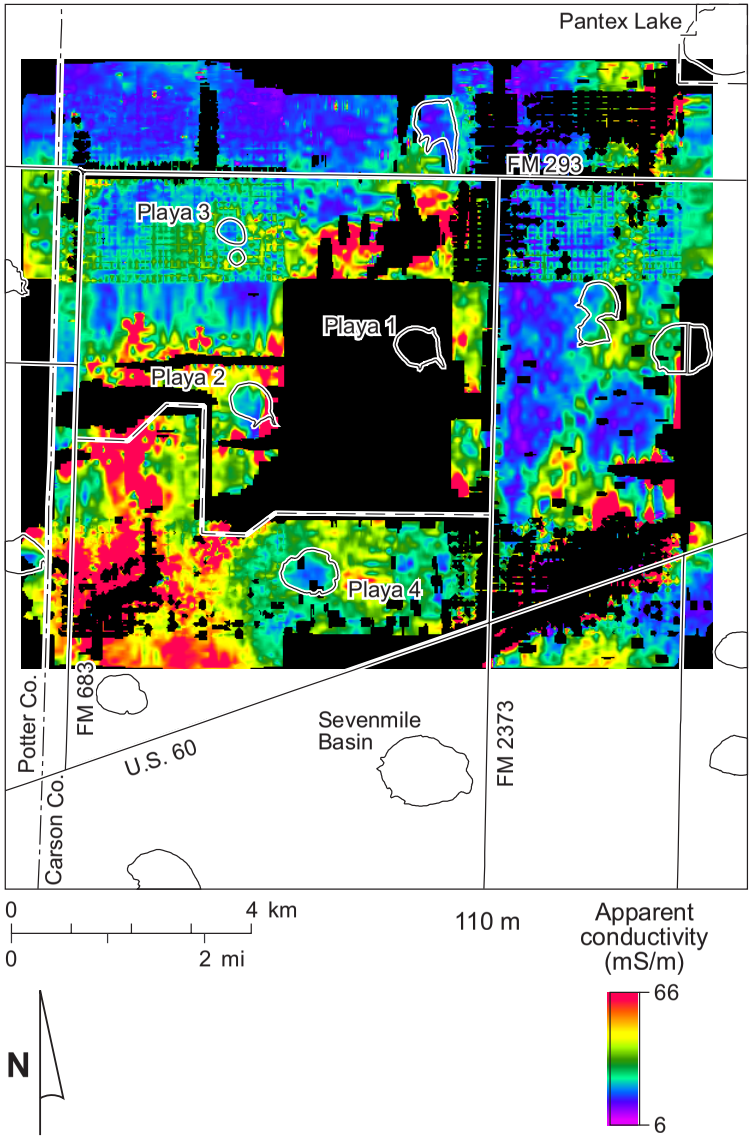


Figure C11. Apparent conductivity at a depth of 110 m.

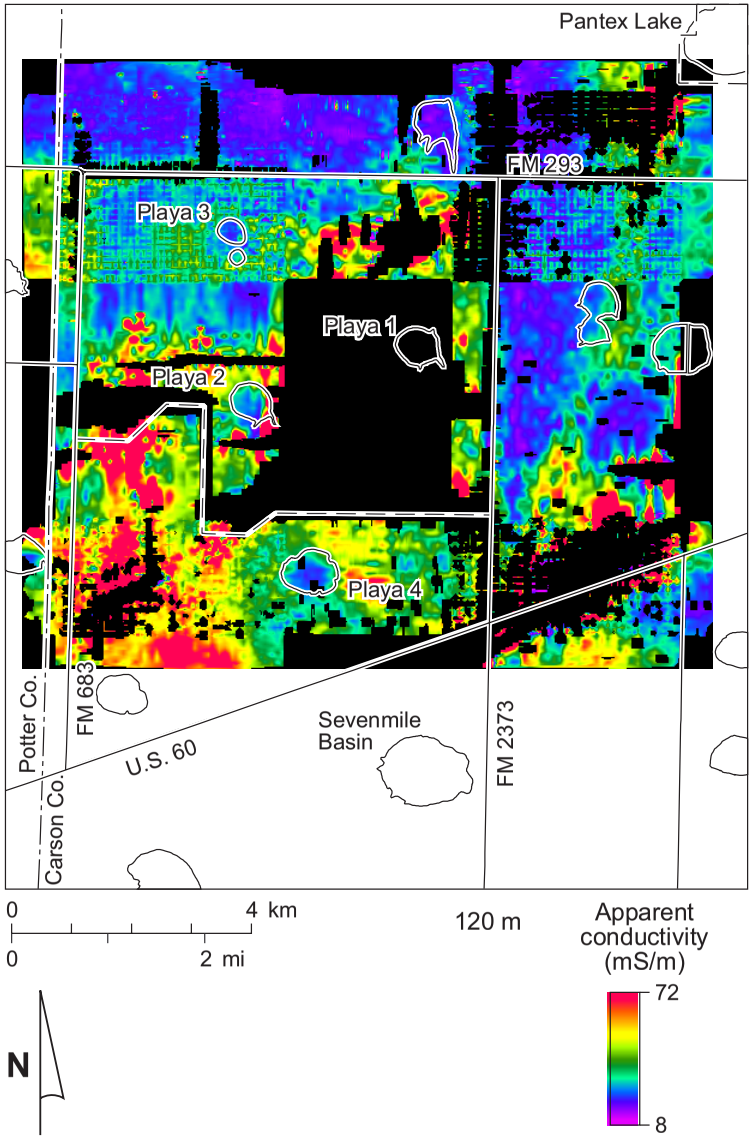


Figure C12. Apparent conductivity at a depth of 120 m.

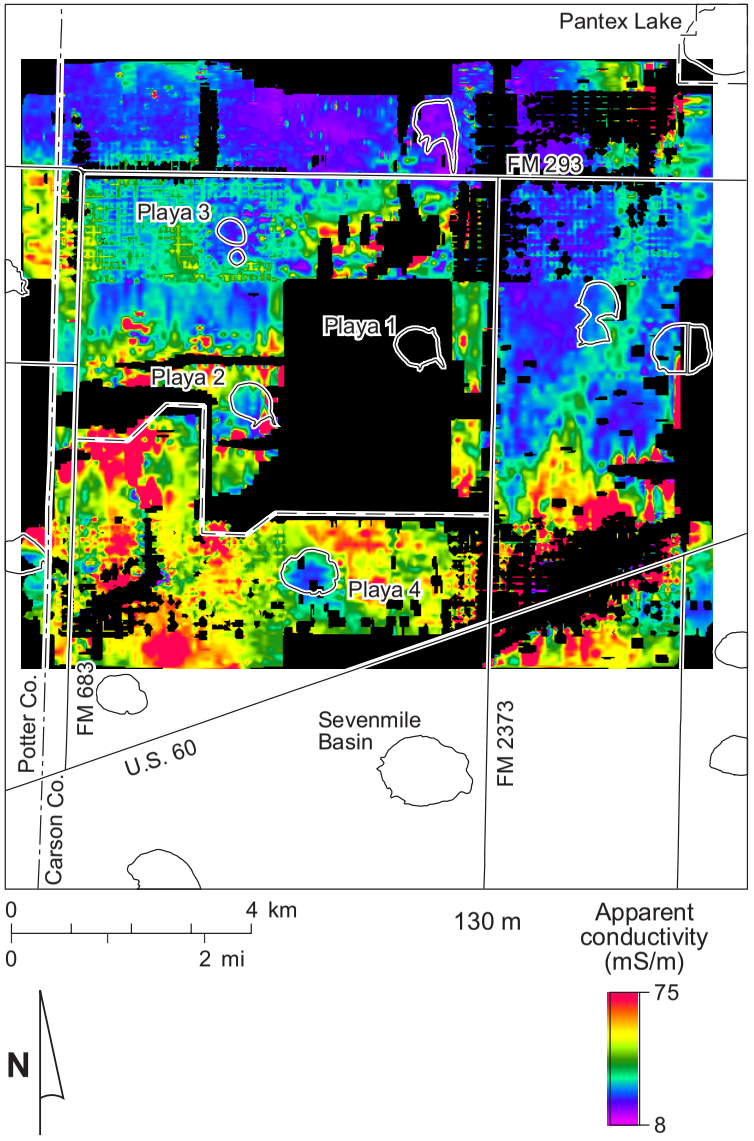


Figure C13. Apparent conductivity at a depth of 130 m.

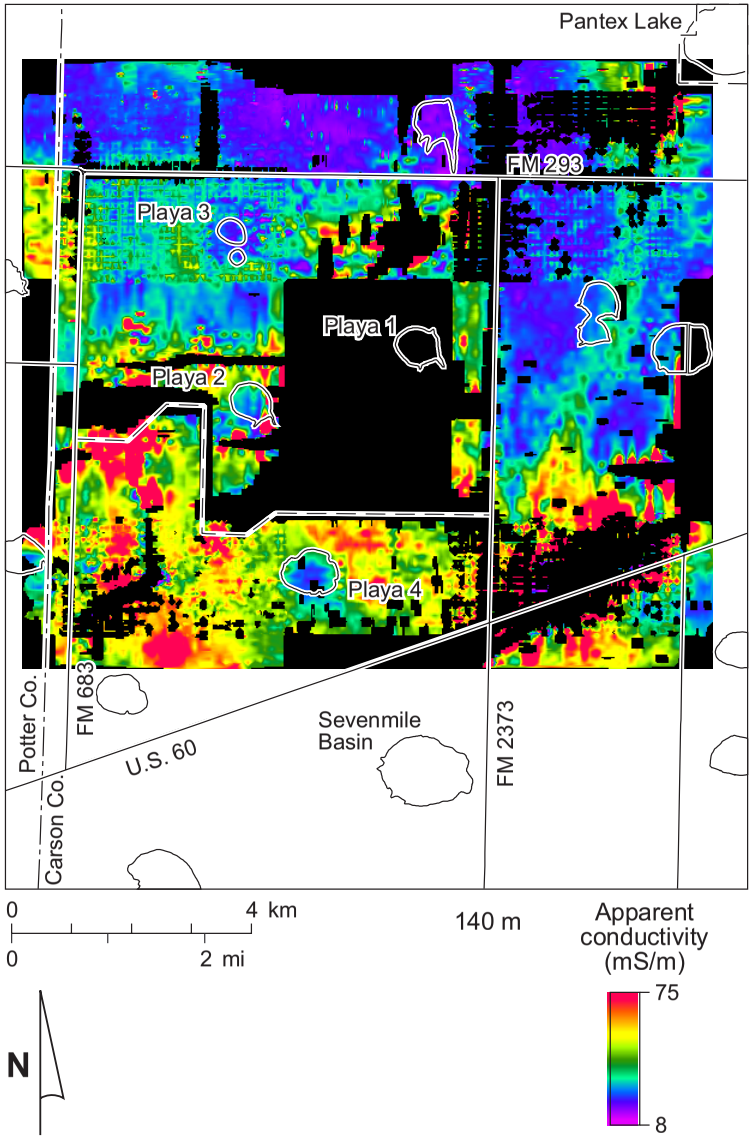


Figure C14. Apparent conductivity at a depth of 140 m.

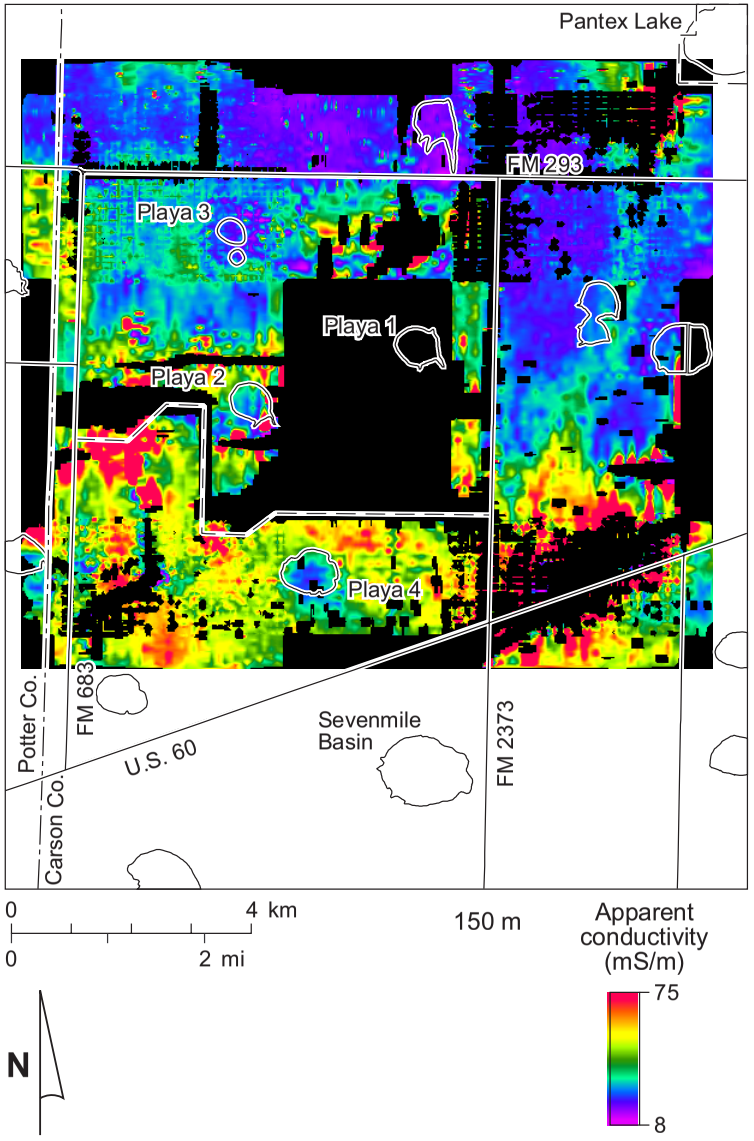


Figure C15. Apparent conductivity at a depth of 150 m.

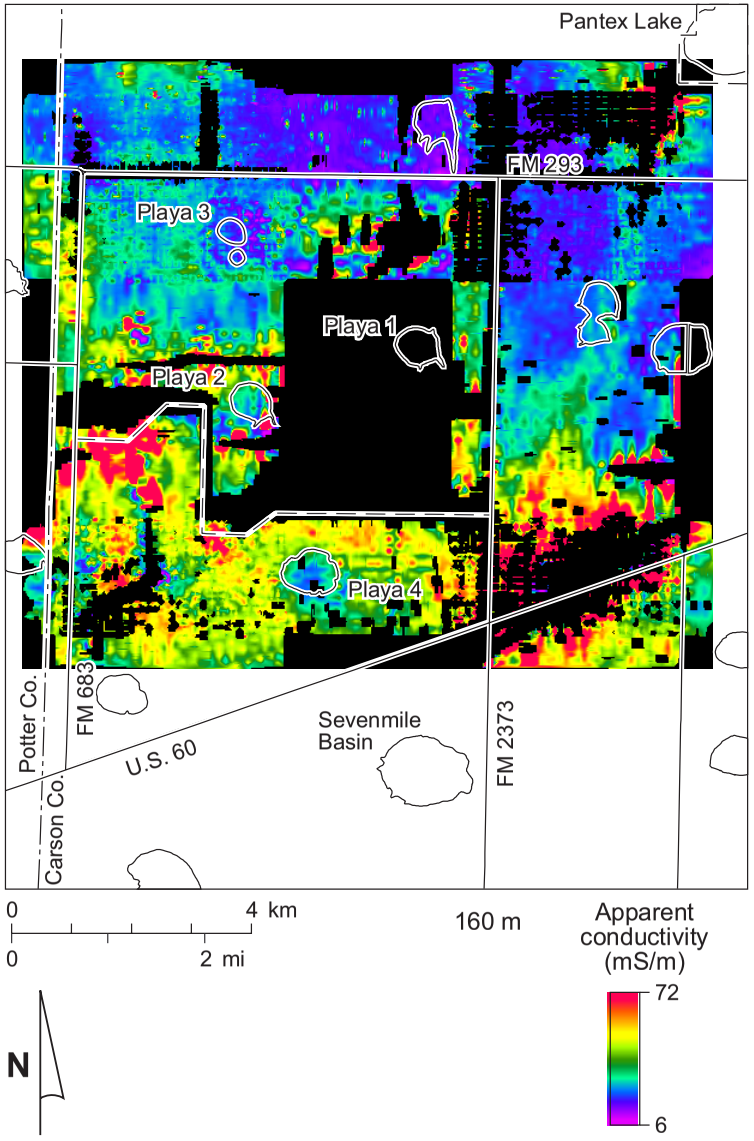


Figure C16. Apparent conductivity at a depth of 160 m.

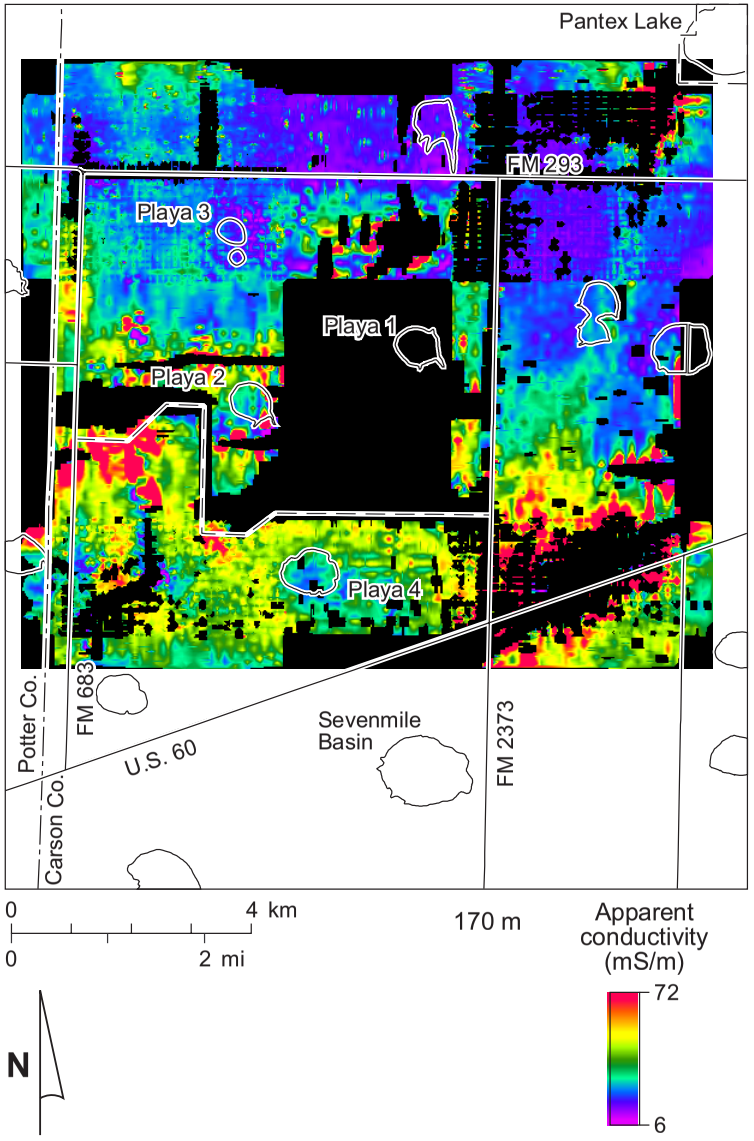


Figure C17. Apparent conductivity at a depth of 170 m.

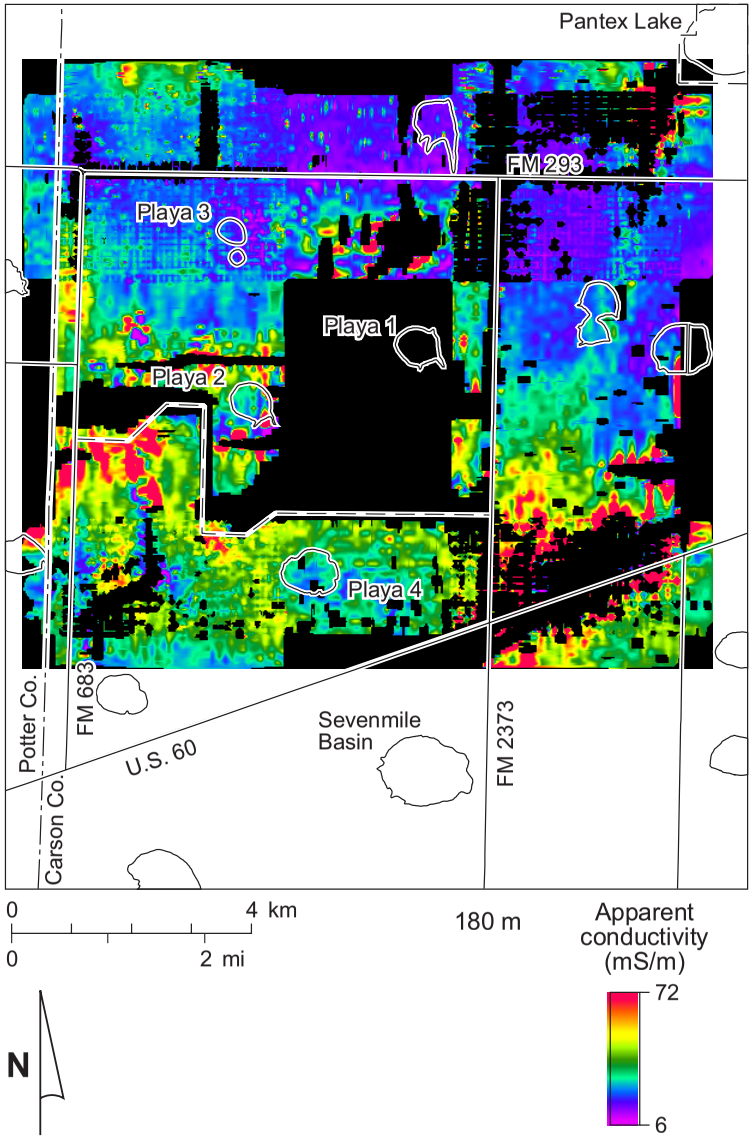


Figure C18. Apparent conductivity at a depth of 180 m.

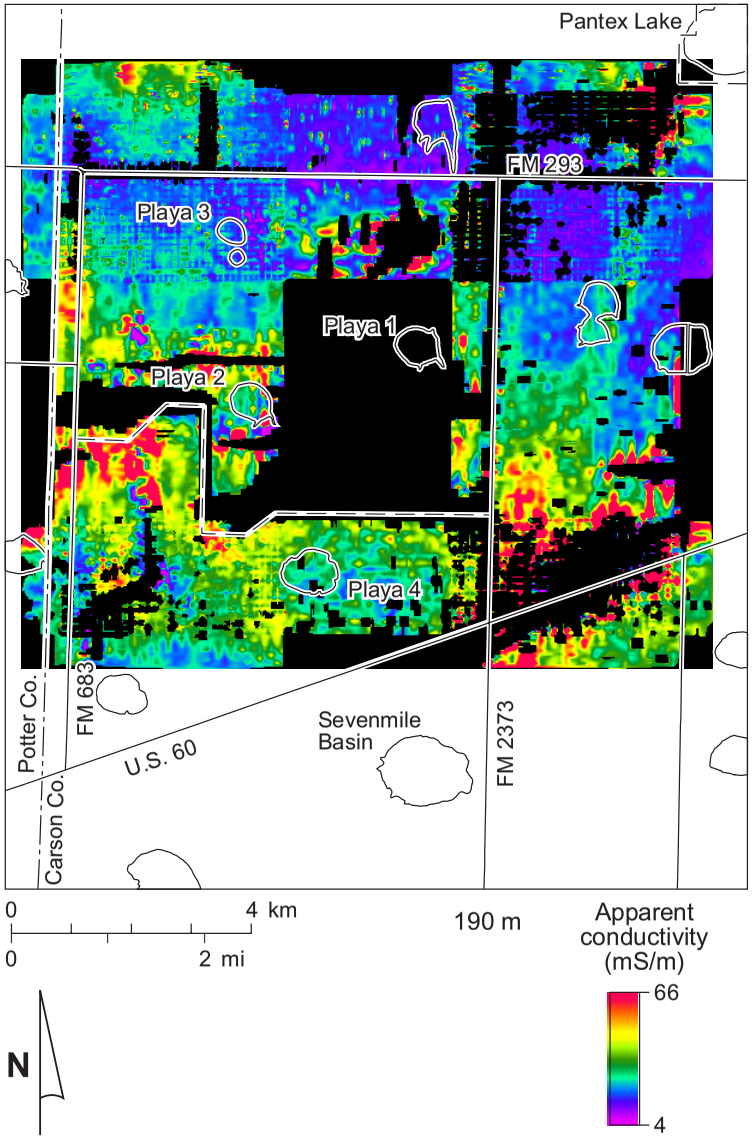


Figure C19. Apparent conductivity at a depth of 190 m.

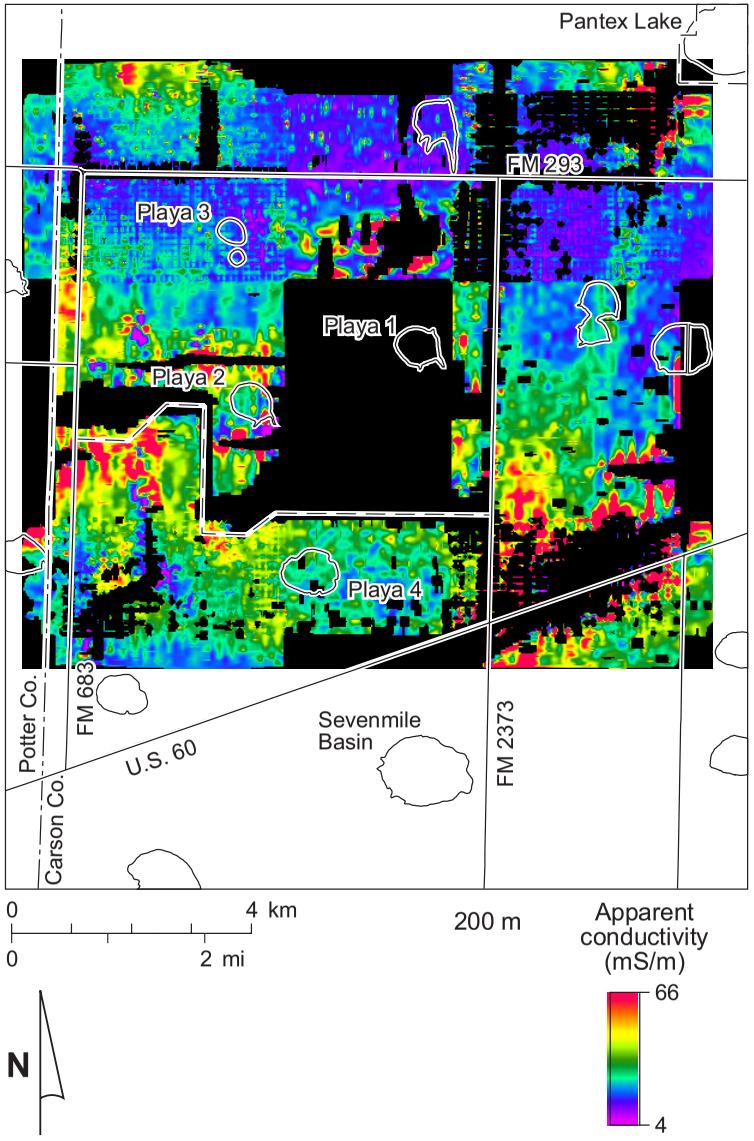


Figure C20. Apparent conductivity at a depth of 200 m.